

FABRIC FORMATION AND CONTROL IN FINE-GRAINED MATERIALS

A Thesis
Presented to
The Academic Faculty

by

Angelica M. Palomino

In Partial Fulfillment
of the Requirements of the Degree
Doctor of Philosophy in Civil and Environmental Engineering


Georgia Institute of Technology
December 2003


Copyright © 2003 by Angelica M. Palomino

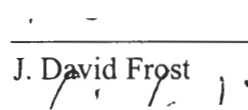
FABRIC FORMATION AND CONTROL IN FINE-GRAINED MATERIALS

Approved:

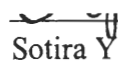



J. Carlos Santamarina, Chairman


Susan E. Burns


J. David Frost


Kimberly Kurtis


Sotira Yiacoumi

Date approved: 12 / 02 / 2003

DEDICATION

To John

ACKNOWLEDGMENT

First, I would like to thank my husband, John Heflin, for his support, patience and encouragement throughout my years at Georgia Tech. I also want to thank my family, Mary, Gilbert, Al and Nancy for always believing I could accomplish anything.

I am especially grateful to my advisor, Dr. J. Carlos Santamarina, for being an excellent mentor and friend. His teachings transcend the realm of research into my everyday life. I have learned more by his example than I could ever express and am forever thankful to him. I would also like to acknowledge his family for their support.

I would like to thank my first advisor, Dr. Dennis G. Grubb, for the many opportunities he has given me and for encouraging me to enter into graduate studies. I also wish to acknowledge my thesis committee: Susan E. Burns, J. David Frost, Kimberly Kurtis and Sotira Yiacoumi. I appreciate their useful comments and suggestions. I also wish to thank Dr. Xianguang Zhu and Dr. Patricia Dove for their guidance.

I would like to thank past and present members of the Particulate Media Laboratory for their assistance and encouragement: Maria Guimaraes, Jose Alvarells, Jong-Sub Lee, Franco Francisca, Tae-Sup Yun, Hyunki Kim, and Guillermo Narsilio, Katherine Klein, Gye Chun Cho, Yu-Hsing Wang, Julio Valdes, and Dante Fratta. I am also thankful to friends and former students I met during this journey: Bill Diesing and Daniel Landers.

I wish to acknowledge the National Science Foundation and Georgia Mining Association for providing funding for this research.

TABLE OF CONTENTS

| | |
|---|-------|
| DEDICATION | iii |
| ACKNOWLEDGMENTS | iv |
| TABLE OF CONTENTS..... | v |
| LIST OF TABLES | x |
| LIST OF FIGURES | xii |
| LIST OF MATHGRAMS | xvii |
| SUMMARY | xviii |
| CHAPTER I INTRODUCTION..... | 1 |
| 1.1 Fine-Grained Materials | 1 |
| 1.2 Motivation – Georgia Kaolin | 1 |
| 1.3 Thesis Organization | 4 |
| CHAPTER II MICROSCALE PHENOMENA AFFECTING | |
| FABRIC FORMATION | 7 |
| 2.1 Particle Size | 7 |
| 2.2 Mineralogy..... | 9 |
| 2.3 Structural Charge | 11 |
| 2.4 Fluid Interactions and Electrical Double Layer Formation | 13 |
| 2.5 Influence of pH and Ionic Concentration..... | 16 |
| 2.5.1 Structural Charge | 16 |
| 2.5.2 Adsorbed Protons (σ_H) and Ions (Δq) | 16 |
| 2.5.3 Charge Balance | 17 |
| 2.5.4 Particle Charge – Special Cases..... | 18 |
| 2.5.5 Dissolution | 18 |
| 2.6 Particle Geometry | 21 |
| 2.6.1 Specific Surface | 21 |

| | |
|--|--------|
| 2.6.2 Edge and Face Double Layers | 23 |
| 2.7 Particle-Particle Interactions..... | 23 |
| 2.8 Proposed Kaolin Fabric Map in the pH Ionic Concentration Space | 26 |
| 2.9 Previous Macroscale Observations | 28 |
| 2.9 Conclusions..... | 29 |
| CHAPTER III MATERIALS AND METHODS | 30 |
| 3.1 Materials | 30 |
| 3.2 Procedures..... | 39 |
| 3.2.1 Kaolin Conversion to Na-Form | 39 |
| 3.2.2 Sedimentation | 42 |
| 3.2.3 Viscosity | 43 |
| 3.2.4 Liquid Limit | 43 |
| 3.3 Physics and Interpretation Guidelines | 44 |
| 3.3.1 Sedimentation | 44 |
| 3.3.2 Rheology | 51 |
| 3.3.3 Liquid Limit | 52 |
| 3.4 Summary | 54 |
| CHAPTER IV FABRIC IN SINGLE MINERALS: EFFECTS OF pH AND IONIC CONCENTRATION | 55 |
| 4.1 Introduction..... | 55 |
| 4.2 Materials and Procedures | 55 |
| 4.2.1 Materials | 55 |
| 4.2.2 Electrolyte pH-Ionic Concentration Matrix | 58 |
| 4.2.3 Sedimentation | 58 |
| 4.2.4 Viscosity | 58 |
| 4.2.5 Liquid Limit | 58 |
| 4.3 Experimental Study 1: Sedimentation | 58 |
| 4.3.1 Results..... | 58 |
| 4.4 Experimental Study 2: Rheological Tests..... | 63 |
| 4.4.1 Results..... | 63 |
| 4.5 Experimental Study 3: Liquid Limit..... | 66 |

| | |
|--|-----|
| 4.5.1 Results..... | 66 |
| 4.6 Discussion..... | 66 |
| 4.6.1 Low/Intermediate Solids Concentration | 66 |
| 4.6.2 High Solids Concentration..... | 73 |
| 4.6.3 Relation to Proposed Fabric Map (Figure 2.9) | 76 |
| 4.7 Conclusions..... | 78 |
| CHAPTER V FABRIC IN SINGLE MINERALS – POLYMER-BASED CONTROL | 80 |
| 5.1 Introduction..... | 80 |
| 5.2 Sodium Polyacrylate (NaPAA)..... | 82 |
| 5.2.1 Adsorption Mechanisms on Kaolinite | 85 |
| 5.2.2 Adsorption Mechanisms on Calcium Carbonate | 87 |
| 5.2.3 Influence of Calcium Chloride (CaCl ₂) | 90 |
| 5.3 Materials and Procedures | 91 |
| 5.3.1 Materials | 91 |
| 5.3.2 Sedimentation | 92 |
| 5.3.3 Viscosity | 92 |
| 5.3.4 Liquid Limit..... | 93 |
| 5.4 Results..... | 94 |
| 5.4.1 Sedimentation | 94 |
| 5.4.2 Viscosity | 97 |
| 5.4.3 Liquid Limit..... | 99 |
| 5.5 Discussion..... | 99 |
| 5.5.1 Kaolinite..... | 102 |
| 5.5.2 Calcium Carbonate..... | 105 |
| 5.6 Conclusions..... | 107 |
| CHAPTER VI TWO-MINERAL MIXTURES WITHOUT POLYMER | 118 |
| 6.1 Introduction..... | 118 |
| 6.1.1 Mineral Mixtures | 118 |
| 6.1.2 Particle Shape..... | 121 |
| 6.1.3 Size..... | 126 |

| | |
|---|-----|
| 6.2 Materials and Procedures | 126 |
| 6.2.1 Materials | 126 |
| 6.2.2 Sedimentation | 128 |
| 6.2.3 Viscosity | 128 |
| 6.2.4 Liquid Limit | 128 |
| 6.3 Experimental Results | 128 |
| 6.3.1 Sedimentation Tests | 128 |
| 6.3.2 Rheological Tests | 136 |
| 6.3.3 Liquid Limit | 138 |
| 6.4 Discussion | 138 |
| 6.4.1 Sedimentation | 138 |
| 6.4.2 Rheology | 140 |
| 6.4.3 Liquid Limit | 142 |
| 6.5 Conclusions | 143 |
| CHAPTER VII TWO-MINERAL MIXTURES WITH POLYMER | 144 |
| 7.1 Introduction | 144 |
| 7.2 Materials and Procedures | 145 |
| 7.2.1 Materials | 145 |
| 7.2.2 Sedimentation | 145 |
| 7.2.3 Viscosity | 146 |
| 7.2.4 Liquid Limit | 146 |
| 7.3 Results | 146 |
| 7.3.1 Sedimentation Tests | 146 |
| 7.3.2 Viscosity | 155 |
| 7.3.3 Liquid Limit | 155 |
| 7.4 Discussion | 159 |
| 7.5 Conclusions | 171 |
| CHAPTER VIII CONCLUSIONS AND RECOMMENDATIONS | 179 |
| 8.1 Conclusions | 179 |
| 8.2 Recommendations | 181 |

| | |
|------------------|-----|
| REFERENCES | 183 |
| VITA..... | 193 |

LIST OF TABLES

| Table | Page |
|--|------|
| 1.1 Traditional Uses of Select Clay Minerals (After Murray, 2000). | 2 |
| 3.1 Tested Materials and Their Manufacturers | 31 |
| 3.2 Characteristics of Wilklay RP2 and SA1 Kaolin Clays (data provided by manufacturer) | 32 |
| 3.3 Characteristics of Premier Kaolin Clay (data provided by manufacturer). | 33 |
| 3.4 Characteristics of #12 White GCC (data provided by manufacturer) | 33 |
| 3.5 Comparison of Tested Materials | 34 |
| 3.6 Characteristics of Colloid 211 Sodium Polyacrylate (data provided by manufacturer). | 41 |
| 3.7 (a) Observed Suspension Settlement Modes as Defined by Previous Researchers..... | 47 |
| 3.7 (b) Observed Suspension Settlement Modes Defined for This Study | 48 |
| 4.1 Selected Studies: Influence of Ionic Concentration on Kaolinite Sedimentation Velocity and Volume | 56 |
| 4.2 Observed Sedimentation Behavior of Kaolinite Suspensions | 60 |
| 4.3 Results Summary for Sedimentation, Viscosity, and Fall Cone Tests | 69 |
| 4.4 Effects of Clay Dissolution on Pore Fluid pH..... | 74 |
| 5.1 Effect of pH on NaPAA Ionization | 84 |
| 5.2 Observed Sedimentation Behavior of Mineral Suspensions | 95 |
| 5.3 Mineral Suspensions pH in deionized water, with NaPAA and with NaPAA plus CaCl ₂ | 95 |
| 5.4 Results Summary for Sedimentation, Viscosity, and Fall Cone Tests | 103 |
| 6.1 Typical Measured Optical Coating Properties | 122 |
| 6.2 Properties of Select Kaolin and Calcium Carbonate Pigments | 125 |

| | | |
|-----|--|-----|
| 6.3 | Observed Sedimentation Behavior for RP2-GCC Mixtures | 130 |
| 7.1 | Observed Sedimentation Behavior for Premier-PCC Mixtures | 148 |
| 7.2 | Supernatant pH of Premier-PCC Mixtures..... | 148 |
| 7.3 | Observed Sedimentation Behavior for Premier-PCC Mixtures with CaCl_2 | 154 |
| 7.4 | Supernatant pH of Premier-PCC Mixtures with CaCl_2 | 154 |
| 7.5 | Estimated Ratios of added Ca^{2+} to NaPAA Monomers $[\text{Ca}^{2+}]_{\text{add}}/C_{\text{PPA}}$ for Premier Kaolinite (calculations are given in Mathgram 7.1)..... | 168 |

LIST OF FIGURES

| Figure | Page |
|---|------|
| 2.1 Relative contributions of skeletal, capillary, and van der Waals forces acting on a particle. At point 1, capillary forces begin to dominate with respect to the particle weight, at point 2 van der Waals forces become more relevant, and at points 3 and 4 capillary forces begin to exceed the contributions due to skeletal forces at confinements of 1 MPa and 10 kPa, respectively (Santamarina, 2002) | 8 |
| 2.2 Clay minerals. The primary building blocks (a) and (b), (c) structure of clay minerals, (d) edge and face termination sites, and (e) particle size and adsorbed layers..... | 10 |
| 2.3 Kaolinite molecular model. The primary building blocks (a) and (b), and (c) structure of clay minerals. Images are prepared with MDL Chime® web browser plug-in (Barak and Nater, 2003). | 12 |
| 2.4 Ionic distribution and variation in electrical potential adjacent to a negatively charged particle. | 15 |
| 2.5 Dissolution rate data based on Si release for kaolinite as a function of pH and temperature, summarized by Nagy (1995). Complete references for data points can be found in Nagy (1995). | 20 |
| 2.6 Kaolinite dissolution-stability diagram. The concentration of aluminum ions is used to monitor the evolution of dissolution. Stability constants used to compute this plot are found in Drever (1997)..... | 20 |
| 2.7 Idealized hexagonal kaolinite particle with size d and thickness t | 22 |
| 2.8 Long-range interparticle force - DLVO Theory. It combines van der Waals attraction (slightly sensitive to c_0) and double layer repulsion (determined by c_0) | 25 |
| 2.9 Summary of postulated particle associations (preferred minimum energy configurations) of kaolinite in NaCl electrolytes. | 27 |
| 3.1 Grain size distribution curves of kaolinites RP2 and SA1, and GCC #12 White. Size ranges for Premier and PCC are inferred from SEM micrographs. | 35 |
| 3.2 Scanning electron micrographs of kaolin clays (a) RP2 and (b) SA1 | 36 |
| 3.3 Scanning electron micrograph of Premier clay in (a) as-received dry form and (b) dispersed. | 37 |

| | | |
|------|---|----|
| 3.4 | Scanning electron micrographs of calcium carbonates (a) GCC #12 White and (b) Rhombic PCC..... | 38 |
| 3.5 | Measured conductivity of NaCl and CaCl ₂ solutions at various concentrations | 40 |
| 3.6 | SEM micrographs of kaolinite structure resulting from (a) flocculation sedimentation and (b) dispersed (accumulation) sedimentation (Pierre et al., 1995) | 49 |
| 3.7 | Sedimentation behavior classification (after Patton, 1979)..... | 50 |
| 3.8 | Rheological behavior. (a) Viscosity profiles for shear thinning, shear thickening and Newtonian fluids (b) clay flow unit response to applied shear. | 53 |
| 4.1 | Kaolinite sedimentation curves. Cases are for target pore fluid pH: (a) 3, (b) 5, (c) 7 and (d) 9. Pore fluid NaCl concentrations in mol/L.. | 59 |
| 4.2 | Kaolinite suspension initial settling velocity α . Target electrolyte pH: 3, 5, 7 and 9 | 62 |
| 4.3 | Kaolinite sedimentation height at 91 days. target electrolyte pH: 3, 5, 7 and 9 | 64 |
| 4.4 | Typical kaolinite suspension rheological behavior (data shown for 0.1 mol/L NaCl concentration) | 65 |
| 4.5 | Kaolinite suspension viscosities at 100 RPM Using Spindle #1 | 65 |
| 4.6 | Kaolinite fall cone penetration lines. Cases are for target pore fluid pH: (a) 3, (b) 5, (c) 7 and (d) 9. Pore fluid NaCl concentrations in mol/L..... | 67 |
| 4.7 | Kaolinite fall cone liquid limits. Target electrolyte pH: 3, 5, 7 and 9. The Cassagrande tests are performed on RP2 kaolinite without first rendering the clay monoionic, nor altering or measuring the solution pH(Klein, 1999). | 68 |
| 4.8 | Slopes of the kaolinite fall cone liquid limit lines. Target electrolyte pH: 3, 5, 7 and 9 | 68 |
| 4.9 | SEM micrographs of RP2 kaolinite exposed to sedimentation test conditions at $c=10^{-5}$ M NaCl and (a) pH=3 and (b) pH=9..... | 71 |
| 4.10 | Changes in fluid pH due to particle dissolution during fall cone tests. Closed symbols represent electrolyte pH prior to mixing and open symbols represent the measured pore fluid pH after mixing | 75 |
| 4.11 | Kaolinite RP2 fabric map. | 77 |

| | | |
|------|--|-----|
| 5.1 | Organic ion adsorption sites on clay mineral surfaces. (a) Exposed oxygen and hydroxyl cleavage planes, and broken bonds on the mineral edges, (b) interlayer space in swelling 2:1 clays and dioctahedral 1:1 clay minerals, (c) exposed surfaces (outer surface and internal tunnels) of sepiolite and palygorskite (attapulgite) particles, and (d) within the interparticle spacing of particle flocs (listed cases from Yariv & Cross, 2002 – graphical interpretation in this figure by the author). | 81 |
| 5.2 | Sodium polyacrylate. (a) Chemical structure of sodium polyacrylate and (b) dissociation of Na^+ ions from NaPAA polymer and subsequent negative charge development in water (after Mukerjee, 2000). | 83 |
| 5.3 | Hypothesized surface interactions of the polyacrylate molecule with (a) protonated aluminol and silanol edge groups of kaolinite and (b) surface calciums of CaCO_3 | 88 |
| 5.4 | Solubility of CaCO_3 in the presence of sodium polyacrylate. The solids volume fraction is 0.02 and the molecular weight of the sodium polyacrylate is 2000 g/mole (data points from Järnström, 1993) | 89 |
| 5.5 | Induction periods of mineral suspensions (solids volume fraction 0.02). Cases: without additives, with sodium polyacrylate, and with sodium polyacrylate plus 0.002 M calcium chloride. | 96 |
| 5.6 | Comparison of mineral suspension sediment heights at approximately 31000 minutes. Cases: without additives, with sodium polyacrylate, and with sodium polyacrylate plus 0.002 M calcium chloride. | 96 |
| 5.7 | Comparison of viscosity measurements at 100 RPM for mineral suspensions with 0.07 solids volume fraction. Cases: without additives, with sodium polyacrylate, and with sodium polyacrylate plus 0.002 M calcium chloride. The viscosity of the RP2 kaolin suspension without additives is high so it is measured with Spindle #3. All other suspension viscosities are measured with Spindle #1. | 98 |
| 5.8 | Fall cone penetration lines for (a) kaolins SA1 and RP2 and (b) GCC and PCC. Cases: without additives, with sodium polyacrylate, and with sodium polyacrylate plus 0.002 M calcium chloride. | 100 |
| 5.9 | Liquid limits comparison. Cases: without additives, with sodium polyacrylate, and with sodium polyacrylate plus 0.002 M calcium chloride. The liquid limits for the Premier case are not measurable. | 101 |
| 5.10 | Slopes of the kaolin and calcium carbonate fall cone liquid limit lines. | 101 |

| | | |
|------|---|-----|
| 5.11 | SEM micrographs of SA1 in the presence of (a) NaPAA and (b) NaPAA with CaCl_2 . | 106 |
| 6.1 | Viscosity of dispersed kaolinite-latex sphere mixtures. The clay mean equivalent spherical diameter $d_{\text{esd}}=0.7\mu\text{m}$. Sphere diameters are 0.1, 0.2 and $0.5\mu\text{m}$, and total solids volume content $\phi=0.55$ (Aline and Lepoutre, 1983a and b). | 127 |
| 6.2 | Sedimentation curves at 21 days for RP2–GCC mixtures (a) 100% RP2 through 50% RP2 and (b) 50% RP2 through 100% GCC by mass | 129 |
| 6.3 | Mixture Suspensions – RP2–GCC Initial Settling Velocity α | 132 |
| 6.4 | Sediment heights for RP2-GCC and SA1-GCC mixtures at 24 hours | 132 |
| 6.5 | Supernatant pH of RP2 Kaolinite -GCC Mixtures | 134 |
| 6.6 | Sedimentation curves at 11.4 days for SA1–GCC mixtures. (a) Suspension height and (b) sediment height | 135 |
| 6.7 | Viscosity measurements of SA1-PCC mixtures | 137 |
| 6.8 | Liquid limits for SA-1–GCC mixtures and sensitivity to moisture content. | 139 |
| 6.9 | Possible particle associations between SA1 and GCC and maximum number of particle attachments: (a) clay particle edge to GCC face and (b) clay particle face to GCC face. Maximum number of particle attachments assuming clay particle thickness $t=0.07\mu\text{m}$ (estimated from SEM micrograph), and spherical GCC shape with $d=12\mu\text{m}$. | 141 |
| 7.1 | Sedimentation curves at 23 days for Premier-PCC mixtures. | 147 |
| 7.2 | Sediment heights of Premier-PCC mixtures at 23 days | 150 |
| 7.3 | Sedimentation curves at 23 days for Premier-PCC mixtures with CaCl_2 . | 151 |
| 7.4 | Premier-PCC sediment heights at 23 days with and without CaCl_2 | 151 |
| 7.5 | Premier-PCC suspension induction times with CaCl_2 . | 152 |
| 7.6 | Viscosity measurements of Premier-PCC suspensions | 156 |
| 7.7 | SEM micrographs for Premier-PCC mixtures prepared as suspensions with the same solids volume fraction $\phi=0.07$ as the viscosity tests: (a) 100:0, (b) 75:25, (c) 25:75 and (d) 0:100 Premier:PCC. | 157 |
| 7.8 | Premier-PCC suspension viscosities with CaCl_2 and 25:75 Premier-PCC without CaCl_2 . | 158 |

| | | |
|------|---|-----|
| 7.9 | Premier-PCC viscosity at 100 RPM with and without CaCl_2 | 158 |
| 7.10 | Liquid limits of Premier-PCC mixtures with and without CaCl_2 | 160 |
| 7.11 | Effects of (a) particle packing and (b) flocculation on sediment height. | 161 |
| 7.12 | Pseudo edge-to-face flocculation of kaolinite and PCC particles. | 164 |
| 7.13 | Premier kaolinite particle associations in the presence of Ca^{2+} : (a) edge-to-edge and (b) edge to face. | 169 |

LIST OF MATHGRAMS

| Mathgram | Page |
|--|------|
| 5.1(a) Estimated RP2 Particle Edge Area..... | 109 |
| 5.1(b) Estimated SA1 Particle Edge Area..... | 110 |
| 5.2 $[\text{Ca}^{2+}]_{\text{add}}/\text{C}_{\text{PPA}}$ Ratios. | 111 |
| 7.1 $[\text{Ca}^{2+}]_{\text{add}}/\text{C}_{\text{PPA}}$ Ratios | 173 |

SUMMARY

Clay is one of the most important natural fine-grained particulate materials. The study of clay behavior has distinct relevance to a wide range of disciplines such as geology and geotechnical engineering, material science, and industrial applications. Furthermore, the optimal use of clay resources can have a critical impact on local economies. In particular, Georgia is one of the world's leading producers of high-quality kaolinite, which is used both as pigment and filler in paints and paper coating.

Non-gravimetric electrical forces, i.e., van der Waals attraction and double layer repulsion, dominate clay behavior under low effective stress conditions. Grain mineralogy and pore fluid chemistry determine surface charge distribution, interparticle electrical forces, the ensuing fabric formation and its potential alteration during pore fluid changes.

This study encompasses a comprehensive investigation of fine particle behavior, its dependence on pore fluid characteristics, and the application of this enhanced understanding to fabric control for the development of engineered fabrics. The systematic physical analysis of previously published studies is complemented with an extensive battery of tests that take into consideration surface charge control through pore fluid characteristics (i.e., pH and ionic concentration), single mineral systems and mixtures (kaolinite and calcium carbonate) and mineral surface modification with polymers. Additional considerations include the effects due to mineral dissolution, particle shape (platy, blocky and rhombahedral), relative particle sizes and masses. The

behavior of both individual mineral systems and mineral mixtures is studied through macroscale tests involving a wide range of solid volume fractions and strain levels. Scanning electron microscopy is also used to verify particle associations.

A detailed fabric map on the pH-ionic concentration space is suggested on the basis of physical analyses, and it is experimentally corroborated. Furthermore, the influence of an anionic polymer on single or mixed mineral systems is surface-charge dependent, i.e. the response depends on the type of kaolinite or calcium carbonate particles and the pore fluid characteristics. Single minerals become more readily dispersed, while the tendency to particle association prevails in kaolin-carbonate mineral systems. Electrostatic interactions, particle shape, and relative mineral content determine the final fabric of mixed-mineral systems. In the presence of a divalent cation, the ratio of added cations to the number of polymer binding sites determines the level of particle associations within single and mixed mineral systems treated with a polymer.

CHAPTER 1

INTRODUCTION

1.1 Fine-Grained Materials

The study of fine-grained particulate materials is relevant to geotechnical engineering, construction, agriculture, medicine, and materials science. The most common natural fine-grained material is clay. Clay behavior depends on particle size and shape, particle size distribution, surface chemistry, surface area and surface charge. The surrounding fluid environment influences some of these properties.

Of particular interest are clay particle interactions at low effective stress conditions: for micron-sized particles, the electrical van der Waals attraction force is dominant at confinements lower than 0.1 kPa. Even though most engineering conditions exceed this boundary, fine particle fabric formation, and ensuing soil behavior, results primarily from electrical forces (Santamarina, 2002).

1.2 Motivation – Georgia Kaolin

Many types of clay minerals are utilized as industrial materials over a broad range of applications depending on their physical and mineralogical characteristics. Table 1 lists traditional applications of kaolin as well as other clays; the most profitable use is for paper filler and coating.

The kaolin deposits in Georgia are concentrated along what was the shoreline of the Atlantic Ocean during the Cretaceous period (about 70 million years ago). This ancient shoreline stretches from Columbus to Augusta and is known as the Fall Line. The Fall

Table 1.1 Traditional Uses of Select Clay Minerals (After Murray, 2000).

| Kaolins | Smectites | Palygorskite and Sepiolite |
|--------------------|-----------------------|-----------------------------------|
| Paper coating | Drilling mud | Drilling fluids |
| Paper filling | Foundry bond clay | Paint |
| Paint extender | Pelletizing iron ores | Agricultural carriers |
| Ceramic ingredient | Sealants | Industrial floor absorbents |
| Rubber filler | Animal feed bonds | Tape joint compounds |
| Plastic filler | Bleaching clay | Cat box absorbents |
| Ink Extender | Agricultural carriers | Suspension fertilizers |
| Cracking catalysts | Cat box absorbents | Animal feed bonds |
| Fiberglass | Adhesives | Catalyst supports |
| Cement | Pharmaceuticals | Adhesives |
| Adhesives | Emulsions stabilizers | Paper |
| Enamels | Desiccants | Pharmaceuticals |
| Pharmaceuticals | Catalysts | Anti-caking agent |
| Crayons | Cosmetics | Reinforcing fillers |
| Molecular sieves | Paint | Environmental absorbent |

Line divides the Piedmont Plateau (north of the line) from the Atlantic coastal plane (south of the line). The Piedmont formation consists of metamorphic rocks, such as schists and gneisses, and igneous rocks such as granite. Intense weathering of the feldspar-rich granite produced large quantities of kaolinitic clays along with feldspars and mica that were carried away by rivers and streams and eventually deposited in wetlands along the ancient coastline. The feldspars further weathered in situ to produce kaolin. These deposits were eventually covered by a thick layer of sediments (CCPA, 2003; UGA, 2003).

Kaolin is one of Georgia's most important natural resources. As the leading state producer, Georgia was responsible for 24% of the total U.S. clay production in 2001 (USGS, 2001). In 2002, the paper industry consumed 53% of the kaolinite mined for domestic use (USGS, 2003). However, a recent shift from acid to alkaline papermaking processes has decreased the demand for kaolinite and increased the use of calcium carbonate as filler, especially precipitated calcium carbonate (Baumgartner, 2002). The solubility of calcium carbonate is low at high pH, and calcium carbonate improves the brightness and bulk of the paper.

The clay market has improved over the last few years due to advances in kaolin processing and an increasing market for non-traditional uses. Better particle size separation techniques and chemical structuring of kaolin particles to achieve particular size distributions have contributed to the industry shift toward unique kaolin-based coating products (Moore, 2002). The growth market for kaolin also includes calcined products for use as a TiO_2 extender in paper coatings and as filler in plastics and paints,

surface-treated products for dispersion in organophilic and hydrophobic systems, and products suitable for engineered paper coatings (Murray, 2000).

The growing trend is to engineer these coatings to meet the increasing demands for achieving specific levels of opacity, brightness, whiteness, gloss and print quality. Paper coatings fill in fiber voids; improve brightness, opacity, whiteness, and gloss; improve ink receptivity; increase resistance to picking and linting; and improve image quality. These properties depend on the coating fabric, which must survive high application shear rates (~ 28 m/sec for blade coaters). The wet coating viscosity must be low enough to minimize resistance during application, yet high enough to cling to the paper fibers until dry. The pigments within the coating suspension must remain well-mixed to help ensure a uniform coating. The final fabric is a function of the pigment minerals interparticle forces before, as well as after application. Hence, by engineering the coating, the desired coating properties can be achieved.

In addition to its relevance in the paper coating industry, clay fabric plays a critical role in determining the engineering behavior of fine-grained soils. For two similar soils at the same void ratio, the soil with the more flocculated fabric, or structure, will have a higher porosity, yet higher strength (interparticle Coulombian attractive forces), lower compressibility, and higher permeability (presence of large voids) than the dispersed soil (Lambe & Whitman, 1969).

1.3 Thesis Organization

The goals of this research are to develop a comprehensive understanding of fine particle behavior, its dependence on pore fluid characteristics, the application of this

enhanced understanding to fabric control, and the development of engineered fine particle fabrics.

In Chapter 2, this study first addresses microscale phenomena governing soil fabric formation, including particle mineralogy, particle-fluid interactions (electrical double layer formation and relative particle thickness), pore fluid chemistry (pH and ionic concentration), and particle-particle interactions due to the competing forces of electrical double layer repulsion and van der Waals attraction (DLVO).

Chapter 3 describes the materials and procedures used throughout the thesis. Also, the physical principles and interpretation guidelines for each test are presented.

Once the underlying mechanisms controlling particle behavior have been established, Chapter 4 focuses on sedimentation behavior, fabric and subsequent response by sediments formed by a single mineral (kaolinite). Particle associations are mapped and interpreted across the pH-ionic concentration space. The experimental methodology varies not only pH and ionic concentration, but solids content and strain conditions as well. It consists of performing sedimentation tests, obtaining rheological profiles, and measuring the liquid limit. Microscale fabric is verified using scanning electron microscopy techniques. In Chapter 5, the fabric formation in single mineral sediments (either kaolinite or calcium carbonate) is affected by adding a polymer with and without an added divalent cation..

Fabric formation and control in single minerals is extended to mineral mixtures in Chapter 6 (kaolinite and calcium carbonate) for various solids content and applied strain levels. The experimental methodology is similar to the methodology applied in previous chapters. Exploratory considerations include differing particle mineralogy and surface

charge, pore fluid changes in pH due to dissolution, differing particle shapes (platy vs. rhombahedral), relative particle sizes and masses. Chapter 7 extends these studies to affect mixed-particle interactions by incorporating both a polymer and an added divalent cation. Finally, conclusions and recommendations for future work are presented in Chapter 8.

CHAPTER 2

MICROSCALE PHENOMENA AFFECTING FABRIC FORMATION

The purpose of this chapter is to study and analyze the role of mineralogy, and the role of pore fluid polarity, pH and ionic concentration on clay interparticle associations and soil fabric formation. The concepts presented in this chapter provide the physicochemical basis for explaining behaviors explored in the following chapters.

The contents and structure of this chapter evolves from previous studies by Klein (1999) and Santamarina et al. (2002) with updated information and references. First, the relevance of size, mineralogy and surface charge is presented. Second, the influence of the pore fluid, including the formation of the electrical double layer and the differences in particle edge and face charges, is discussed. Finally, the expected particle associations based on the dominant interparticle forces with varying pH and ionic concentration are summarized for kaolinite in a pH-ionic concentration fabric map.

2.1 Particle Size

Due to their size (and resulting specific surface) clay particle behavior under low confinement is dominated by electrical forces. Figure 2.1 maps the regions of relevant forces acting on a particle for the given range of particle sizes. Points 1 ($d \approx 3\text{mm}$) and 2 ($d \approx 30\mu\text{m}$) indicate the particle diameters at which the influence of weight becomes less significant compared to capillary and van der Waals forces, respectively. For particle diameters $d < 20\mu\text{m}$ (Point 3) and $d < 0.2\mu\text{m}$ (Point 4) capillary forces begin to exceed the contributions due to skeletal forces at confinements of 1 MPa and 10 kPa, respectively. Particles are considered “fine” when contact-level capillary and electrical forces control

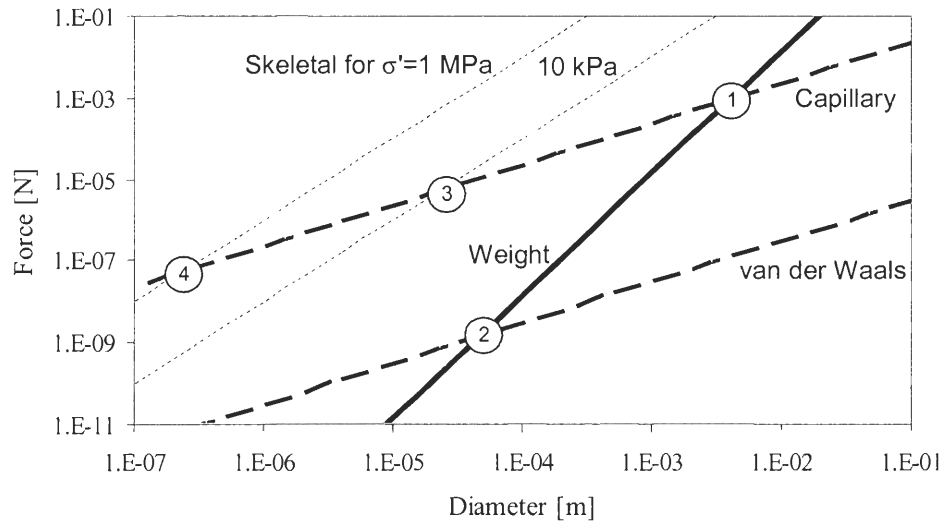


Figure 2.1 Relative contributions of skeletal, capillary, and van der Waals forces acting on a particle. At point 1, capillary forces begin to dominate with respect to the particle weight, at point 2 van der Waals forces become more relevant, and at points 3 and 4 capillary forces begin to exceed the contributions due to skeletal forces at confinements of 1 MPa and 10 kPa, respectively (Santamarina, 2002).

their behavior. These forces gain relevance at low effective stresses and particle sizes smaller than $d \approx 10\mu\text{m}$.

2.2 Mineralogy

Clay minerals are classified as phyllosilicates, referring to the layered, or sheet, structure and the base silica sheet. Layered silicates typically consist of some combination of two sheet types with silicon tetrahedra and aluminum or magnesium octahedra as the basic units (Figure 2.2-a). The silicon tetrahedron – four O^{2-} at the vertices surrounding a central Si^{4+} – is the basic unit of the silica sheet, while the aluminum or magnesium octahedral – six OH^- at the vertices around a central Al^{3+} or Mg^{2+} – serves as the basic unit of the octahedral sheet. Gibbsite refers to octahedral sheets whose cations are primarily aluminum, while brucite refers to an octahedral sheet whose cations are mostly magnesium. These sheets are held together through hydrogen bonding or with linking ions (Mitchell, 1993).

The clay mineral type depends on the sheet stacking sequence. Two common stacking arrangements form the 1:1 and the 2:1 clay minerals. Kaolinite, a 1:1 clay mineral, consists of individual layers of one silica and one gibbsite sheet. The layers have a basal spacing of 7.2 \AA . The sheets within the layers are held together by sharing oxygen atoms between the silicon and the aluminum (the oxygen at the silica tetrahedron tip also acts as an octahedron vertex). Layers are held together with hydrogen bonds linking the silica tetrahedral O^{2-} to the gibbsite OH^- (Mitchell, 1993; Bohn et al., 1985). The silica and gibbsite stacking of kaolinite leaves O^{2-} termination sites on the silica face, OH^- termination sites on the gibbsite face, and O^{2-} and OH^- termination sites along the edges (Figure 2.2-d).

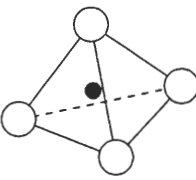
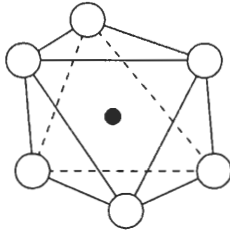
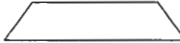
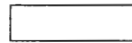
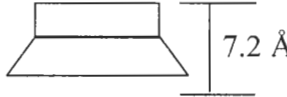
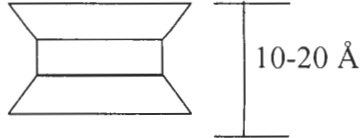
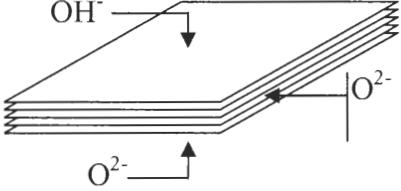
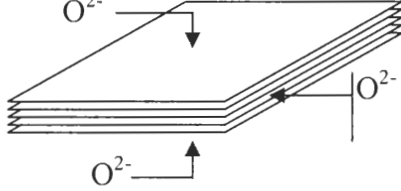
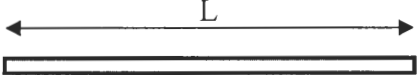
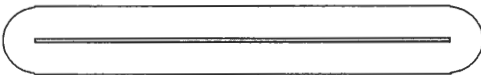
| | | |
|---|---|---|
| (a) Basic Units | <p>Si Tetrahedron</p>  <p>● Si⁴⁺ ○ O²⁻</p> | <p>Al or Mg Octahedron</p>  <p>● Al³⁺ or Mg²⁺ ○ OH⁻ or O²⁻</p> |
| (b) Sheets |  <p>Si tetrahedral - Silica</p> |  <p>Al octahedral sheet: Gibbsite</p> |
| | 1:1 Minerals - Kaolinite | 2:1 Minerals - Montmorillonite |
| (c) Mineral Structure |  <p>7.2 Å</p> |  <p>10-20 Å</p> |
| (d) Termination Sites on Particle Faces and Edges |  |  |
| (e) Particle Size and Adsorbed Layers | <p>L = 1-20 μm Thickness t ≈ L/30 Adsorbed layer 100 Å</p>  <p>Adsorbed layer plots thinner than the trace used for the edge</p> | <p>L < 100t < 0.1 μm Thickness t ≈ 9.6 Å Adsorbed layer 100 Å</p>  |

Figure 2.2 Clay minerals. The primary building blocks (a) and (b), (c) structure of clay minerals, (d) edge and face termination sites, and (e) particle size and adsorbed layers.

The 2:1 clay minerals, such as montmorillonite, illite, and chlorite, are formed by layers of either a gibbsite or brucite sheet stacked between two silica sheets. The sheets within the layers are bonded through oxygen sharing as in the 1:1 minerals. Interlayer bonding occurs by van der Waals forces, linking cations, and/or water molecules. The termination sites at the faces of the 2:1 clay minerals contain O^{2-} from the silica sheets, while both O^{2-} and OH^- occupy the edge termination sites (Figure 2.2-d).

A kaolinite molecular model is presented in Figure 2.3. The model shows the relative placement and bonding between single silica tetrahedral and aluminum octahedral groups to form sheets and the final mineral structure. The silica face O^{2-} , gibbsite face OH^- , and edge O^{2-} and OH^- termination sites are clearly depicted.

2.3 Structural Charge

Clay particles have a net charge, or ion exchange capacity, due to their crystalline structure. Structural charge is considered to be quite stable, but it can be affected by mineral dissolution (Section 2.5.5) and by very slow ionic diffusion within the solid phase. Sources of structural charge include isomorphic substitution, broken bonds along termination sites (mineral sheets have finite size), structural disorder and crystal defects (Grim, 1968; Sposito, 1989).

During mineral formation, isomorphic substitution of higher valence ions with lower valence ions renders a net negative charge while preserving the structure of the sheets. For example, Al^{3+} may substitute for Si^{4+} in the silicon tetrahedra, while Mg^{2+} may substitute for Al^{3+} in the aluminum octahedra (Mitchell, 1993). Substitutions occur according to ion availability, charge, and similarity in size (Lambe & Whitman, 1969). However, the formation of kaolinite involves very little isomorphic substitution; only one

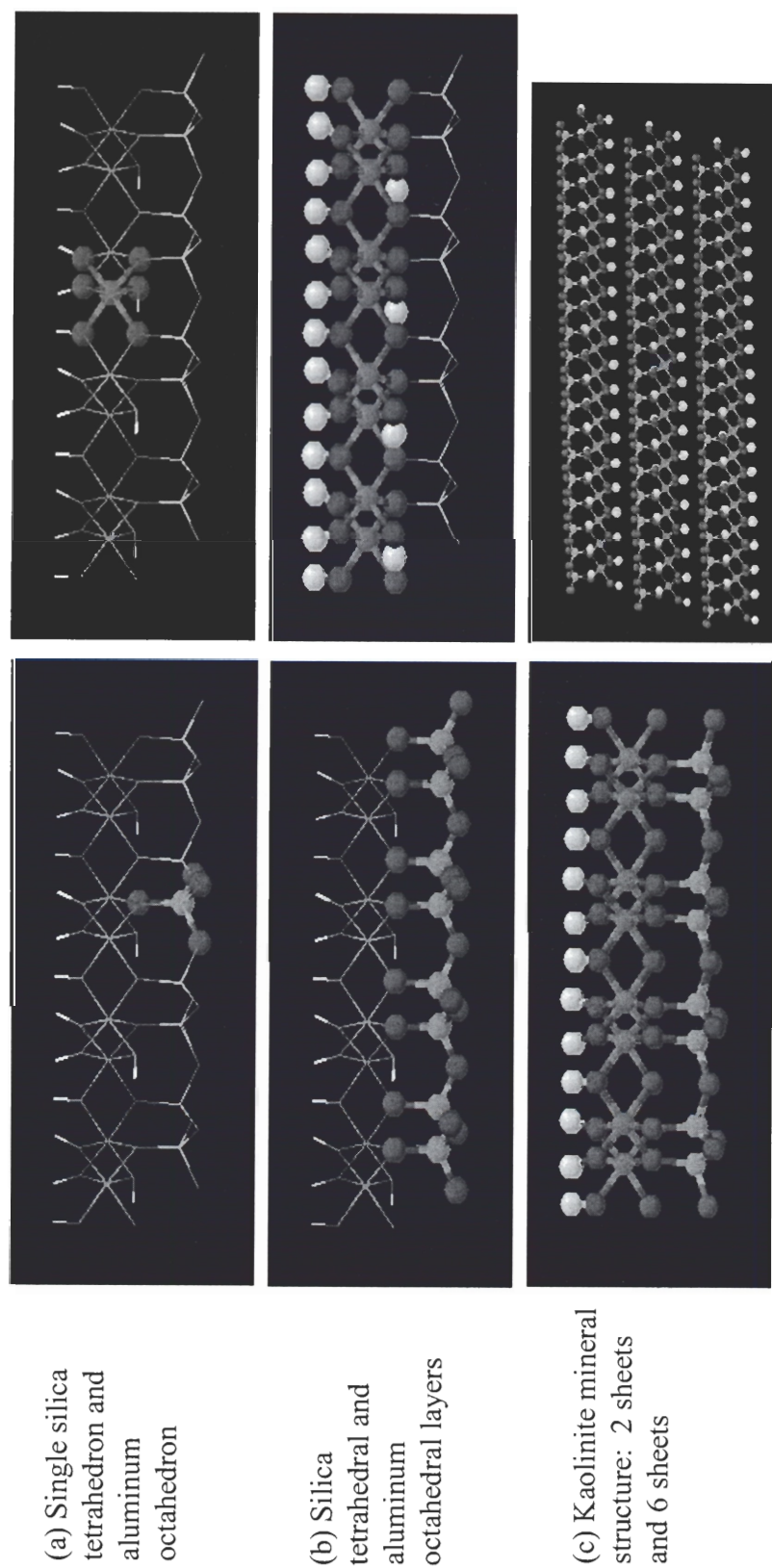


Figure 2.3 Kaolinite molecular model. The primary building blocks (a) and (b), and (c) structure of clay minerals. Images are prepared with MDL Chime® web browser plug-in (Barak and Nater, 2003).

Al^{3+} replacing every 400th Si^{4+} is needed to account for the net charge in a kaolinite particle (van Olphen, 1977; Schofield & Samson, 1953). In fact, Ma and Eggleton (1999) concluded that less than 5% of the exchange capacity of kaolinite is due to isomorphic substitution.

Locally unsatisfied bonds exist along the edges of mineral sheets. In infinite sheets, electrical neutrality is achieved among neighboring units by sharing oxygens O^{2-} in Si-tetrahedral units and hydroxyls OH^- in octahedral units. Since minerals do not exist in infinitely long sheets, charges at lateral boundaries remain uncompensated. The number of broken bonds tends to increase as the particle size decreases and as lattice distortions increase. Locally unsatisfied bonds are one of the major sources of exchange capacity in kaolinite minerals (Grimm, 1968; Ma & Eggleton, 1999).

Hydrogen atoms on the exposed plane of hydroxyls in octahedral sheets may be replaced with other cations such as Na^+ or Ca^{2+} . Because the octahedral sheet comprises a basal plane in kaolinite minerals, this source of exchange capacity is also important (Grim, 1968; Ma & Eggleton, 1999).

2.4 Fluid Interactions and Electrical Double Layer Formation

Under dry conditions, clay structural charges are compensated with counterions closely bound to the mineral surface. Excess ions around the particles are in the form of salt precipitates. Upon wetting, these precipitated salts hydrate and form the bulk fluid electrolyte.

Under the influence of water polarity and thermal agitation-induced diffusion, the surface-bound counterions tend to move away from the particle surface. This movement is limited by the attraction force between the counterions and the charged surface. A

characteristic ion concentration distribution called the diffuse double layer develops from the competing effects of thermal agitation and electrostatic forces. For a clay mineral with net negative surface charge, there will be a high concentration of cations near the surface with a corresponding low anion concentration. Further away from the surface, the concentration of cations decreases while the anion concentration increases asymptotically reaching bulk fluid concentrations, c_0 , at some distance from the mineral surface as depicted in Figure 2.4. The Stern layer describes the tightly bound ions remaining near the mineral surface and extends for only a few angstroms, while the Gouy layer is defined as the region of diffuse ions beyond the Stern layer. The boundary between the Stern and Gouy layers is called the outer Helmholtz plane (Lyklema, 1995).

The Gouy layer outer boundary is not well-defined due to the random movements of the hydrated ions. The “thickness of the diffuse double layer”, or the Debye-Hückel length, ϑ is taken to be the distance at which the potential, Ψ , decays to $1/e$ of the Stern potential Ψ_{stern} , and it is equal to

$$\vartheta = \left(\frac{\varepsilon' k T}{2 c_0 e_o^2 z^2 N_{av}} \right)^{1/2} = \left(\frac{\varepsilon' R T}{2 c_0 z^2 F^2} \right)^{1/2} \quad 2.1$$

where T is absolute temperature [K], c_0 is the ionic concentration in the bulk solution [mol/m³], ε' is the real permittivity of the solution [farad/m], and z is the valence of the prevailing cation. The constants invoked are the elementary charge ($e_o = 1.602 \cdot 10^{-19}$ C),

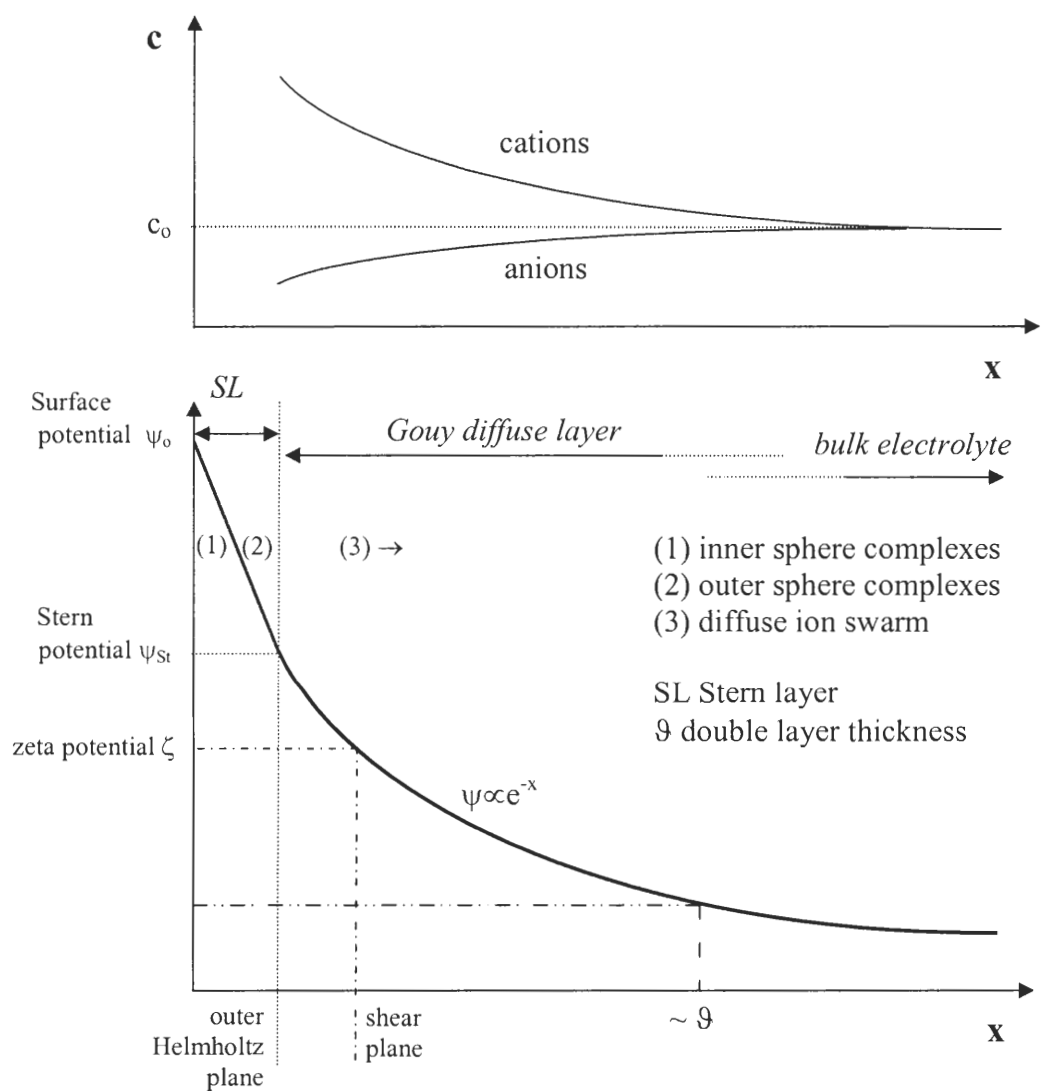


Figure 2.4 Ionic distribution and variation in electrical potential adjacent to a negatively charged particle.

Boltzmann's constant ($k=1.38 \cdot 10^{-23}$ J/K), Avogadro's number ($N_{av}=6.022 \cdot 10^{23}$ mol⁻¹), the gas constant ($R=8.3145$ J/mol·K), and Faraday's constant ($F=96485.3$ C/mol).

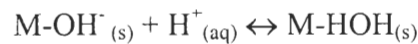
2.5 Influence of pH and Ionic Concentration

2.5.1 Structural Charge

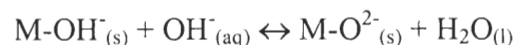
The structural charge, σ_0 , is the permanent mineral charge stemming from isomorphic substitution, uncompensated charges along termination sites, structural disorder and crystal defects (Section 2.4; Grim, 1968; Sposito, 1989).

2.5.2 Adsorbed Protons (σ_H) and Ions (Δq)

Particle excess structural charges are balanced by the adsorption of protons and other ions. The adsorption process depends on the affinity of an ion for the mineral and on the availability, or concentration, of those ions. Associations tend to be greater between a mineral and its constituent species. These species act as potential-determining ions, i.e., they determine the particle surface electrical potential. For oxides in water, proton H^+ (H_3O) and hydroxyl OH^- are often potential-determining ions in that protonation, H^+ adsorption at termination sites, increases the surface positive charge and OH^- -surface interactions increase the surface negative charge. Protonation increases the net positive charge according to:



where M represents a metal. Negative surface charges are increased through deprotonation, which is the removal of protons from OH^- termination sites to form water (Lyklema, 1995; Stumm, 1992):



Both protons and hydroxyls play key roles in both 1:1 and 2:1 clay minerals, specifically on the octahedral face of 1:1 minerals (e.g., gibbsite face of kaolinite) and on the OH⁻ termination sites on the edges of both 1:1 and 2:1 clay minerals (Figure 2.2).

In addition to OH⁻ and H⁺, other ions may adsorb onto the particle by forming inner and outer sphere complexes. Inner sphere complexes are counterions that remain near the particle surface without water molecules separating the ion from the surface, the counterions having lost at least part (or all) of their primary hydration shell. Outer sphere complexes remain near the surface with their primary hydration shell intact.

Cation adsorption is the prevailing mechanism altering the charge of surfaces with O²⁻ termination sites, such as on silica faces (the basal plane of a Si-sheet has an O²⁻ termination site every 4.8 Å²). The Stern potential decreases (becomes less negative) with increasing ionic concentration. At large concentrations, the particle can be rendered neutral or even positively charged. Both the charge and size of the cation determine the efficiency of surface charge modification, as in the case of Al³⁺ ions (see Amirtharajah and Mills, 1982; Lovgren et al., 1990). Cation complexation can take place in the hexagonal cavities between the O²⁻ on the Si-sheet basal plane and near hydroxyl surface sites (Hayes and Leckie, 1987; Nishimura et al., 1994). Therefore, protonation and cation complexation are not independent processes.

2.5.3 Charge Balance

The strength of Coulombian forces requires that the particle and its adsorbed ions satisfy electroneutrality. Therefore,

$$\sigma_o + (\sigma_H + \Delta q) = 0 \quad 2.1$$

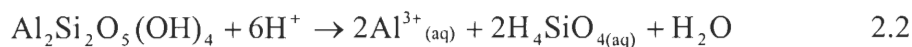
2.5.4 Particle Charge – Special Cases

Two important cases of particle charge are the “point of zero charge” and the “isoelectric point” (Sposito, 1998). The point of zero charge is the pH at which the Stern potential is zero and is typically measured with potentiometric titration. The isoelectric point is the pH at which the zeta potential (potential at the shear plane) is zero. Using electrophoresis, the IEP is the point at which the particle mobility is zero. Mobility is the velocity of a charged particle normalized with respect to the applied electric field. Both the PZC and IEP vary with the availability of potential-determining surface sites (OH⁻ termination sites in the case of clay minerals) and the electrolyte conditions.

Differences in termination sites on clay particle basal surfaces and edges leads to variation between the two surface types in protonation and ion complexation. Hence, the net charge on the basal plane differs from that of the edges, and each surface may have its own corresponding IEP.

2.5.5 Dissolution

Mineral stability depends on the surrounding fluid pH, ionic concentration, ion type, and temperature. The pH-dependence of kaolinite dissolution involves two distinct mechanisms. At low pH, aluminum preferentially dissociates according to the protonation reaction (Wieland and Stumm, 1992):



At moderate to high pH, silica preferentially dissociates. Converting aqueous Al^{3+} species to $\text{Al}(\text{OH})_4^-$, the dissociation reaction may be written as (Nagy, 1995):



Deprotonation of Si-OH sites promote silicate dissolution at $\text{pH} > 8$ according to:



This reaction weakens adjacent Si-O bonds, releasing Si^{4+} into solution. For aluminosilicates, this silica release appears to control the detachment of non-silica complexes at high pH. The rate-limiting silica dissolution reaction is (Brady and Walther, 1989)



where $\text{Si-O}^- \cdot n\text{H}_2\text{O}$ is the activated complex and n is the number of water molecules. Hence, the Si-O^- concentration increases with increasing pH, and the dissolution reaction rate increases. Figure 2.5 summarizes kaolinite dissolution rates as a function of pH and temperature based on Si dissociation data. Clearly, the

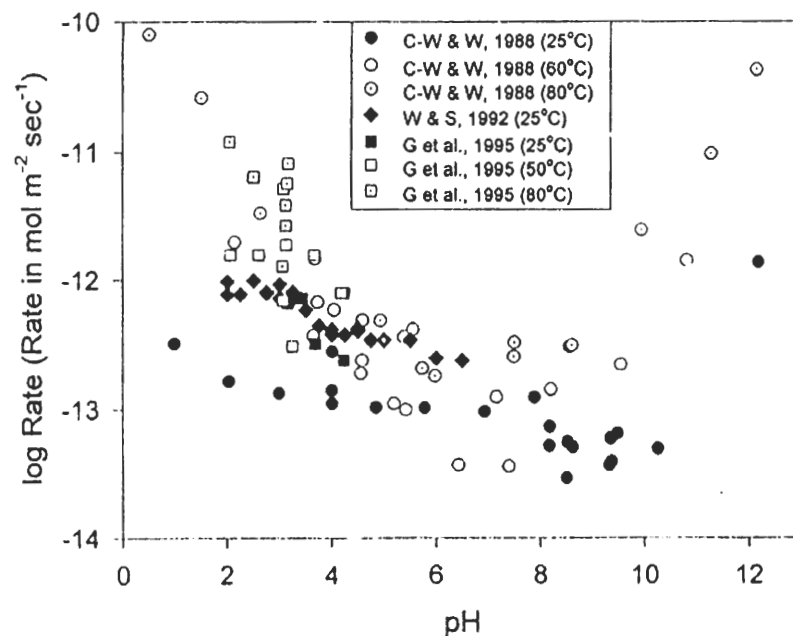


Figure 2.5 Dissolution rate data based on Si release for kaolinite as a function of pH and temperature, summarized by Nagy (1995). Complete references for data points can be found in Nagy (1995).

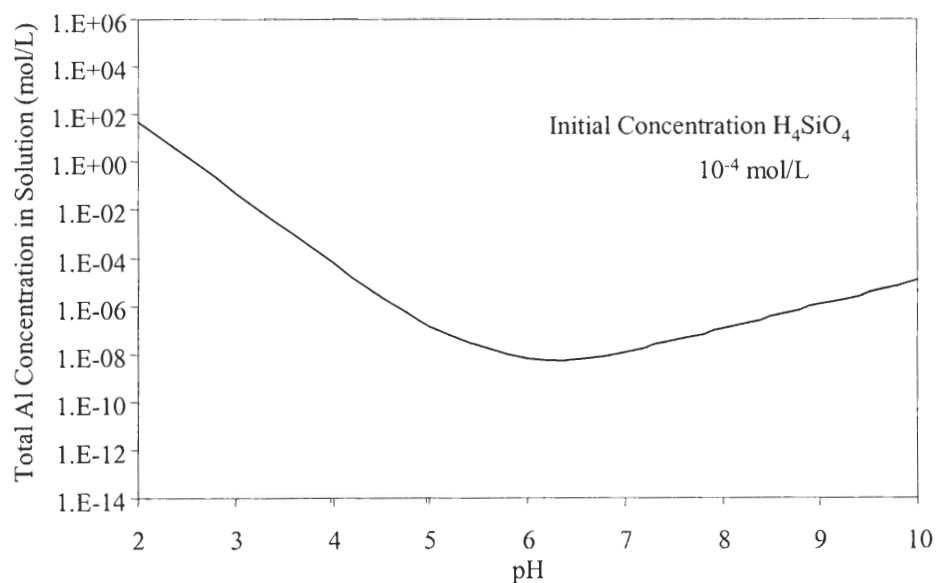


Figure 2.6 Kaolinite dissolution-stability diagram. The concentration of aluminum ions is used to monitor the evolution of dissolution. Stability constants used to compute this plot are found in Drever (1997).

measured dissolution rates are much higher at extreme values of pH than at moderate pH.

The stability of kaolinite at an initial H_4SiO_4 concentration of 10^{-4} mol/L (typical of fresh, river water) and over a range of pH values is plotted in Figure 2.6. Mineral precipitation occurs when the total aluminum species concentration in the fluid is greater than the stability value, while dissolution takes place in the opposite case.

Mineral dissolution shifts the pH towards a stable value corresponding to the particular mineral-fluid system by consuming H^+ at low pH and OH^- at high pH. The liberated ions, such as Al^{3+} at low pH ($\text{pH} < 2$) cause the rapid coagulation of suspensions in primarily face-to-face aggregation (Rand et al., 1980).

2.6 Particle Geometry

2.6.1 Specific Surface

The specific surface may be defined as the ratio of the particle surface area to its weight. A square plate with length L , thickness t , and density ρ , has a specific surface:

$$S_a = \frac{2L^2 + 4tL}{tL^2\rho} = \frac{2}{t\rho} \left(1 + 2\frac{t}{L} \right) \quad 2.6$$

Equation 2.7 shows the significant influence of particle thickness on the specific surface. The specific surface of an ideal kaolin particle of size d and thickness t is (see Figure 2.7):

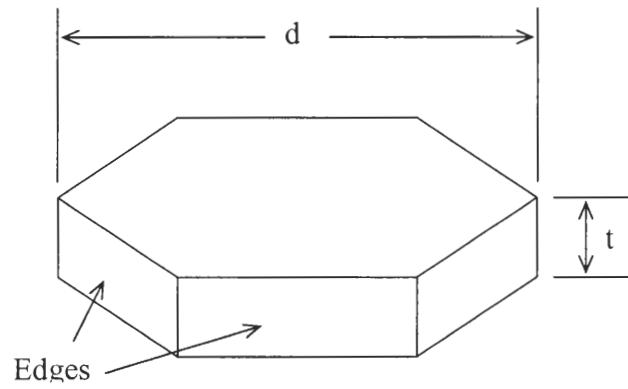


Figure 2.7 Idealized hexagonal kaolinite particle with size d and thickness t .

$$S_{z,kaolin} = \frac{8}{\sqrt{3}dp} + \frac{2}{tp} \quad 2.7$$

where $8/(\sqrt{3}dp)$ and $2/tp$ are the components due to the edge area and basal planes, respectively. Equation 2.7 implies that the specific edge surface area depends on the particle size, while the specific basal area depends on the particle thickness (Ma and Eggleton, 1999).

2.6.2 Edge and Face Double Layers

Figure 2.2(e) illustrates two important concepts in the relationship between particles and their respective double layers. First, the impact of the double layer increases with decreasing particle size and thickness. Second, the edge potential may be hidden by the face double layer when particles are thin $t < \delta$. Numerical determinations of electrostatic potential around a montmorillonite particle show that the impact of the face potential on the net edge potential increases as concentration decreases (double layer thickness increases), the ratio of the edge charge density to face charge density decreases, and the ratio of the particle length to thickness increases (Secor and Radke, 1985 – Additional corroborating results can be found in Delville, 2002).

2.7 Particle-Particle Interactions

Governing interparticle forces are reflected in the association between two particles. Three minimum energy particle associations are edge-to-face EF, edge-to-edge EE, and face-to-face FF (van Olphen, 1977). A fourth association often observed in SEM

images is shifted face-to-face (Shifted FF). Interparticle forces that promote these associations include:

- Coulombian attraction between a positive edge and a negative face, resulting in EF flocculation (Schofield and Samson, 1954). EF associations are often detected with rheological parameters such as the Bingham yield stress. In a suspension, decreasing the supernatant pH changes the behavior of the clay particles from stable (deflocculated, dispersed) to shear-resistant. The edge IEP is the transition pH at which the increase in resistance occurs.
- Osmotic repulsion and van der Waals attraction between two surfaces (edge or face) with the same charge. The fluid permittivity between the particles (Hamaker constant) determines the van der Waals attraction, while the ionic concentration more readily influences the Stern potential, and consequently the Debye-Hückel length (double layer thickness). Figure 2.8 is a plot of the net force between two particles as a function of the distance between them. When van der Waals attraction prevails, particle association tends toward FF aggregation.
- Prevailing van der Waals attraction at intermediate concentrations, where EF Coulombian attraction and FF repulsion decrease, resulting in EE flocculation (van Olphen, 1951).

Groups of associated particles form conglomerates, which in turn form sediments. The density and mechanical properties reflect the type of interparticle associations. For example, FF aggregations typically form high-density flocs, and EF flocs

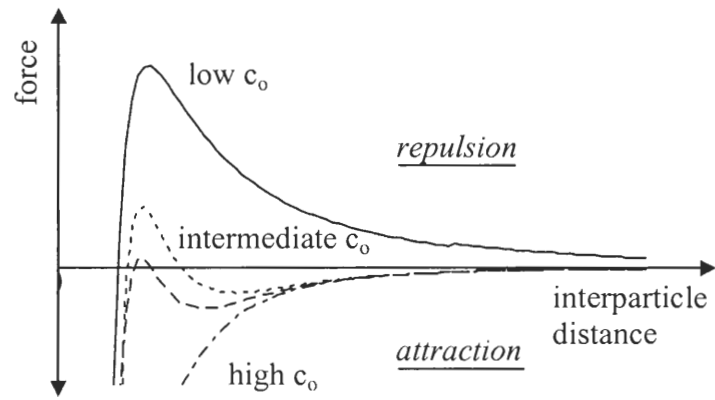


Figure 2.8 Long-range interparticle force - DLVO Theory. It combines van der Waals attraction (slightly sensitive to c_0) and double layer repulsion (determined by c_0).

experience strong Coulombian and van der Waals attraction forces. The macroscale manifestations are explored in subsequent chapters.

2.8 Proposed Kaolin Fabric Map in the pH Ionic Concentration Space

The previous discussion defines particle associations and resulting fabric formation as a function of pH and ionic concentration. Figure 2.9 summarizes particle interactions for kaolinite across a range of pH values and ionic concentrations found in the literature. The prevailing considerations for each region in the proposed “pH-concentration fabric map” follow:

- *Low ionic concentration.* At high pH, both the particle edges and faces are negatively charged, the double layer is large, and repulsion prevails. The particles are therefore deflocculated and dispersed. As the pH decreases and becomes less than the edge IEP (pH~7.2), the edges become positively charged. Electrostatic attraction favors EF associations. When the pH approaches the particle (face) IEP, van der Waals-dominated associations prevail. At low pH, both the particle edges and faces are positively charged resulting in deflocculated-dispersed structure.
- *High ionic concentration.* At NaCl electrolyte concentrations greater than 0.1 to 0.15 M, the double layer is thin and van der Waals attraction dominates. Particles associate by FF aggregation. Shifted FF may be observed in the pH region below the edge IEP and above the face IEP. These aggregates link through EE and EF interactions and form high void ratio networks (van Olphen, 1977; Rand and Melton, 1977; Melton and Rand, 1977; O’Brien, 1971).

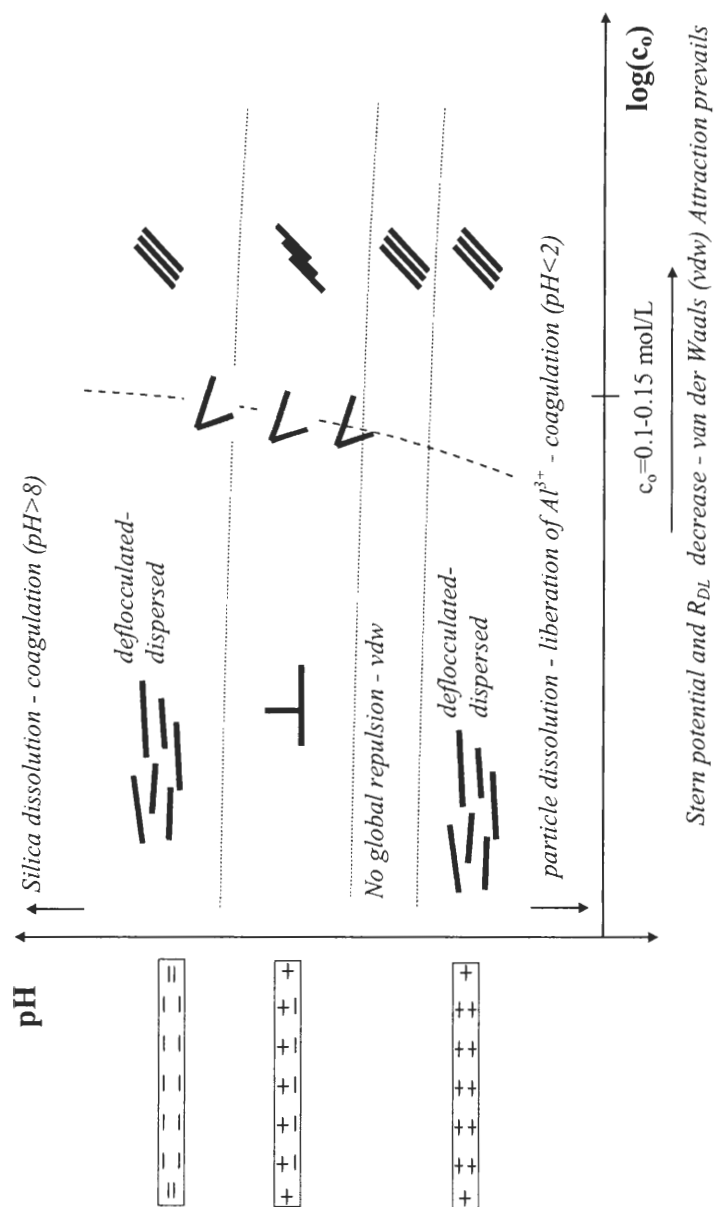


Figure 2.9 Summary of postulated particle associations (preferred minimum energy configurations) of kaolinite in NaCl electrolytes.

- *Moderate ionic concentration.* As the ionic concentration increases from low to high, particles associations shift from deflocculated-dispersed or EF to FF aggregation. In the transition region (~ 0.1 M NaCl), the expected particle association is EE and is independent of pH.
- *Extreme pH.* Mineral dissolution and release of Al^{3+} ions at extremely low pH (< 2) and silica dissolution at high pH (> 9) are expected to induce particle coagulation.

An analogous discussion addressing the fabric map of montmorillonite can be found in Santamarina et al. (2002).

2.9 Previous Macroscale Observations

The previous discussions suggest that mineralogy and pore fluid chemistry define interparticle forces, and therefore fabric formation. Particle associations are often inferred from rheological studies, but other testing techniques provide insight into the nature of the final fabric. Examples include monitoring hydraulic conductivity, sedimentation, liquid limit and shear strength. Published studies related to variations in the mechanical properties of kaolinite and montmorillonite in relation to changes in pore fluid chemistry are summarized in Santamarina et al. (2002). The following observations can be made:

Many trends appear to be the immediate consequence of changes in double layer thickness ϑ : as the double layer thickness increases, interparticle repulsion forces and porosity increase. This is particularly the case in high specific surface montmorillonite: as ϑ increases, the sedimentation volume and the liquid limit increase.

Deviations from this general trend are more common in kaolinite than in montmorillonite, especially when changes in permittivity are involved (the Hamaker constant in the van der Waals force depends on permittivity).

2.10 Conclusions

The behavior of small particles ($< 10\mu\text{m}$) under low stresses is dominated by van der Waals attraction and double layer repulsion. Mineralogy and pore fluid determine the chemical-electrical characteristics of mineral surfaces, the ensuing interparticle electrical forces, and fabric formation and its potential alteration during pore fluid changes. Therefore, a detailed analysis of chemical-mechanical coupling must take into consideration changes in surface charge density and double layer formation, the geometric characteristics of the particles, the characteristics of the pore fluid (pH, concentration, ion type), and recognize the interplay between the particle and pore fluid characteristics.

In its simplest form, fabric formation and alteration in clay minerals can be captured in the pH-concentration space. The resulting fabric formation map is different for different clay minerals, and it may also vary with the valence and size of prevailing ions.

Macroscale testing offers insight into the prevailing particle associations by relating observed trends in fabric properties, such as changes in sedimentation height, hydraulic conductivity, or liquid limit, with changes in pore fluid ionic concentration, ion valence, pH and permittivity.

CHAPTER 3

MATERIALS AND METHODS

The purpose of this chapter is to summarize the characteristics of the materials used throughout this study, to define the governing phenomena involved in each test procedure, and to provide guidelines for the physical interpretations of measured parameters. Any deviations from the general procedures are presented in the relevant chapter.

3.1 Materials

This study focuses on the behavior of five minerals: three types of kaolin and two types of calcium carbonate. Tables 3.1 through 3.5 list their sources and properties. Grain size distribution curves are presented in Figure 3.1.

Scanning electron micrographs of the kaolins are shown in Figures 3.2 and 3.3, while micrographs of the calcium carbonates are presented in Figure 3.4. Notice the particle size differences between the RP2 and SA1 kaolin clays. The RP2 clay (Figure 3.2-a) has many smaller, more randomly-shaped particles than the SA1 (Figure 3.2-b). The larger SA1 particles tend to have the characteristic pseudo-hexagonal shape. Premier kaolin is shown in in the dry, as-received form and after dispersing in deionized water in Figure 3.3. In dry form, the Premier particles are bound together in spherical units much larger than the clay particles themselves, $\sim 100\ \mu\text{m}$ compared to $\sim 2\ \mu\text{m}$.

Both the size and shape of the GCC particles are much different than the clay particles. Where the RP2 and SA1 particles are platy and have $d_{50} = 0.36\ \mu\text{m}$ and $d_{50} = 1.1\ \mu\text{m}$, respectively, the GCC particles are bulkier $d_{50} = 12\ \mu\text{m}$ with irregular

Table 3.1 Tested Materials and Their Manufacturers

| Material | Manufacturer Designation | Manufacturer | Location |
|--|---------------------------------|--------------------------------------|-------------------|
| Kaolin, air-float processed | Wilklay RP2 | Wilkinson Kaolin Associates | Gordon, Georgia |
| Kaolin, air-float processed | Wilklay SA1 | | |
| Kaolin, NaPAA-treated, coating quality | Premier (dry form) | Imerys, Pigments and Additives Group | Roswell, Georgia |
| Precipitated Calcium Carbonate (PCC) | Rhombic | | |
| Ground Calcium Carbonate (GCC) | #12 White | Georgia Marble Company | Kennesaw, Georgia |

Table 3.2 Characteristics of Wilklay RP2 and SA1 Kaolin Clays (data provided by manufacturer)

a) Typical Properties

| Property | RP2 | SA1 |
|---|-----------|-------|
| Specific Gravity | 2.6 | 2.6 |
| GE Brightness, % Average | 78 | 79.5 |
| pH (28% solids), Average | 5.2 | 5.4 |
| Median Particle Diameter, (μm) | 0.36 | 1.1 |
| Oil Absorption, g/100g Clay | 40 | 32 |
| Minimum Dispersed Viscosity, 70% solids, cps* | Not Fluid | -- |
| Minimum Dispersed Viscosity, 62% solids, cps* | 4000 + | -- |
| Viscosity, 62% solids, cps*, Maximum | -- | 400 |
| Raw Color | Cream | Cream |

*Brookfield No.2 Spindle, 20 rpm.

b) Chemical Analysis

| Chemical Component | RP2 | SA1 |
|--------------------------------|--------|--------|
| SiO ₂ | 45.60% | 45.60% |
| Al ₂ O ₃ | 38.40 | 38.40 |
| Fe ₂ O ₃ | 0.88 | 0.40 |
| TiO ₂ | 1.69 | 1.50 |
| CaO | 0.05 | 0.06 |
| MgO | 0.02 | Trace |
| K ₂ O | 0.15 | 0.18 |
| Na ₂ O | 0.21 | Trace |
| LOI | 13.70 | 13.82 |

Table 3.3 Characteristics of Premier Kaolin Clay (data provided by manufacturer).

| | |
|--|-------|
| Specific Gravity | ~2.6 |
| Bro: optimum/20/#1/ @70% solid | 292 |
| Brightness (% Reflectance) | 87.96 |
| pH (as is solids) | 7.19 |
| Particle Size Distribution (% , < 2 μ m) | 90.3 |
| Hurcules: rpm @ 18 dynes | 2481 |
| % Moisture | 0.5 |
| Dispersant (Sodium Polyacrylate), % by wt. | ~0.35 |

Table 3.4 Characteristics of #12 White GCC (data provided by manufacturer)

a) Typical Properties

| | |
|--------------------------------------|------|
| Specific Gravity | 2.71 |
| Dry Brightness | 93 |
| Median Particle Diameter, (μ m) | 12 |
| Oil Absorption | 6.5 |
| Hardness (Moh's Scale) | 3.0 |

b) Chemical Composition

| | |
|-----------------------|----------|
| CaCO ₃ | 95% Min. |
| MgCO ₃ | <3.00 |
| Other Acid Insolubles | <3.00 |

Table 3.5 Comparison of Tested Materials

| Material | Specific Gravity ¹ | Size ¹ [μm] | pH ² | Conductivity ² , σ [$\mu\text{S/cm}$] | Liquid Limit ³ |
|-------------------|-------------------------------|--|-----------------|--|---------------------------|
| Kaolinite RP2 | 2.6 | $d_{50} = 0.36$ | 4.66 | 11.98 | 78 |
| Kaolinite SA1 | 2.6 | $d_{50} = 1.1$ | 6.50 | 16.38 | 43 |
| Kaolinite Premier | 2.6 | 95% < 2 | 6.39 | 323 | -- |
| GCC #12 White | 2.71 | $d_{50} = 12$ | 8.76 | 54.60 | 28 |
| PCC Rhombic | 2.71 | $d_{50} = 1$ | 9.87 | 101.90 | 52 |

¹Manufacturer data, ²measurements of supernatant made at volumetric solids content $\phi=0.02$ in deionized water after centrifuging suspensions, ³measured with fall cone device (BS 1377).

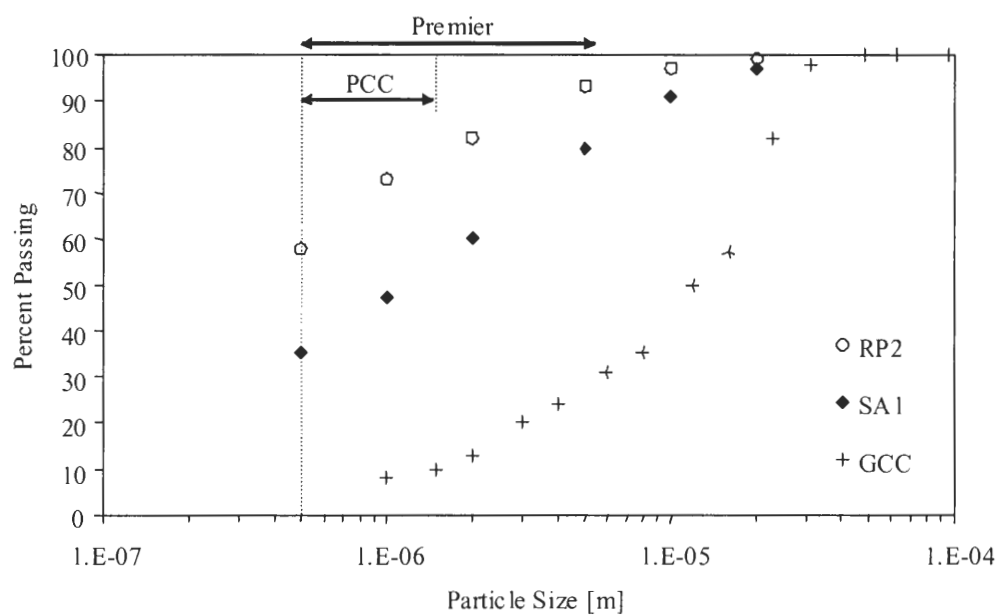
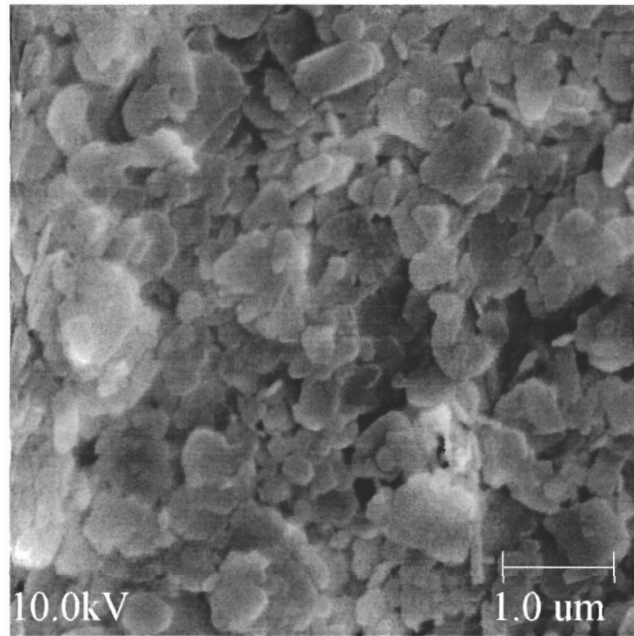
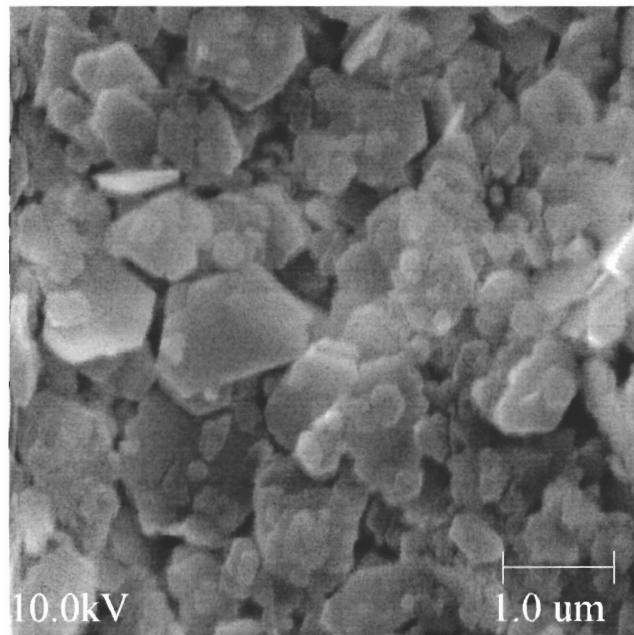


Figure 3.1 Grain size distribution curves of kaolinites RP2 and SA1, and GCC #12 White. Size ranges for Premier and PCC are inferred from SEM micrographs.

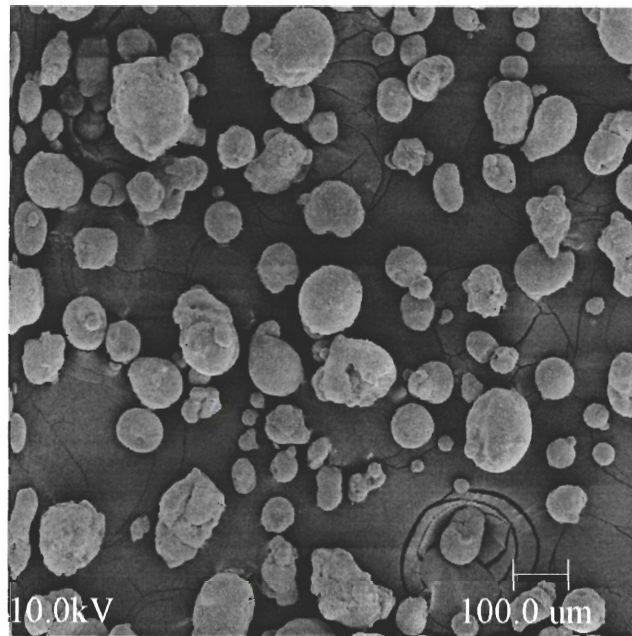


(a)

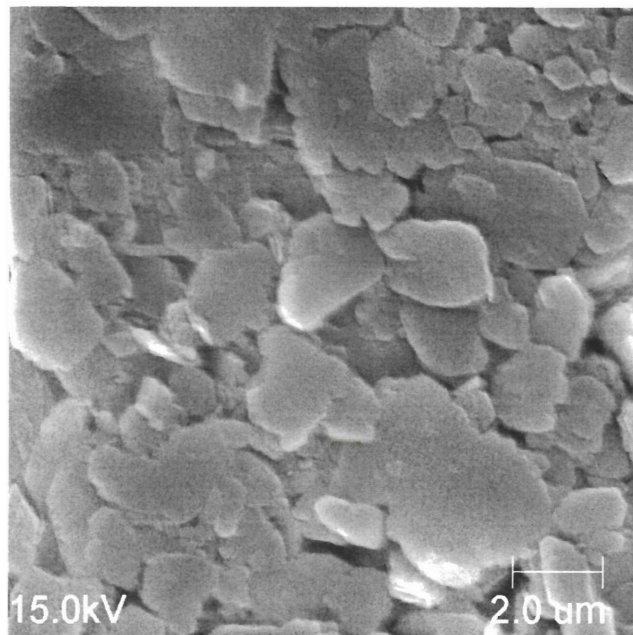


(b)

Figure 3.2 Scanning electron micrographs of kaolin clays (a) RP2 and (b) SA1.

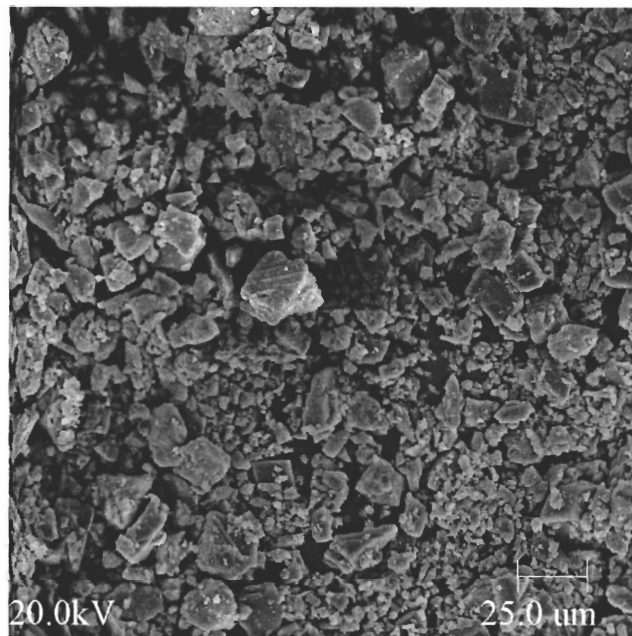


(a)

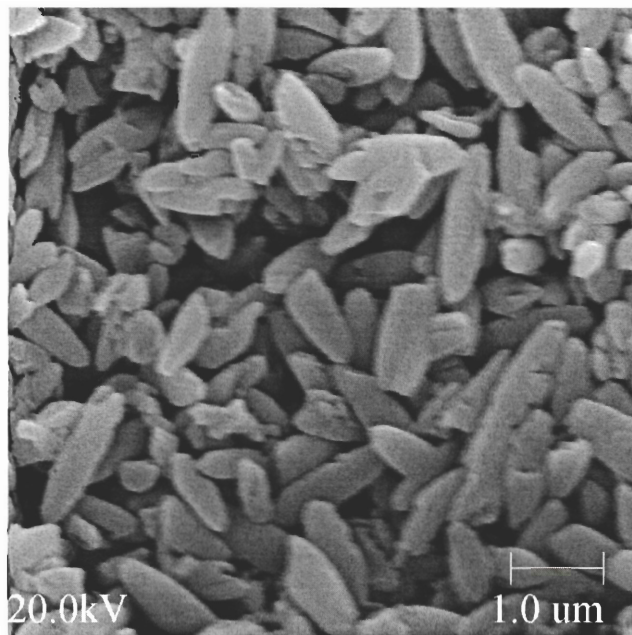


(b)

Figure 3.3 Scanning electron micrograph of Premier clay in (a) as-received dry form and (b) dispersed.



(a)



(b)

Figure 3.4 Scanning electron micrographs of calcium carbonates (a) GCC #12 White and (b) Rhombic PCC.

surfaces. The individual PCC particles shown in Figure 3.4-b are very uniform with an elongated crystalline shape. The size of the particles is on the order of 1 μm . The PCC is received in a dry, cake form, so the material is ground with a pestle and mortar prior to testing.

Other chemicals used in this study include two salts, NaCl and CaCl_2 (Fisher Scientific), and a commercially available sodium polyacrylate (NaPAA) designated Colloid 211 (Rhône-Poulenc, Vinings Industries, Marietta, GA). Figure 3.5 plots the measured conductivity of NaCl and CaCl_2 solutions at various concentrations. The NaPAA properties are listed in Table 3.6.

3.2 Procedures

3.2.1 Kaolin Conversion to Na-Form

The kaolin used for studies performed in Chapter 4 is rendered monoionic before testing using procedures similar to those outlined by van Olphen (1977). The clay is vigorously mixed with a 2 M NaCl solution at approximately 3 mL solution per gram kaolinite. The suspension is left for 48 hours, during which the clay particles are allowed to settle. The supernatant is siphoned and replaced with a 1 M NaCl solution, mixed and left for 24 hours. The process is repeated with another 1 M NaCl solution wash for a total equilibrium time of 96 hours. After the final salt wash, the excess salt is removed through several washings with deionized water (typically 10 or more). The supernatant conductivity is measured periodically with an Omega Conductivity Meter (model CDB 420). The clay is considered monoionic with no excess salts when the supernatant

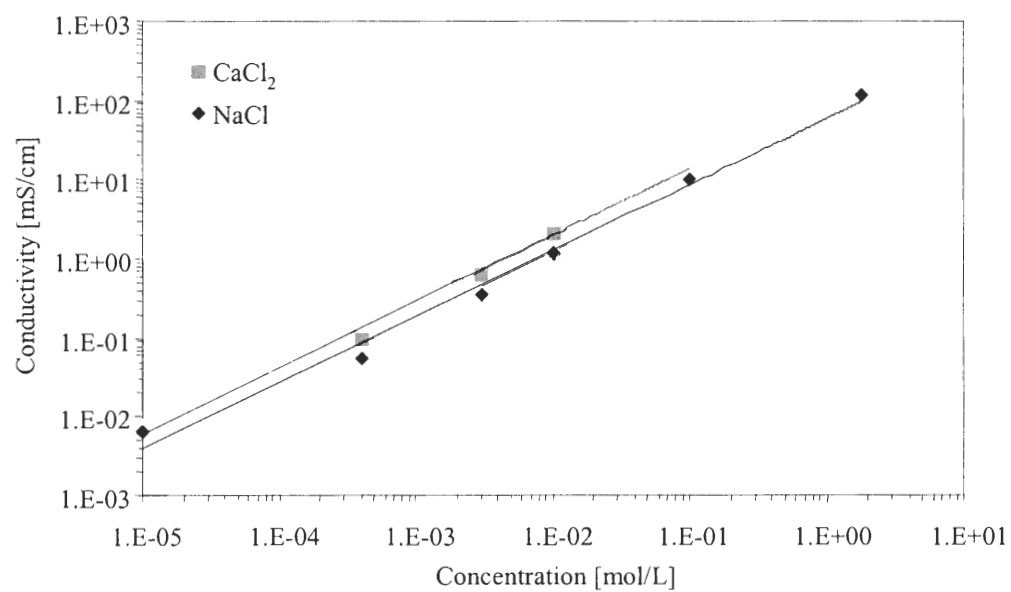


Figure 3.5 Measured conductivity of NaCl and CaCl₂ solutions at various concentrations.

Table 3.6 Characteristics of Colloid 211 Sodium Polyacrylate (data provided by manufacturer)

| | |
|--|---------------------------|
| Appearance | Clear, light amber liquid |
| % Nonvolatile Matter (NVM ¹) | 43 |
| pH | 7.2 |
| Viscosity ² at 25°C (cps) | 250 |
| Specific Gravity at 25°C | 1.30 |
| Molecular Weight (g/mole) | 3400 |
| Solubility | Water-soluble |

¹NVM = ½ gram sample at 130°C for ½ hour, ²Brookfield #2 Spindle at 30 RPM.

conductivity is $<100 \mu\text{S}/\text{cm}$. The clay is then oven-dried and ground using a pestle and mortar.

3.2.2 Sedimentation

All the sedimentation suspensions are prepared so that the final solids volume fraction $\phi=0.02$. The solids volume fraction ϕ is the total volume of solids divided by the total suspension volume. A 2.54 cm-diameter acrylic cylinder is filled with approximately 10 to 20 mL of a pore fluid solution or deaired deionized water, depending on the test conditions. The appropriate amount of clay, calcium carbonate or a combination of both is then gently mixed with the fluid in the cylinder. The total mass of solids added to the cylinder varies according to the mineral specific gravity in order to attain a pre-selected volume fraction ϕ . Additional pore fluid water is poured into the cylinder to reach a total height of 15.5 cm corresponding to 78.5 mL or 17 cm corresponding to 86.1 mL. The final volume varies with the test series, but the volume fraction is the same in each case. The suspensions are slowly mixed with a perforated plunger until a uniform appearance is observed. The suspensions hydrate overnight and are then remixed.

Entrapped air is removed with a low vacuum, $u \cong -5\text{kPa}$. Once the air evacuates (no evidence of bubble formation), and without releasing the vacuum, each cylinder is repeatedly inverted for approximately one minute.

After the last inversion, the cylinder is placed on a level surface. This point is defined as time zero. The vacuum is removed, and the cylinder is capped with a rubber stopper. Both the suspension and sediment heights are monitored with time. The heights are recorded for at least two weeks starting at $t = 15$ seconds. Each subsequent reading is

taken at twice the time interval of the previous reading, i.e., $t_1 = 15$ seconds, $t_2 = 30$ seconds, $t_3 = 1$ minute, etc. The supernatant pH of each suspension is measured using an Accumet AR50 pH meter (Fisher Scientific) after the last suspension and sediment heights are recorded.

3.2.3 Viscosity

For each test condition, the solids mass appropriate for forming a suspension with a solids volume fraction of $\phi=0.07$ is placed in a 600-mL beaker and mixed with the selected pore fluid solution. The total volume, either 400 mL or 500 mL, depends on the test series. The beaker is placed on a Corning magnetic stirrer and mixed for at least eight hours before measurement.

The suspension viscosities are measured using a Brookfield DV-E Viscometer fitted with spindles #1, 2 or 3. Spindle #1 has the largest diameter of the disk spindle set and is used for taking measurements within the lower range of the viscometer. The spindle rotational speed is varied between 1 RPM and 100 RPM, and the viscosity reading as well as torque % and degree of settlement are recorded after 1.5 minutes for every rotational speed setting. Between readings, the suspensions are mixed well for approximately 20 seconds to counteract any particle settlement that may have taken place. The final pore fluid pH is determined by centrifuging a small sample and measuring the supernatant.

3.2.4 Liquid Limit

The fall cone test procedure is based on the British Standard 1377. Penetration measurements are taken with a Wykeham Farrance cone penetrometer at four moisture

contents for each remolded mineral mixture. The first moisture content is obtained by mixing approximately 50 to 100 mL of deionized water or a chemically modified solution with 200 g to 350 g of solids. Typical solid-liquid volume fraction in liquid limit tests are $\phi=0.50$ to 0.85. In cases where the pore fluid chemistry is altered, the exact solution volumes are recorded. The soil mixture hydrates for at least eight hours before obtaining the first measurement point. After the equilibration time, the soil is thoroughly re-mixed and carefully placed in a metal cup, 2 1/2" x 1 3/4", avoiding air entrapment. The excess material is scraped off the top leaving a smooth even surface. Once an acceptable penetration depth is recorded, 10 to 30 g of material are removed to determine the moisture content. The pore fluid pH is measured by placing a small amount of the mineral paste on the reactive portion of a ColorpHast pH strip (Fisher Scientific) and allowing the pore fluid to leach onto the paper. The remaining soil is then mixed with an additional fluid volume to increase the moisture content for the next penetration measurement. The cone penetration depths are plotted against the percentage moisture contents. Reading from a best-fit line drawn through the measured points, the liquid limit is the moisture content corresponding to a penetration depth of 20 mm.

3.3 Physics and Interpretation Guidelines

3.3.1 Sedimentation

Gravimetric sedimentation is a widely used method for indirectly determining particle size (Hunter, 1993). The popularity of this method stems from its simplicity, its applicability to a wide range of particle sizes, the limited equipment that is necessary, i.e.

a graduated cylinder, and both accurate and reproducible results (Orr & Dallavalle, 1959).

Stoke's Law was first utilized for particle size measurement in 1904 (Irani & Callis, 1963). Stokes' law relates the terminal velocity of a falling particle to the particle size and fluid characteristics. For a smooth, rigid sphere falling at its terminal velocity in an infinite homogeneous fluid medium within the laminar flow regime ($Re < 0.2$), the Stokes settling velocity is (Allen, 1990):

$$v_{St} = \frac{(\rho_s - \rho_f)gd^2}{18\eta} \quad 3.1$$

where ρ_s and ρ_f are the densities of the solid and fluid respectively, g is the acceleration due to gravity, η is the fluid viscosity and d is the particle diameter. The modified Stokes' equation for non-spherical particles, such as clays, assumes a Stokes' diameter, d_{St}^2 defined as (Allen, 1990):

$$d_{St}^2 = \frac{d_v^3}{d_d} \quad 3.2$$

where d_v is the diameter of a sphere with the same volume as that of the particle and d_d is the diameter of a sphere experiencing the same drag force as the particle when moving at the same terminal velocity in an identical fluid. Therefore, the Stoke's diameter is the equivalent diameter of a sphere with the same density and terminal velocity as the

particle in the same fluid within the laminar flow regime. Hindered settling is minimized at volume fractions $\phi=0.002$ to 0.005 (Irani and Callis, 1963).

In the case of flocculated particles, the densities of the formed flocs vary with floc size. Due to their fractal nature, the floc density decreases with increasing floc diameter (Lagvankar & Gemmell, 1968; Klimpel et al., 1986; Hogg et al., 1987; Fogle et al., 1991; Gregory, 1997). Hence, the settlement rate will vary as the floc characteristics vary. Therefore, one method of assessing the state of dispersion of a clay suspension at the macroscale is sedimentation analysis.

The state of dispersion of a suspension with a low solids content may be inferred from the settlement behavior just after mixing as well as the final sediment volume. Table 3.7-a summarizes the various sedimentation modes observed by several authors. It is important to note that these authors make no distinction between EF flocculation or FF aggregation within the flocculation sedimentation behavior classification. Pierre et al. (1995) verified the structures for kaolinite sediments formed from suspensions exhibiting flocculation and dispersed settling behaviors using SEM. Pictures are shown in Figure 3.6. For this study, sedimentation behavior is categorized as EF flocculated, FF aggregated, dispersed, or mixed-mode as defined in Table 3.7-b. Also, particle associations are defined as flocculated for EF associations, aggregated for FF associations and dispersed for particles with minimal interaction. The major characteristics of EF flocculated, FF aggregated, and dispersed sedimentation modes are presented schematically in Figure 3.7.

Table 3.7 (a) Observed Suspension Settlement Modes as Defined by Previous Researchers

| Sedimentation Characteristics | Mode | | | | |
|----------------------------------|--|---|---|---|---|
| | Free ¹ /Dispersed Free ² /Stable ³ Settling; Accumulation ⁴ Sedimentation | Hindered ¹ /Zone ² / Flocculated ³ Settling; Flocculation ^{3,4} Sedimentation | Flocculated Free Settling ² | Consolidation Settling (High solids content) ² | Mixed Flocculation- Accumulation ⁴ Sedimentation |
| Particle Interaction | Minimal; Any aggregates formed remain dispersed | Strong; flocs readily form | Flocs of differing sizes form, but flocs remain dispersed | No distinct floc formation | Minimal → Floc formation |
| Suspension Appearance | Increasing density from top to bottom | Uniform density | Increasing density from top to bottom | Hair cracks form in suspension | Top to bottom increasing density → uniform |
| Supernatant Appearance | Cloud of suspended fine particles | Clear | Cloud of suspended flocs | Clear | Cloudy → Clear |
| Suspension-Supernatant Interface | None | Well-defined, moves downward as flocs settle | None | Well-defined, moves downward | None → Well-defined |
| Suspension-Sediment Interface | Well-defined, moves upward as sediment builds | None | Well-defined, moves upward as sediment builds | None | Well-defined → None |
| Settlement Rate | Very slow | Rapid, constant | Slow | Slow | Slow → Rapid |
| Sediment Formation | Particles settle into lowest possible position and according to size, largest first | Flocs settle in random pile | Flocs settle according to size | Settles as a whole due to self-weight | Particles settle according to size → Formed flocs settle uniformly |
| Sediment Volume | Compact; strongly resists redispersion | Voluminous; easily redispersed | Between compact and voluminous | -- | Thin layer of compact sediment below thicker layer of voluminous sediment |

¹Patton (1979), ²Imai (1980), ³Ravisangar (2001), ⁴Pierre and Ma (1999).

Table 3.7 (b) Observed Suspension Settlement Modes Defined for This Study

| Sedimentation Characteristics | Mode | | | |
|----------------------------------|---|--|---|---|
| | Dispersed Sedimentation | EF Flocculation Sedimentation | FF Aggregation Sedimentation | Mixed-Mode Sedimentation |
| Particle Interaction | Minimal; Any aggregates formed remain dispersed | Strong; flocs readily form | Strong; aggregates readily form | Minimal → Floc/Agg. formation |
| Suspension Appearance | Milky with increasing density from top to bottom | Uniform density | Uniform density | Top to bottom increasing density → uniform |
| Supernatant Appearance | Cloud of suspended fine particles | Clear | Clear | Cloudy → Clear |
| Suspension-Supernatant Interface | None | Well-defined, moves downward as flocs settle | Well-defined, moves downward as aggregates settle | None → Well-defined |
| Suspension-Sediment Interface | Well-defined, moves upward as sediment builds | None | None | Well-defined → None |
| Settlement Rate | Very slow | Rapid, constant | Very rapid, constant | Slow → Rapid |
| Sediment Formation | Particles settle into lowest possible position and according to size, largest first | Flocs settle in random pile | Aggregates settle according to size | Particles settle according to size → Formed flocs/aggregates settle uniformly |
| Sediment Volume | Compact; strongly resists redispersion | Voluminous; easily redispersed | Compact to voluminous | Layer of compact sediment below layer of voluminous sediment |

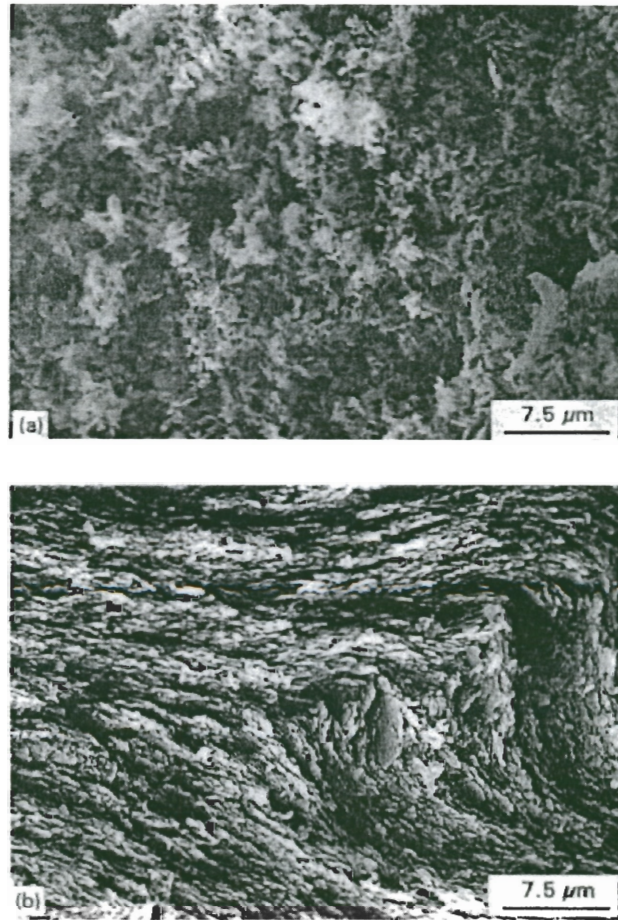
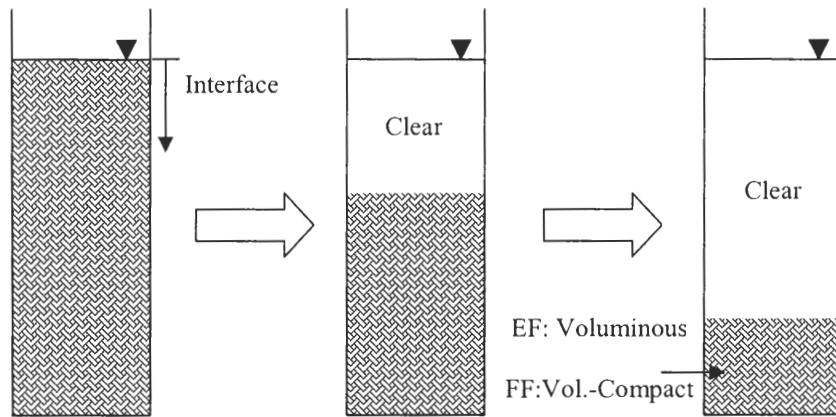
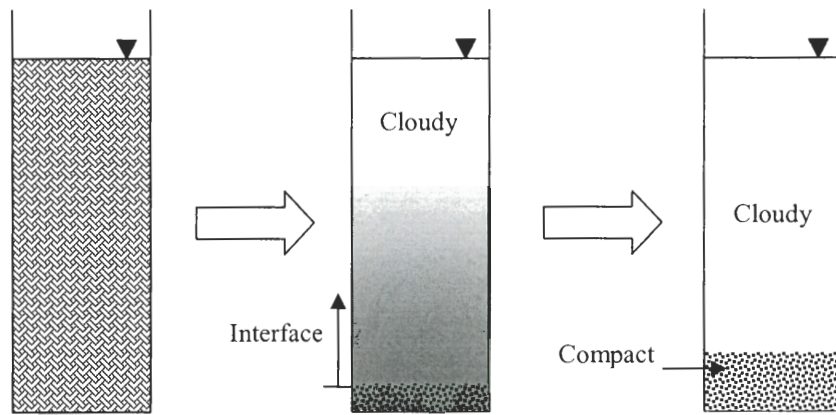


Figure 3.6 SEM micrographs of kaolinite structure resulting from (a) flocculation sedimentation and (b) dispersed (accumulation) sedimentation (Pierre et al., 1995).



(a) EF flocculation/FF aggregation sedimentation



(b) Dispersed sedimentation

Figure 3.7 Sedimentation behavior classification (after Patton, 1979).

3.3.2 Rheology

Viscosity is the resistance of a fluid to shear. In general, the viscosity of a suspension is greater than that of the pure fluid. Particles cause perturbations in stream lines under laminar conditions such that the rate of energy dissipation is increased. Therefore, the presence of particles increases the viscosity compared to the pure fluid (Hiemenz, 1986).

The rheological behavior of a suspension depends on the fluid viscosity, solids concentration, shape and size of the particles, and the state of dispersion or particle interactions (van Olphen, 1977). Einstein's equation relates the solids volume fraction, ϕ , to the suspension viscosity, η , may be written as (Hiemenz, 1986):

$$\frac{\eta}{\eta_o} = 1 + K\phi \quad 3.3$$

where η_o is the fluid viscosity and K is a constant that depends on the particle characteristics and particle interactions. This expression presumes the suspension has a constant viscosity, the flow velocity is laminar, the suspension has a very low solids concentration, the particles are large relative to the liquid molecules so that the fluid may be considered a continuum, and the particles are small relative to the viscometer so that wall effects can be ignored.

At sufficiently low solids concentrations, ϕ may be replaced with ϕ_f , the volume fraction of flocs, so that the K value may be related to the degree of flocculation (Rand &

Melton, 1977; Hunter, 2001). For uncharged rigid spherical particles, $K = 2.5$. For well-dispersed kaolinite suspensions at high pH, and at low ϕ values, K is approximately 10 (Nicol & Hunter, 1970; Michaels & Bolger, 1964; Rand & Melton, 1977).

However, clay suspensions may exhibit non-Newtonian behavior (Figure 3.8-a). Decreasing viscosity with increasing shear rate characterizes shear thinning or pseudoplastic fluid. If this effect depends on the shear history of the fluid, the behavior is termed thixotropic and is a typical characteristic of flocculated clay suspensions (Hiemenz, 1986; van Olphen, 1977).

Shear thinning behavior is associated with deflocculation in that the number of interparticle bonds in a flocculated suspension decreases with increasing shear rate (Hunter 2001). In other words, increasing the applied stress breaks down the suspension structure into smaller flow units whose size and particle associations depend on the interparticle forces (Rand & Melton, 1977), as depicted in Figure 3.8-b. Deflocculation results in a decrease in viscosity by reducing the flow unit anisotropy and by releasing fluid trapped within the floc, reducing the effective solids volume fraction (Sacks, 2001).

Well-dispersed kaolinite suspensions at low solids content have been shown to yield a much lower, constant viscosity than that of a flocculated system with an equal solids content (Rand & Melton, 1977; Nicol & Hunter, 1970; Michaels & Bolger, 1964). Low viscosity, even at increasing applied shear rates, is due to particle or flow unit alignment so that the platy particles have a minimal contribution to flow resistance (Figure 3.8-b).

3.3.3 Liquid Limit

The fall cone test (BS 1377 1990) permits determining the liquid limit of high specific surface soils. The liquid limit is the water content boundary dividing the plastic

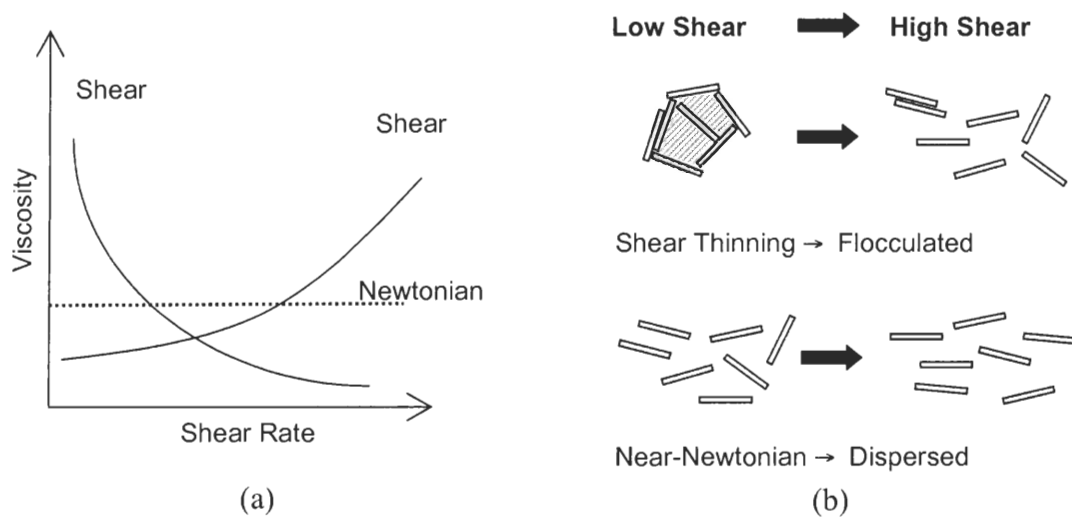


Figure 3.8 Rheological behavior. (a) Viscosity profiles for shear thinning, shear thickening and Newtonian fluids (b) clay flow unit response to applied shear.

and liquid behavioral states of a soil. The British Standard defines the liquid limit as the water content at which an 80-g stainless steel cone with a 30° angle penetrates a remolded soil specimen 20 mm when the cone is released at the soil surface.

Soils at the liquid limit have a shear strength between 1.3 and 2.4 kPa (Wroth and Wood, 1978). The shear strength of a clay at its liquid limit depends on the soil fabric. The particles or aggregates interact to supply the resistance to shear (Mitchell, 1993). Since the pore fluid chemistry determines the soil fabric, changing the pore fluid pH and/or ionic strength will alter the soil resistance to shear and in turn the liquid limit. The sensitivity to pore fluid content is denoted by the slope of the measured cone penetration vs. water content at the liquid limit. The greater the slope, the more rapidly the soil shear strength reduces for a given increase in water content.

3.4 Summary

This study focuses on the behavior of two mineral groups: kaolinite and calcium carbonate. These two groups are represented by three different types of kaolin and two types of carbonate, which encompass five different particle shapes. Minerals are carefully prepared to render homo-ionic particles with no excess salts. Fluids are aqueous electrolytes with controlled pH and ionic concentration, and often include a polymer.

The soil-fluid mixtures are prepared at different volume fractions and tested to different strain levels using sedimentation tests (~ zero strain), liquid limit (~100% strain), and viscosity (infinite strain).

CHAPTER 4

FABRIC IN SINGLE MINERALS: EFFECTS OF pH AND IONIC CONCENTRATION

4.1 Introduction

Clay fabric formation depends primarily on particle size and shape, clay mineralogy, and pore fluid chemistry. These parameters determine the nature of the dominant forces acting on the particles as reviewed in Chapter 2. The purpose of this chapter is to experimentally explore clay particle interactions across the pH-ionic concentration space, and over a range of solids concentrations and physical disturbances. Table 4.1 summarizes some of these effects on kaolinite as reported by previous researchers. Particle interactions are determined by assessing the state of dispersion of clay specimens mixed with pH-modified electrolytes. Three different test series are performed to study the effects of pH and ionic concentration on clay fabric: sedimentation tests, rheological tests, and liquid limit measurements. These tests involve a wide range of solids concentration as well as degree of system disturbance.

4.2 Materials and Procedures

4.2.1 Materials

The clay used in these studies is kaolinite Wilklay RP2 (Chapter 3). It is rendered monoionic using the procedure outlined in Section 3.2.1.

Table 4.1 Selected Studies: Influence of Ionic Concentration on Kaolinite Sedimentation Velocity and Volume

| Purpose | Specimen | Effect on Settlement Velocity | Effect on Sedimentation Volume | Reference |
|--|---|---|--|----------------------------|
| Effect of ionic concentration, valence, dielectric constant, and clay mineralogy on sediment volume | Solids content= 10 g soil/100 mL NaCl concentration= 10^{-3} to 2N | | \uparrow conc. \rightarrow \uparrow sed. vol. | Sridharan & Prakash (1999) |
| Effect of ionic concentration and pH on kaolinite sediment volume | Solids content= 9.1 & 4.75 wt%. NaCl concentration= 0.06 to 1.0 mol/L, pH=3 to 10 | | At pH < edge IEP, \uparrow conc. \rightarrow \downarrow sed. vol. At pH > edge IEP, \uparrow conc. \rightarrow \uparrow sed. vol. | Melton & Rand (1977) |
| Effect of ionic concentration and clay type on clay sensitivity | Solids content= 10 g/100 mL NaCl concentration= 0.031 to 0.5 mol/L | \uparrow conc. \rightarrow \uparrow set. vel. | \uparrow conc. \rightarrow \downarrow sed. vol. | Fam & Dusseault (1998) |
| Effect of ionic concentration, valence, and pore fluid dielectric permittivity on sedimentation volume | Solids content= 50 g/L NaCl concentration= 10^{-4} to 1.0 mol/L | \uparrow conc. \rightarrow \downarrow set. vel. | \uparrow conc. \rightarrow \downarrow sed. vol. | Chen & Anandarajah (1998) |
| Effect of ionic concentration and valence on sedimentation volume | Solids content= 50 g/L NaCl concentration= 0.002 to 1.0 mol/L | | \uparrow conc. \rightarrow \downarrow sed. vol. | Anandarajah (1997) |
| Effect of pore fluid chemistry on sediment stability | Solids content= 333 g/L NaCl concentration= 4×10^{-3} to 0.1 mol/L pH=4 to 9 | At pH<5: \uparrow conc. \rightarrow \uparrow set. vel. | Low pH: \uparrow conc. \rightarrow \downarrow sed. vol. High pH: \uparrow conc. \rightarrow \uparrow sed. vol. | Ravisangar (2001) |

Table 4.1 (cont'd)

| Purpose | Specimen | Effect on Settlement Velocity | Effect on Sedimentation Volume | Reference |
|--|--|--|--|----------------------|
| Effect of ionic concentration on the structure of kaolinite aggregates | Solids content= 0.5% by mass (total vol.= 100 mL) FeCl ₃ concentration= 0, 0.17, 0.67, 1.67, 3.33 mmol/L | | Conc. \leq 0.67 mmol/L: ↓conc. → ↓sed. vol. Conc. \geq 0.67 mmol/L ↑conc. → ↑ sed. vol. Max sed. vol. at 0.67 mmol/L | Pierre et al. (1995) |
| Effect of ionic concentration and pH on kaolinite and bentonite aggregates | Solids content= 0.5% by mass (total vol.= 100 mL) AlCl ₃ concentration= 0, 1.0, 2.0, 5.0, 10, 50 mmol/L pH= 2, 4, 6, 8, 9.5, 12 | Conc. \leq 5 mmol/L: ↓conc. → ↓set. vel., except at pH 2 Conc. \geq 5 mmol/L ↑conc. → ↓ set. vel., except at pH 9.5 | Conc. \leq 2 mmol/L: ↓conc. → ↓sed. vol. Conc. \geq 2 mmol/L ↑conc. → ↓ sed. vol., except at pH 12 Max sed. vol. at 2 mmol/L | Pierre & Ma (1999) |

4.2.2 Electrolyte pH-Ionic Concentration Matrix

The pore fluid electrolytes consist of NaCl solutions at concentrations of 10^{-5} , 4×10^{-4} , 3×10^{-3} , 0.1, and 1.8 mol/L (for NaCl electrolytes, the stoichiometric ionic strength is equal to the concentration) and target pH 3, 5, 7, and 9 at each concentration for a total of 20 solutions. The pH is altered with HNO_3 to lower the pH and NaOH to raise the pH.

4.2.3 Sedimentation

Adjustments to pH are made after suspension and sediment heights are recorded for two weeks by adding small volumes of extreme pH solutions prepared at the appropriate salt concentration. The suspensions are remixed and measurements recorded according to the selected time schedule for 91 days.

4.2.4 Viscosity

After the equilibration time, suspensions having a pore fluid pH far from the target pH are modified.

4.2.5 Liquid Limit

No pH modification is attempted.

4.3 Experimental Study 1: Sedimentation

4.3.1 Results

Sedimentation Behavior. Sedimentation trends are plotted in Figure 4.1. A summary of the observed sedimentation behavior for the tested kaolinite suspensions is presented in Table 4.2. Observed suspension modes are categorized according to the definitions presented in Table 3.7-b. Salient observations include:

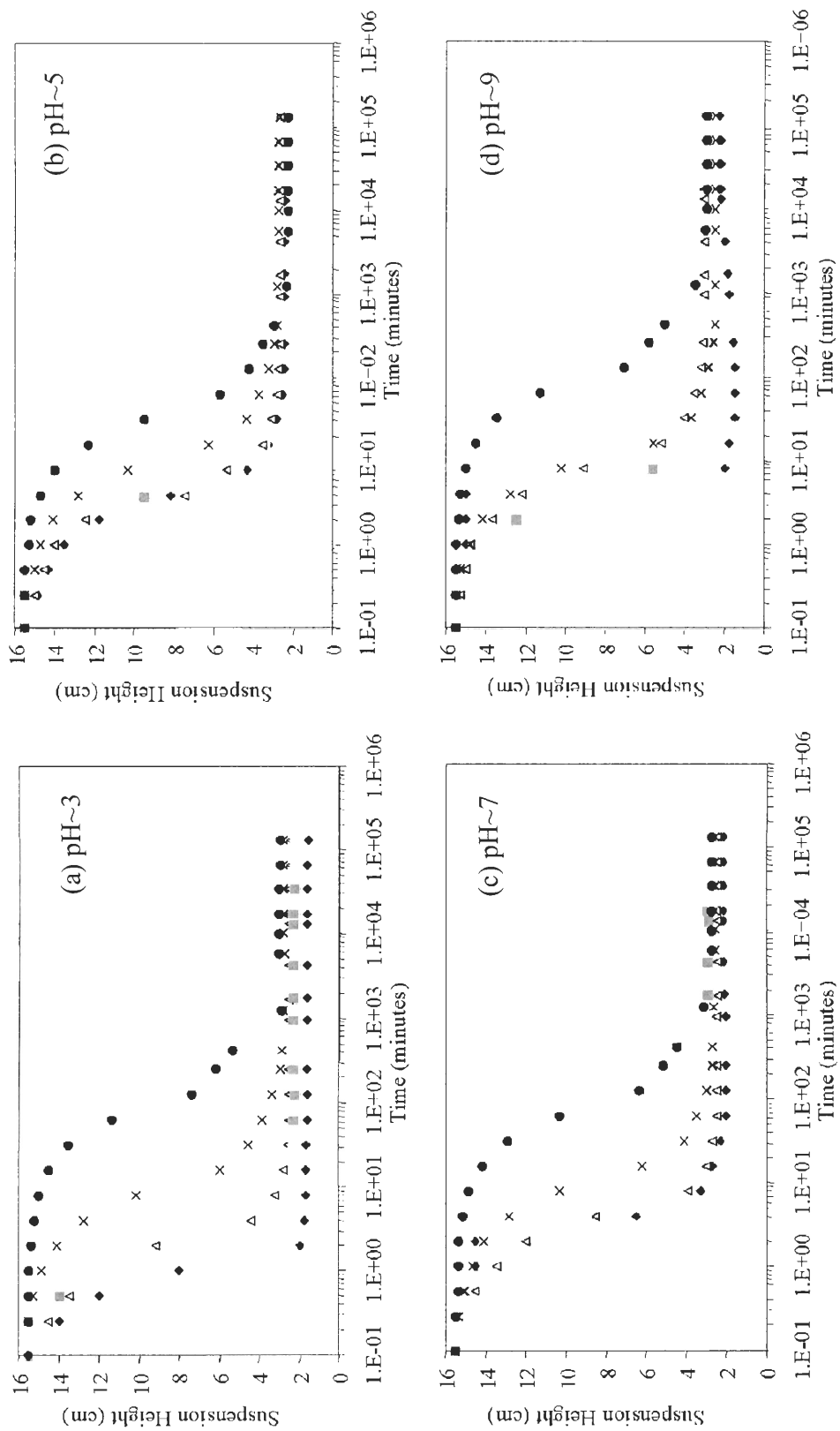


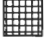





Figure 4.1 Kaolinite sedimentation curves. Cases are for target pore fluid pH: (a) 3, (b) 5, (c) 7 and (d) 9. Pore fluid NaCl concentrations in mol/L: \diamond 10^{-5} \blacksquare 4×10^{-4} \triangle 3×10^{-3} \bullet 1.8 .

Table 4.2 Observed Sedimentation Behavior of Kaolinite Suspensions

| | | Salt Concentration (mol/L) | | | | |
|-----------|---|----------------------------|--------------------|--------------------|----------------|-------------------------------|
| | | 10^{-5} | 4×10^{-4} | 3×10^{-3} | 0.1 | 1.8 |
| Target pH | 9 | Dispersed | Dispersed | Mixed-Mode | Mixed-Mode | Mixed-Mode |
| | 7 | Dispersed | Dispersed | Mixed-Mode | Mixed-Mode | Mixed-Mode |
| | 5 | EF Flocculation | EF Flocculation | EF Flocculation | Mixed-Mode | Mixed-Mode |
| | 3 | FF Aggregation | FF Aggregation | FF Aggregation | FF Aggregation | Flocculation of FF Aggregates |

-  Initially very thick colloidal cloud, duration of one month
-  Initially thick colloidal cloud, duration of several weeks
-  Initially moderate colloidal cloud, duration of several weeks
-  Initially thin colloidal cloud, duration of several hours
-  Initially very thin colloidal cloud, duration of several hours
-  No significant colloidal cloud development

- All suspensions at pH 3 exhibit characteristics consistent with FF aggregation sedimentation independent of ionic concentration
- At pH 5 and high ionic concentration ($c > 0.1$ mol/L), the suspension settling mode is mixed with a thin colloidal cloud lasting for several hours
- At pH 7 and 9 and intermediate salt concentrations ($c = 3 \times 10^{-3}$ to 0.1 mol/L), suspension settling is characterized as mixed-mode, i.e. initially dispersed then EF flocculated settling, while at high salt concentration ($c = 1.8$ mol/L) the behavior is mixed with complete settling of colloidal particles taking several hours
- The settlement time and number of suspended particles in the colloidal clouds varies from several hours to one month, depending on both electrolyte pH and ionic concentration

Settlement Velocity Parameter α The settling velocity parameter, α , is herein defined as the slope of the initial portion of the settlement-time curve known as the induction period. It is calculated from each suspension settlement curve. During the induction period, the initial suspension consists of interconnected flow units with highly tortuous fluid flow paths between them. Hence, initial fluid displacement is hindered. As time progresses, the flow units tend to line up, shortening the flow paths (Michaels & Bolger, 1962). This marks the beginning of hindered settlement. Therefore, α indicates how long the suspension flow units interact with each other and how ordered the suspension structure becomes.

The initial settlement velocity, α (cm/min), for each suspension is plotted in Figure 4.2. There is a general decrease in α with increasing ionic concentration for $c > \sim 10^{-2}$ to $\sim 10^{-1}$

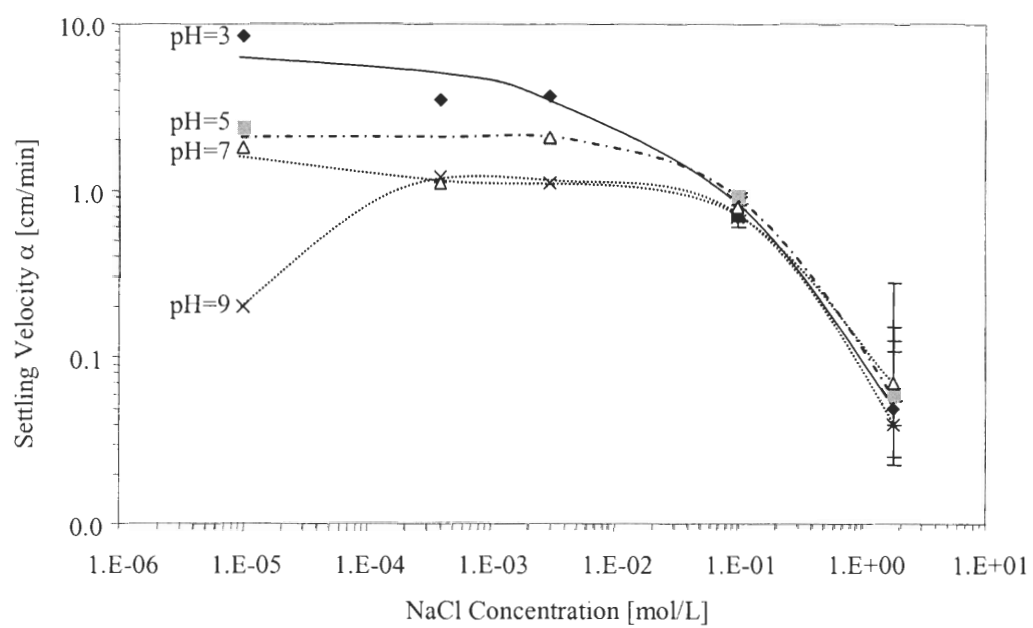


Figure 4.2 Kaolinite suspension initial settling velocity α . Target electrolyte pH: 3, 5, 7 and 9

mol/L. The initial settlement velocity for the specimen with $c=10^{-5}$ mol/L and pH=9 is very low and in agreement with the sediment mode.

Sedimentation Height The final sedimentation height for each suspension is plotted in Figure 4.3. Overall, the sedimentation height tends to increase with increasing ionic concentration, contrary to DLVO predictions. This highlights the role of fabric. Notice the relative height inversion from 10^{-5} mol/L to 1.8 mol/L: the sedimentation height at the lowest ionic concentration increases according to pH 3, 7, and 5, but, at 1.8 mol/L the sedimentation height increases according to pH 5, 7, and 3. The sedimentation height values converge at 0.1 mol/L to a single point of approximately 2.6 cm.

4.4 Experimental Study 2: Rheological Tests

4.4.1 Results

The general rheological response to increasing shear rate for the suspensions tested in this study is shown in Figure 4.4. The observed decrease in measured viscosity with increasing shear rate is typical of a shear-thinning fluid. Also, from Equation 3.3 the K values for the high pH slurries ranged between 200 and 2200. This pronounced deviation from the approximate K value for well-dispersed kaolinite suspensions is consistent with the non-Newtonian behavior exhibited by the tested suspensions. Therefore, Equation 3.3 does not apply.

The viscosity readings at 100 RPM and 1.5 minutes are shown in Figure 4.5. Below the ionic concentration 0.1 mol/L, the viscosities increase with the pH order 9, 3, 5, and 7, indicating the direction of increasing flocculation. At concentration $c \sim 0.1$ mol/L, the viscosities tend toward a single value (~ 49 mPa·s) regardless of pH. Above concentration 0.1 mol/L, the order of increasing viscosity is reversed: pH 7, 5, 3, and 9.

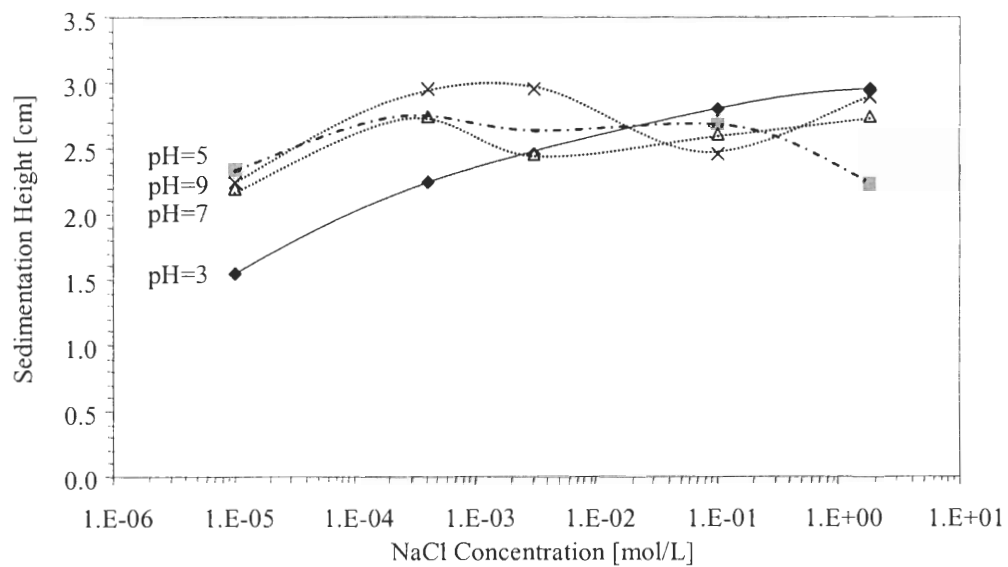


Figure 4.3 Kaolinite sedimentation height at 91 days. target electrolyte pH: 3, 5, 7 and 9

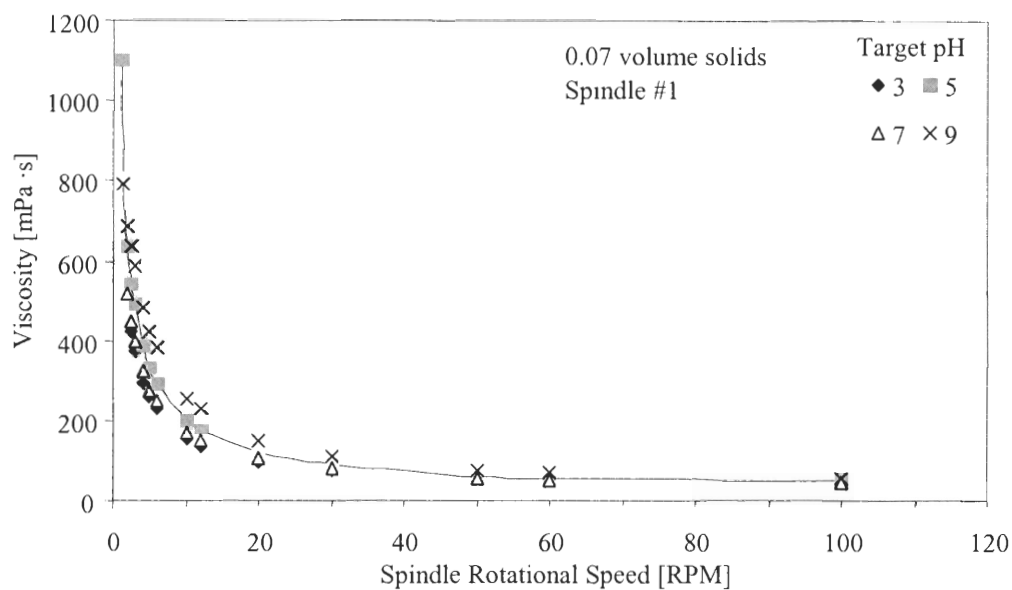


Figure 4.4 Typical kaolinite suspension rheological behavior (data shown for 0.1 mol/L NaCl concentration).

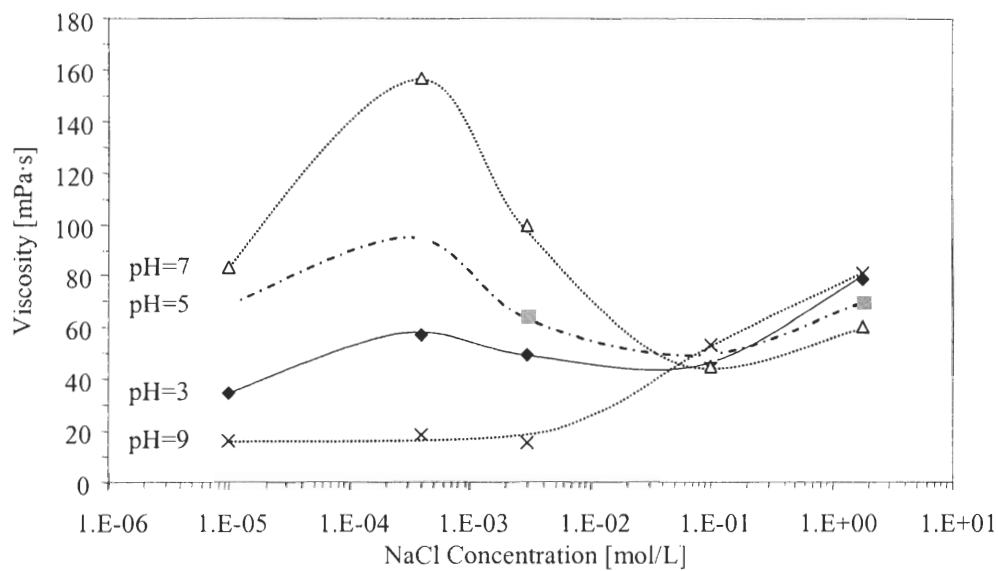


Figure 4.5 Kaolinite suspension viscosities at 100 RPM Using Spindle #1.

4.5 Experimental Study 3: Liquid Limit

4.5.1 Results

Figures 4.6, 4.7 and 4.8 summarize the fall cone penetration lines, measured liquid limits, and calculated liquid limit line slopes, respectively, for all mixtures. Liquid limit data determined using the Cassagrande method is included for comparison in Figure 4.7.

Overall, the liquid limit decreases with increasing salt concentration. Liquid limit for all pH values converge for $c \sim 0.1$ mol/L to a single point $LL \sim 57.5\%$. The solution pH has the most impact on liquid limit at extreme ionic concentrations.

The sensitivity to water content increases with increasing NaCl concentration. Slope values also collapse to a single point at 0.1 mol/L NaCl regardless of solution pH. The solution pH has little impact on water sensitivity except at high NaCl concentrations, especially at 1.8 mol/L.

4.6 Discussion

This chapter maps the interactions of clay particles within a wide range of pore fluid pH and ionic concentration, as well as over a range of solids concentrations and physical disturbances. A summary of all major test results is presented in Table 4.3.

4.6.1 Low/Intermediate Solids Concentration

The DLVO theory predicts particle repulsion and a dispersed system at very low ionic concentrations and low valence, in this case 10^{-5} NaCl. However, the sedimentation and rheological behaviors are all pH-dependent at this concentration. At pH 3, the low final

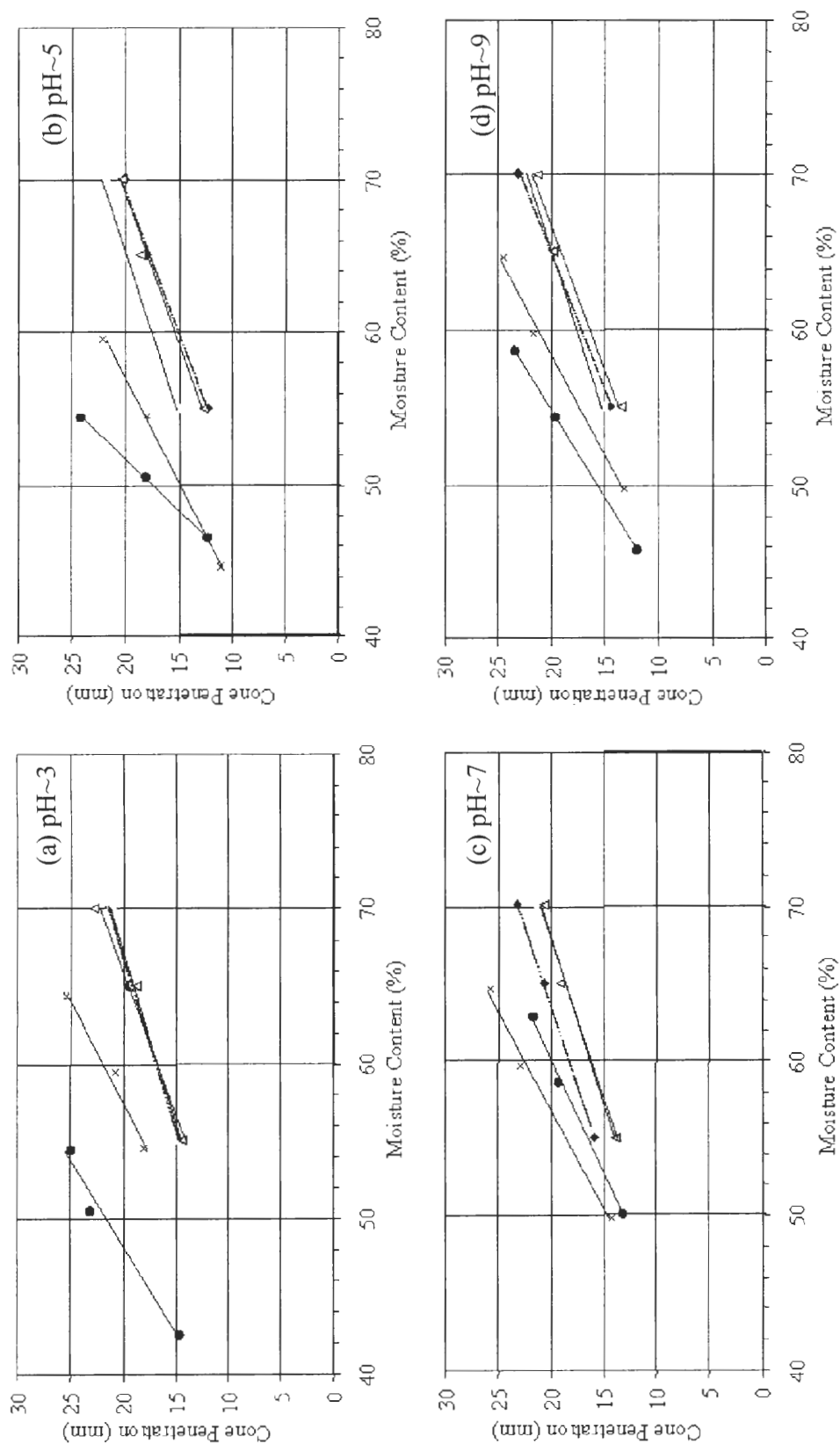


Figure 4.6 Kaolinite fall cone penetration lines. Cases are for target pore fluid pH: (a) 3, (b) 5, (c) 7 and (d) 9. Pore fluid NaCl concentrations in mol/L: $\diamond 10^{-5}$ $\blacksquare 4 \times 10^{-4}$ $\triangle 0.1$ $\bullet 1.8$.

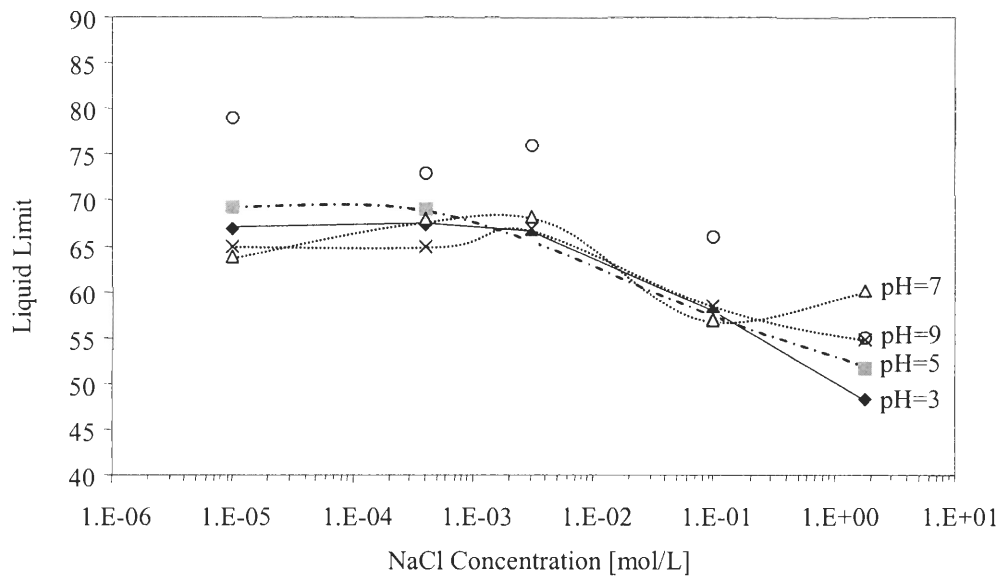


Figure 4.7 Kaolinite fall cone liquid limits. Target electrolyte pH: 3, 5, 7 and 9. The Cassagrande tests (○) are performed on RP2 kaolinite without first rendering the clay monoionic, nor altering or measuring the solution pH (Klein, 1999).

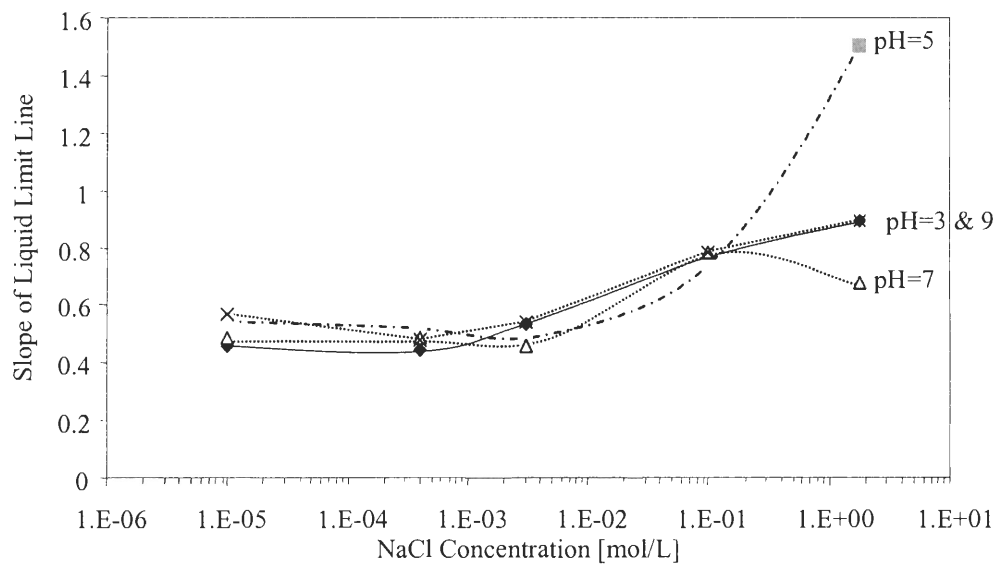


Figure 4.8 Slopes of the kaolinite fall cone liquid limit lines. Target electrolyte pH: 3, 5, 7 and 9.

Table 4.3 Results Summary for Sedimentation, Viscosity, and Fall Cone Tests

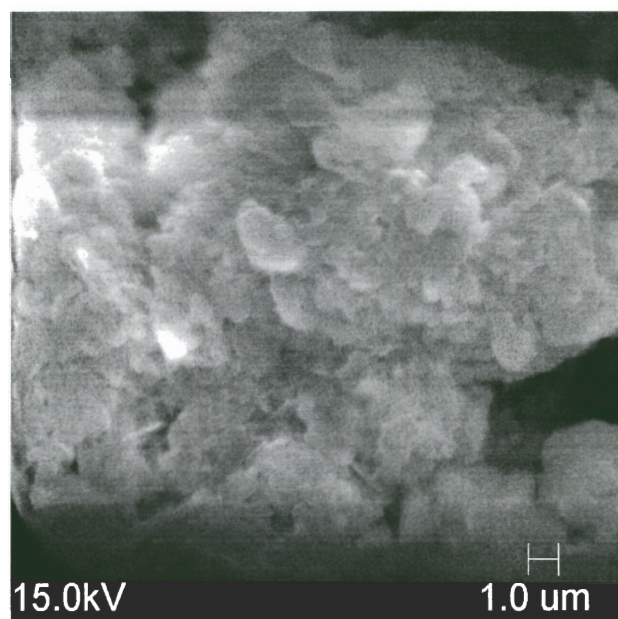
| NaCl Concentration [mol/L] | Target pH | Sedimentation (0.02 solids content) | | | Viscosity (0.07 solids content) | | Fall Cone (0.55 - 0.85 solids content) | | | |
|----------------------------|-----------|-------------------------------------|---------------|-------------------|---------------------------------|-------------|--|-------------|------------------|--------------|
| | | Measured pH | Observed Mode | α [cm/min] | Final Height [cm] | Measured pH | Viscosity [mPa·sec] | Measured pH | LL Slope [mm/w%] | Liquid Limit |
| 10 ⁻⁵ | 3 | 3.03 | Flocculation | 8.5 | 1.55 | 2.91 | 34.5 | 5.3 | 0.457 | 66.9 |
| | 5 | 4.50 | Mixed | 2.4 | 2.35 | 5.07 | 68.6 | 4.7 | 0.544 | 69.3 |
| | 7 | 6.53 | Dispersed | 1.8 | 2.20 | 6.81 | 83.2 | 4.8 | 0.486 | 63.7 |
| | 9 | 8.45 | Dispersed | 0.2 | 2.25 | 8.50 | 16.5 | 5.8 | 0.570 | 65.0 |
| 4×10 ⁻⁴ | 3 | 3.50 | Flocculation | 3.5 | 2.25 | 3.43 | 56.8 | 5.2 | 0.443 | 67.3 |
| | 5 | 4.27 | Mixed | 1.7 | 2.75 | 5.35 | 95.8 | 4.7 | 0.519 | 68.9 |
| | 7 | 6.70 | Dispersed | 1.1 | 2.75 | 6.71 | 156.8 | 5.7 | 0.488 | 68.0 |
| | 9 | 8.55 | Dispersed | 1.2 | 2.95 | 8.11 | 18.2 | 5.7 | 0.477 | 65.0 |
| 3×10 ⁻³ | 3 | 3.33 | Flocculation | 3.7 | 2.45 | 3.44 | 49.1 | 6.0 | 0.536 | 66.0 |
| | 5 | 5.23 | Mixed | 2.0 | 2.65 | 5.03 | 64.4 | 4.3 | 0.476 | 65.3 |
| | 7 | 6.87 | Mixed | 2.1 | 2.45 | 6.51 | 99.5 | 6.0 | 0.455 | 68.1 |
| | 9 | 8.86 | Mixed | 1.1 | 2.95 | 8.99 | 15.8 | 6.0 | 0.543 | 66.7 |
| 0.1 | 3 | 3.39 | Flocculation | 0.7 | 2.80 | 3.10 | 46.5 | 5.7 | 0.755 | 57.7 |
| | 5 | 4.34 | Mixed | 0.9 | 2.70 | 4.62 | 49.6 | 4.3 | 0.742 | 57.0 |
| | 7 | 7.14 | Mixed | 0.8 | 2.60 | 6.37 | 44.8 | 6.0 | 0.785 | 56.8 |
| | 9 | 8.53 | Mixed | 0.7 | 2.45 | 8.67 | 53.5 | 5.8 | 0.780 | 58.4 |
| 1.8 | 3 | 3.35 | Flocculation | 0.05 | 2.95 | 3.26 | 78.8 | 3.8 | 0.895 | 48.2 |
| | 5 | 4.70 | Dispersed | 0.06 | 2.25 | 4.44 | 69.9 | 4.0 | 1.51 | 51.7 |
| | 7 | 7.23 | Dispersed | 0.07 | 2.75 | 6.72 | 60.6 | 3.8 | 0.677 | 60.2 |
| | 9 | 8.56 | Dispersed | 0.04 | 2.90 | 8.82 | 81.4 | 3.8 | 0.894 | 54.8 |

sedimentation height, low viscosity and high initial settling velocity α indicate that the low and moderate solids suspensions are dispersed. But, the settling behavior is observed to have a high degree of particle interaction. In addition, kaolinite particle dissolution is significant at low pH. For this case, it appears that dissolution promotes face to face aggregation forming dense, yet dispersed, aggregates. FF aggregation is verified with SEM in Figure 4.9-a. Dispersed FF aggregates have a high settling velocity due to the increased aggregation, form a more compact sediment, and cause less perturbations in stream lines compared to open EF flocs.

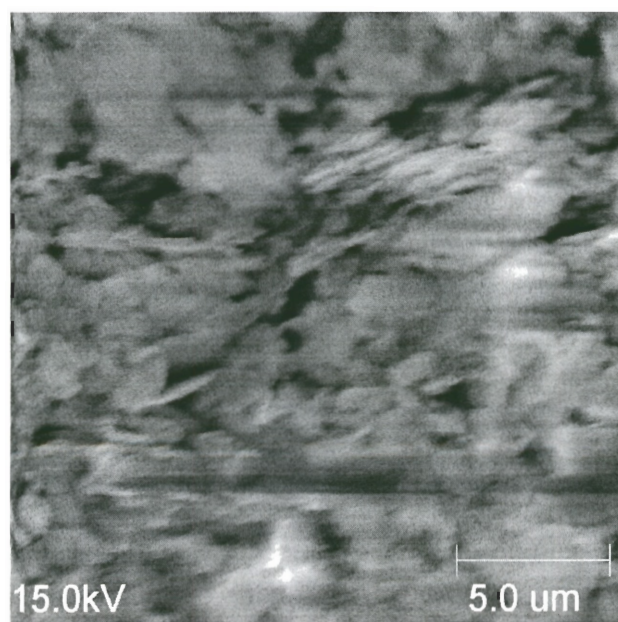
At low ionic concentration and high pH, the observed settlement behavior, settling velocity α and the measured viscosity indicate a dispersed system, which is consistent with previous findings (Rand & Melton, 1977; Nicol & Hunter, 1970; Michaels & Bolger, 1964) and visual observation using SEM (Figure 4.9-b). However, the sedimentation height is greater than expected for a dispersed system. One plausible explanation for this discrepancy is that the particles left in suspension forming the colloidal cloud interact and form EF flocs over time relative to the change in supernatant pH. The flocs eventually settle and form an open-structured layer on top of the initial denser sediment.

At low ionic concentration and moderate pH, the observed and measured parameters indicate a more flocculated structure than that at the extreme pH. Since the measured pore fluid pH is between the edge and particle isoelectric point, the most likely association for these suspensions is edge-to-face.

Increasing the ionic concentration to $c=4 \times 10^{-4}$ and $c=3 \times 10^{-3}$ results in an increase in particle flocculation as indicated by the sedimentation and rheological parameters.



(a)



(b)

Figure 4.9 SEM micrographs of RP2 kaolinite exposed to sedimentation test conditions at $c=10^{-5}$ M NaCl and (a) pH=3 and (b) pH=9.

However, the viscosities measured at high pH for these ionic concentrations indicate dispersed systems. Again, the enlarged sedimentation heights are probably the result of a flocculated colloidal particle layer settling on a more compact structure.

At 0.1 mol/L NaCl, the suspension structure becomes pH independent as observed in both the sedimentation and viscosity measurements. This is consistent with previous findings and attributed to an increase in face-to-face aggregation from edge-to-face due to double layer thinning and subsequent dominance of van der Waals attractive forces (Schofield & Samson, 1954; Rand & Melton, 1977). At this NaCl concentration, the effects of dissolution only contribute to the aggregation process. The extreme pH suspensions show an increase in aggregation, while the moderate pH suspensions tend toward a slight decrease in flocculation behavior compared to the $c=3 \times 10^{-3}$ NaCl suspensions. The thinner double layers allow for edge-to-edge and edge-to-face flocs to form from the face-to-face aggregates.

At $c=1.8$ mol/L NaCl, the relative behaviors of the tested suspensions indicate only a slight dependence on pH. For pH 3, all sedimentation and rheological parameters indicate an increase in flocculation from the $c=0.1$ mol/L NaCl case. The observed settling behaviors for the remaining pH suspensions indicate more dispersed systems. However, initial settling velocities, sedimentation heights, and viscosities show an increase in flocculation. The initial settlement velocity increases with increasing ionic concentration, thus indicating an increase in particle associations with salt concentration. Hence, the FF aggregates tend to form EF flocs.

4.6.2 High Solids Concentration

The effects of ionic concentration on the liquid limit and on the clay sensitivity are seen in Figures 4.7 and 4.8. An increase in the ionic concentration results in a decrease in the liquid limit and an increase in the sensitivity. The liquid limit results agree with findings by previous researchers and are attributed to the decrease in double layer thickness: as the double layers shrink, the clay structure becomes more compact and reduces the amount of pore fluid necessary to induce particle mobilization (Klein, 1999; Di Maio, 1996). The high volumetric solids content and high strain conditions impede EF floc development, so the particles tend to align. Consequently, the liquid limit depends primarily on the thickness of the DDL.

However, the effect of pH on the liquid limit is insignificant at NaCl concentrations less than or equal to 0.1 mol/L. The high solids content increases the buffering capacity of the system through particle dissolution, thereby neutralizing the pore fluid pH. Dissolving kaolinite particles consume H^+ at low pH and OH^- at high pH as discussed in Section 2.5.5, although no chemical analysis is performed. Dissolution also increases the pore fluid ionic strength with the release of aluminum ions. The measured pore fluid pH for these mixtures ranges from 4.3 to 6.0 (Table 4.4, Figure 4.10) even though the starting solution pH prior to mixing with the solids ranges from 2.9 to 8.8. But, at high ionic concentration, 1.8 mol/L, the measured pore fluid pH ranges from 3.8 to 4.0. The initial pH of the corresponding solutions ranges from 2.6 to 8.7. The role of the sodium ions takes precedence at this concentration, exchanging with hydrogen ions on the clay surface to produce a low-pH pore fluid. Cation exchange reactions tend to be both stoichiometric and rapid and so can be seen at this testing timescale (Bohn et al., 1985).

Table 4.4 Effects of Clay Dissolution on Pore Fluid pH

| Target pH | Salt Concentration (mol/L) | Sedimentation | | Viscosity | | Fall Cone | |
|-----------|----------------------------|---------------------|--------------------------|---------------------|------------------------|---------------------|---------------------|
| | | Initial Solution pH | Pore Fluid pH at 2 Weeks | Initial Solution pH | Pore Fluid pH at 8 hrs | Initial Solution pH | Final Pore Fluid pH |
| 3 | 1×10^{-5} | 2.75 | 3.03 | 3.04 | 4.04 | 3.13 | 5.3 |
| | 4×10^{-4} | 3.06 | 5.20 | 3.08 | 5.43 | 3.06 | 5.2 |
| | 3×10^{-3} | 3.10 | 4.96 | 2.98 | 4.35 | 2.95 | 6.0 |
| | 0.1 | 3.16 | 3.85 | 2.89 | 3.83 | 2.92 | 5.7 |
| | 1.8 | 2.84 | 3.60 | 2.70 | 3.39 | 2.6 | 3.8 |
| 5 | 1×10^{-5} | 5.00 | 5.91 | 5.04 | 5.07 | 4.65 | 4.7 |
| | 4×10^{-4} | 5.23 | 5.79 | 5.82 | 6.67 | 4.52 | 4.7 |
| | 3×10^{-3} | 5.02 | 5.23 | 5.83 | 5.03 | 4.70 | 4.3 |
| | 0.1 | 5.29 | 4.34 | 5.18 | 4.25 | 4.46 | 4.3 |
| | 1.8 | 5.74 | 4.18 | 4.50 | 3.68 | 4.48 | 4.0 |
| 7 | 1×10^{-5} | 6.85 | 5.97 | 6.83 | 5.98 | 6.90 | 4.8 |
| | 4×10^{-4} | 6.53 | 5.80 | 6.92 | 6.40 | 6.91 | 5.7 |
| | 3×10^{-3} | 7.13 | 5.28 | 8.99 | 5.11 | 6.87 | 6.0 |
| | 0.1 | 7.56 | 4.60 | 6.29 | 4.21 | 6.81 | 6.0 |
| | 1.8 | 7.10 | 4.27 | 7.67 | 3.87 | 6.92 | 3.8 |
| 9 | 1×10^{-5} | 8.91 | 6.12 | 8.86 | 5.80 | 8.61 | 5.8 |
| | 4×10^{-4} | 8.93 | 5.96 | 9.56 | 5.55 | 8.79 | 5.7 |
| | 3×10^{-3} | 9.11 | 5.72 | 9.96 | 5.55 | 8.75 | 6.0 |
| | 0.1 | 9.05 | 4.59 | 9.76 | 4.37 | 8.80 | 5.8 |
| | 1.8 | 8.76 | 4.64 | 9.67 | 3.83 | 8.77 | 3.8 |

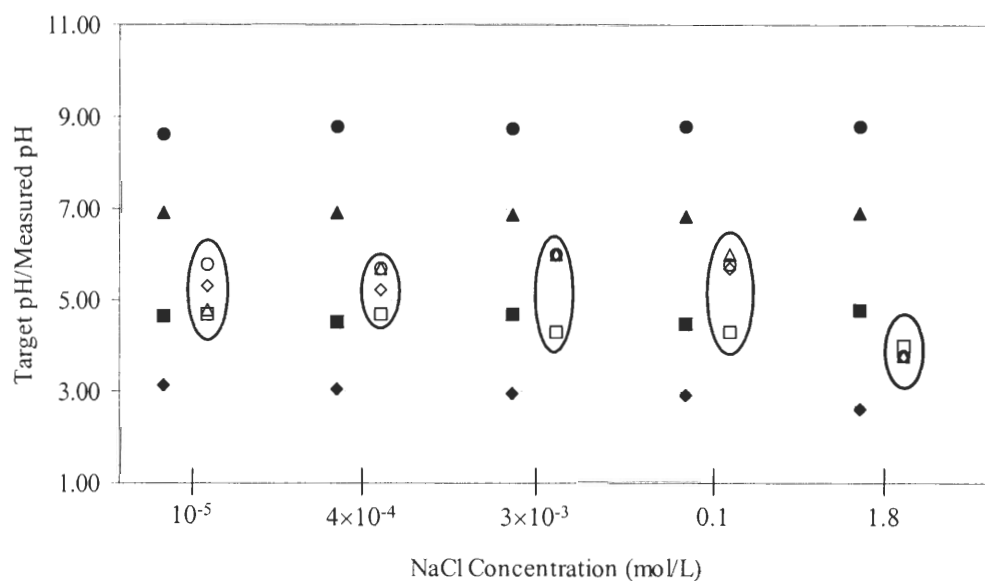


Figure 4.10 Changes in fluid pH due to particle dissolution during fall cone tests. Closed symbols represent electrolyte pH prior to mixing and open symbols represent the measured pore fluid pH after mixing.

Klein (1999) makes similar observations of a decrease in pore fluid pH from 6.01 to 3.82 corresponding to an increase in ionic concentration from 1×10^{-5} to 1.8 mol/L NaCl in low solids content kaolinite suspensions. The $\text{Na}^+ - \text{H}^+$ exchange allows for variation in structure and sensitivity at differing pH.

4.6.3 Relation to Proposed Fabric Map (Figure 2.9)

Three salient global trends are observed taking into consideration the various results at significantly different solids volume fraction ϕ and strain:

- Ionic concentration controls behavior at high concentration ($c > 0.1$ mol/L for this kaolin)
- Conversely, the effects of pH are greatest at NaCl concentrations less than 0.1 M
- The measured suspension/soil mixture parameters converge and cross at 0.1 M NaCl

These trends are consistent with the major characteristics of the proposed fabric map for kaolinite and NaCl presented in Figure 2.9 which was derived on conceptual considerations and published results. An alternate fabric map based on the sedimentation and rheological parameters for the RP2 kaolinite gathered in this research is shown in Figure 4.11.

The two fabric maps are in general agreement. In the low ionic concentration region the kaolinite suspension behavior is pH-dependent. The particles are dispersed in the region where double layers are large and both the edges and faces are negatively charged, i.e. at high pH. By decreasing the pH, the particle net positive edge charge increases due to protonation. Electrostatic attraction develops between the positive edges and negative faces at moderate pH, ~ 5 to 7, and EF flocs begin to form. At low pH, the effects of dissolution dominate particle interactions. Release of Al^{3+} and subsequent

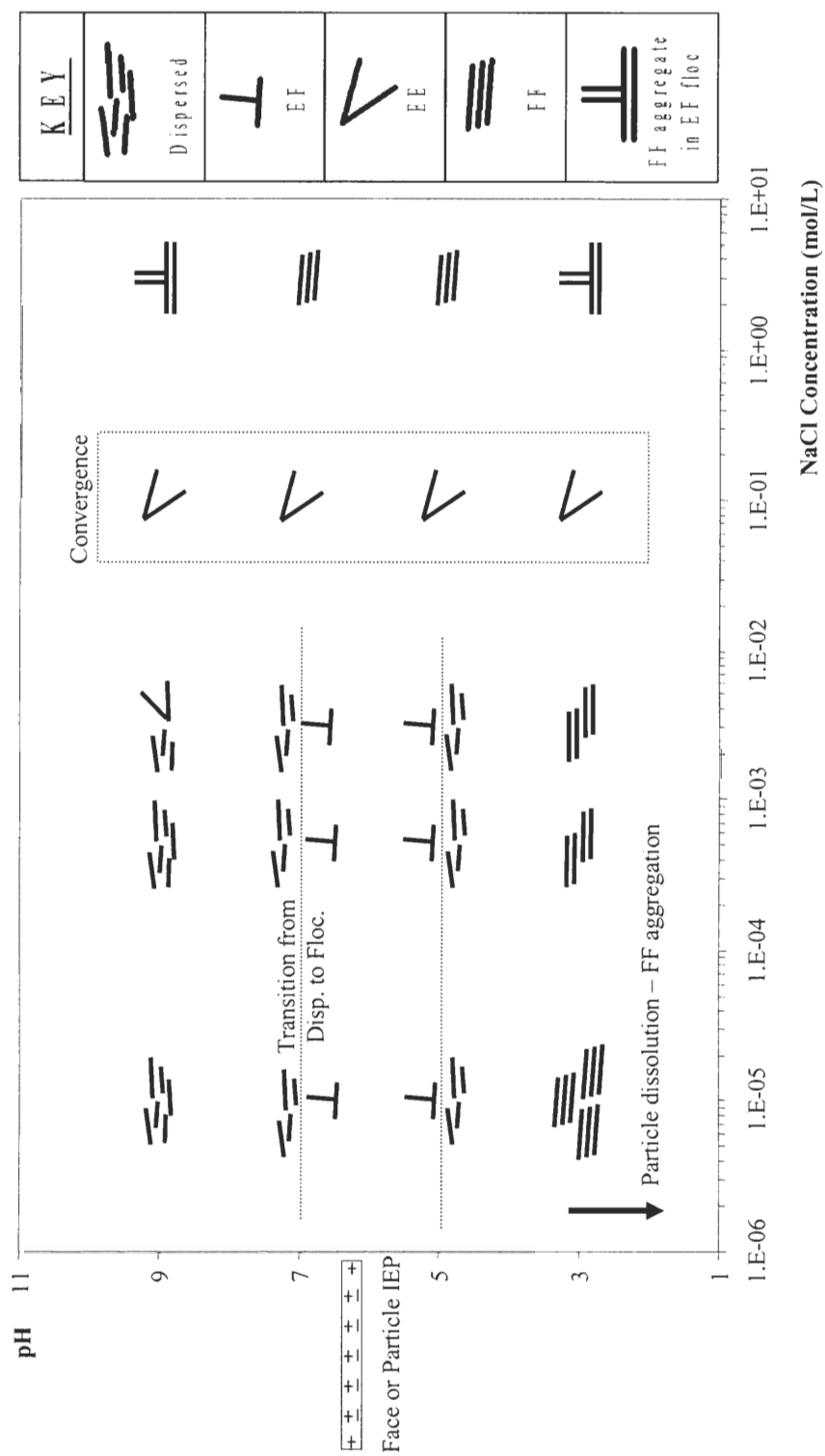


Figure 4.11 Kaolinite RP2 fabric map.

surface readsorption induces particle coagulation (Wieland and Stumm, 1992), which produces dense aggregates.

At high NaCl concentrations, the suspensions exhibit behaviors consistent with aggregated systems. The dominant force in this region is van der Waals attraction between particle basal surfaces resulting in FF aggregates. The open structures in the case of sediment height indicate the presence of EE and EF links between the aggregates.

For moderate ionic concentrations, the suspension behavior is consistent with intermediate particle associations. That is, they range from dispersed or flocculated to aggregated at higher ionic concentrations. As stated above, the transition region is clearly defined at $c \sim 0.1$ mol/L NaCl.

4.7 Conclusions

Fabric formation in kaolinite mixtures governs the settlement and rheological behaviors as well as the measured shear strength. Sedimentation, viscosity and fall cone tests involve widely differing solids volume fraction ϕ and strain conditions. Together, they permit inferring clay particle interactions and resulting fabric.

For the tested kaolinite clay:

pH has the greatest influence at low pore fluid salt concentrations.

There exists a particle association convergence point, i.e. an ionic concentration at which the suspension behavior is no longer pH-controlled. This concentration represents the transition zone between pH-controlled behavior and concentration-controlled behavior.

For high solids concentration mixtures, the clay buffering capacity neutralizes the solution pH. The liquid limit is thereby only dependent on the ionic concentration. Furthermore, high solids volume fraction ϕ and strain hinder natural trends in fabric

formation and encourage particle alignment. Hence, DDL thickness gains increased relevance.

At the highest tested ionic concentration, the sodium-hydrogen ion exchange results in a low pore fluid pH as well as an increase in variation of both the liquid limit and the clay sensitivity at varying initial solution pH.

Finally, the fabric map developed for the particular kaolinite clay tested in this study, RP2, taking into consideration sedimentation, viscosity and liquid limit tests (different ϕ and strain) closely resembles the fabric map proposed in Chapter 2 on the basis of physical processes and scattered data found in the literature (Figure 2.9).

CHAPTER 5

FABRIC IN SINGLE MINERALS – POLYMER-BASED CONTROL

Interparticle forces depend on pore fluid pH and ionic concentration. The ensuing fabrics were observed at various solids volume fraction in Chapter 4. The purpose of this chapter is to explore the effects of sodium polacrylate (NaPAA) and NaPAA in combination with CaCl_2 on a variety of single-mineral suspensions. This chapter provides the behavioral basis for later chapters on mineral mixtures.

5.1 Introduction

Polymers – organic molecules – are often used to aid in dispersing or flocculating particle suspensions. Polymers may adsorb onto clay minerals at different adsorption sites (Figure 5.1): basal surface oxygen and hydroxyl cleavage planes, edge sites, interlayer spacing in swelling clay minerals, and on the external and internal tunnel surfaces of tubular clay particles. Adsorption also occurs in the interparticle spacing within flocs (Yariv and Cross, 2002).

The surface adsorption of polymer molecules alters the clay mineral surface properties and interparticle interactions. In the case of flocculants, polymers bind particles together through polymeric bridging whereby polymer molecules attach to more than one particle, by increasing van der Waals attraction, or by decreasing the repulsive forces. On the other hand, dispersion mechanisms include steric stabilization, decreased van der Waals, or increased repulsive forces (Sacks, 2001). Polymers with chemically identical monomers may either cause dispersion or flocculation depending on their molecular weight or chain length, and the polymer concentration. The chain length is the

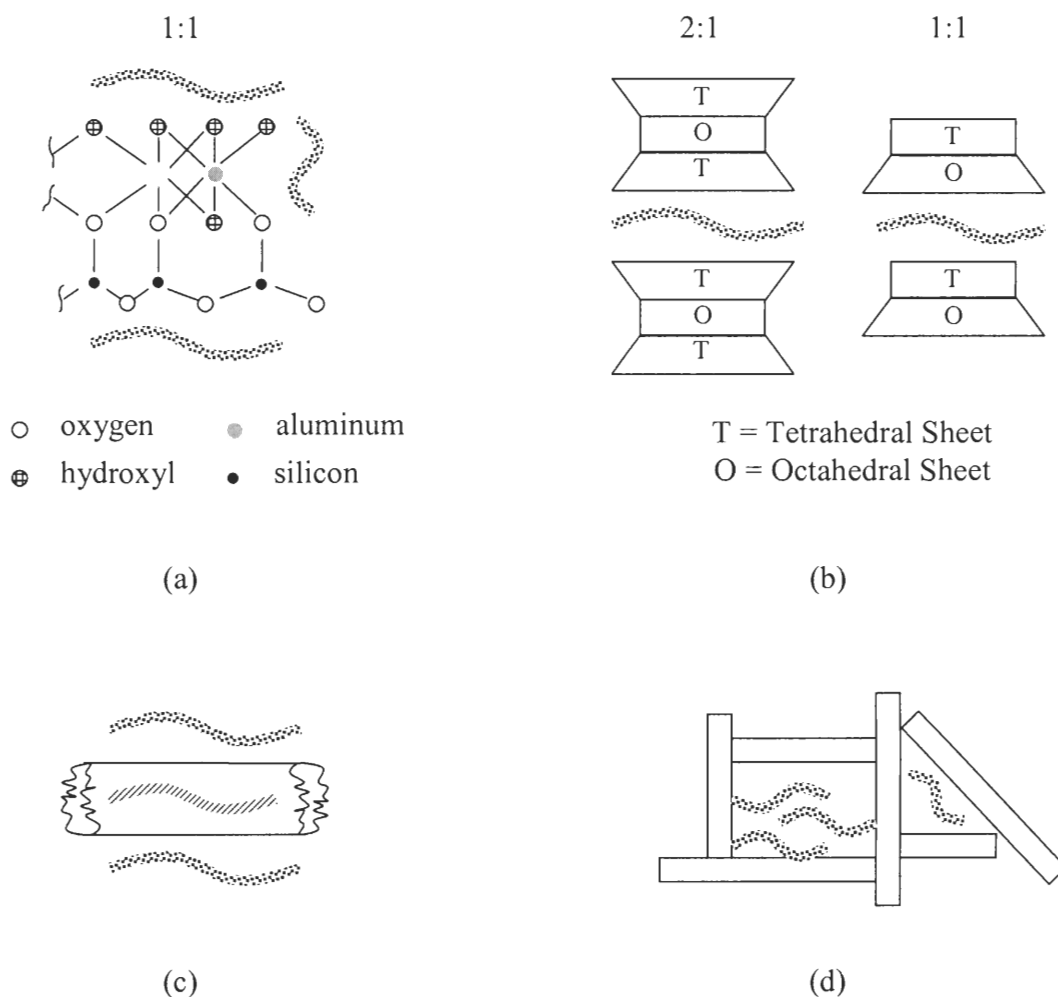


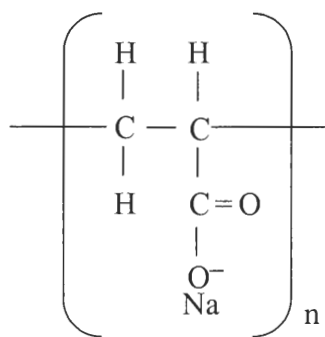
Figure 5.1 Organic ion adsorption sites on clay mineral surfaces. (a) Exposed oxygen and hydroxyl cleavage planes, and broken bonds on the mineral edges, (b) interlayer space in swelling 2:1 clays and dioctahedral 1:1 clay minerals, (c) exposed surfaces (outer surface and internal tunnels) of sepiolite and palygorskite (attapulgite) particles, and (d) within the interparticle spacing of particle flocs (listed cases from Yariv & Cross, 2002 – graphical interpretation in this figure by the author).

number of monomer units per molecule and can be calculated given the polymer molecular weight expressed in grams per mole.

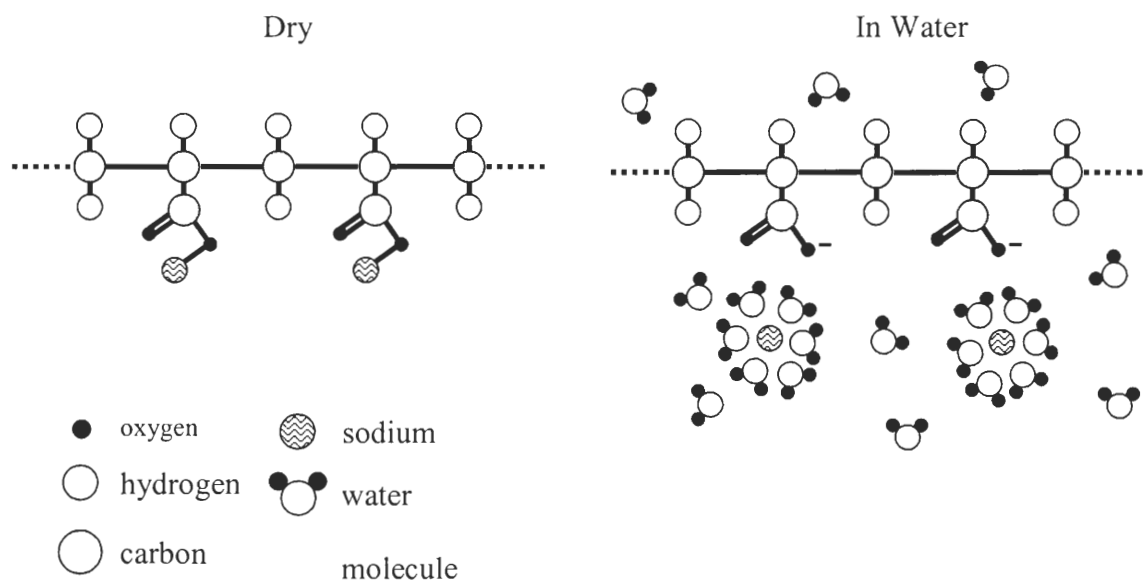
5.2 Sodium Polyacrylate (NaPAA)

The sodium polyacrylate molecule has the chemical formula $[\text{CH}_2\text{CH}(\text{COONa})]_n$ and is considered to be anionic in nature. The molecular structure is linear with a backbone of a long chain of carbon atoms. Branching from the backbone are hydrogens and sodium carboxylate groups, as represented in Figure 5.2-a; notice the position of the sodium ions relative to the carbon backbone. Figure 5.2-b schematically represents the reaction of the NaPAA molecule with water: the sodium ions become hydrated and dissociate from the polymer backbone so that the molecule behaves as a negatively charged body. The polymer molecule then has one negative charge per monomer in its fully dissociated state (Michaels and Morelos, 1955). The number of Na^+ ions that may dissociate depends on both the pH and ionic concentration of the solvent (Rahaman, 1995). Therefore, increasing the solution pH increases the degree of ionization of NaPAA molecules, and near-complete ionization occurs above pH 6.0. Table 5.1 lists the number of negative charges per monomer unit at various pH values based on the measured ionization constant for NaPAA. At high pH (>6), NaPAA molecules uncoil due to their increased intramolecular charge repulsion. As the pH decreases (<6), associations with protons decrease the negative polymer charge density, and molecules begin to coil onto themselves (Micheals and Morelos, 1955).

The electrolyte composition also affects the NaPAA molecule net charge. In the presence of free Ca^{2+} ions, the polyacrylate molecule adsorbs the divalent cations at the negative carboxylate ion sites. Saturation occurs at some critical ratio of total Ca^{2+} ions



(a)



(b)

Figure 5.2 Sodium polyacrylate. (a) Chemical structure of sodium polyacrylate and (b) dissociation of Na^+ ions from NaPAA polymer and subsequent negative charge development in water (after Mukerjee, 2000).

Table 5.1 Effect of pH on NaPAA Ionization

| pH | No. Anions Per Monomer Unit |
|-----------|------------------------------------|
| 8 | 1.0 |
| 7 | 0.99 |
| 6 | 0.94 |
| 5 | 0.60 |
| 4 | 0.13 |

(From Michaels and Morelos, 1955)

to the total number of polyacrylate segments; this ratio approaches 0.3 bound Ca^{2+} ions per polyacrylate monomer at pH 8 (Järnström and Stenius, 1990). Ca^{2+} ion adsorption increases the total positive charge, decreases the molecule extension and causes the molecule to recoil. However, if the Na^+ is added to a Ca-based system, the Na^+ ions will tend to displace the Ca^{2+} ions, and the polyacrylate molecules revert to an extended conformation (Schweins and Huber, 2001).

5.2.1 Adsorption Mechanisms on Kaolinite

The adsorption of organic anions onto kaolinite surfaces may follow one of six mechanisms (Yariv and Cross, 2002): (1) non-specific anion exchange coupled with van der Waals interactions between neighboring nonpolar molecules, (2) non-specific anion exchange coupled with hydrogen bonding between an anion and some Brønsted acid surface group i.e., proton donor site, (3) exposed hydroxyl replacement such as at edges and possibly at the aluminum hydroxide faces, (4) anion coordination with edge nonhydrated polyvalent cations, particularly strong Lewis acid sites i.e., electron-pair accepting sites, (5) sorption onto short-chain hydroxyl cationic groups previously sorbed at particle edge sites, and (6) sorption onto a previously sorbed bi- or polydentate organic cation on the particle edge surface. Attachment mechanisms proposed for the adsorption of polyanions onto kaolinite platelets include electrostatic interactions, hydrogen bonding, or some combination of the two (Theng, 1979; Yariv and Cross, 2002). In addition, the preferred adsorption sites are at broken bonds, or particle edge sites where positive charges prevail (Bergström et al., 1996).

In the special case of NaPAA, the primary mechanisms for its adsorption onto the kaolinite surface are typically thought to be attractive electrostatic interactions between

the negative carboxylate groups and the positive edge and basal sites (Diz and Rand, 1990; Järnström and Stenius, 1990) or hydrogen bonding between the unionized carboxyl groups and the edge oxygens (Michaels and Morelos, 1955). Since the number of edge sites plays a critical role in polyanion adsorption, in the case of kaolinite, the number of edge charges has the largest influence on polymer binding (Theng, 1979; Yariv and Cross, 2002). At moderate pH and without any added salts, NaPAA adsorbs mostly on the particle edges, where the highly negatively charged polymer has strong electrostatic interactions with the aluminol or silanol (protonated) edge groups (Bergström et al., 1996; Theng, 1979).

For pH conditions above the edge isoelectric point (IEP), hydroxyls begin to occupy positions near edge protons or metallic cations. As the number of kaolinite edge positive charges is reduced, adsorption decreases (Bergström et al., 1996). Sjöber et al. (1999) measure very little adsorption of NaPAA onto kaolin particles at pH 8.5, using a polymer with molecular weight 4500 g/mol at a dosage of approximately 0.035 mg polymer/m² clay. Hence, the amount of polymer adsorbed along the particle edges depends on the surrounding pH and ionic concentration (Theng, 1979; Järnström and Stenius, 1990; Ström et al., 1995; Bergström et al., 1996). Salt type also affects adsorption; the influence of CaCl₂ as an added salt will be further discussed in Section 4.2.3.

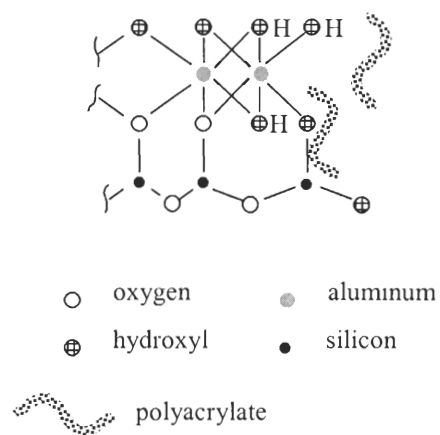
Ström et al. (1995) show that polyacrylate molecules tend to adopt flat conformations on a positively charged surface. Using ellipsometric techniques, they measure the polyacrylate film thickness on a silicon oxide surface treated with polyethylene imine which renders positive sites. Without added salts, the adsorbed polymer layer is very thin, approximately 0.2 nm. A flat conformation at kaolin particle

edges means that the particles stabilize because polymer molecules neutralize the positive edge charges thus, the net negative edge charge increases. In other words, it appears that the polymer molecules do not participate in steric stabilization.

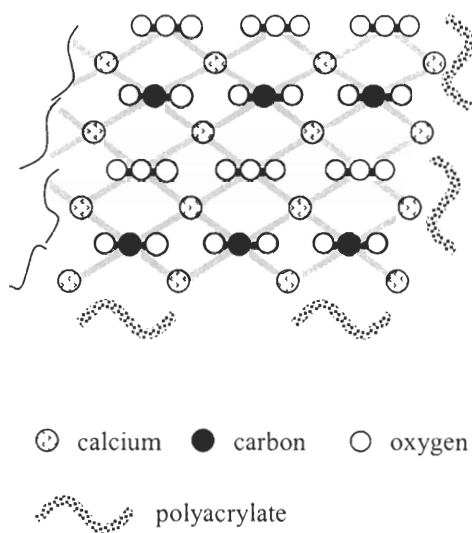
5.2.2 Adsorption Mechanisms on Calcium Carbonate

Two mechanisms have been proposed for the adsorption of NaPAA molecules onto calcium carbonate surfaces. First, adsorption may occur through electrostatic interactions as depicted in Figure 5.3, which depends on the surface charge (Järnström, 1993; Bjorklund et al., 1994). The charge of calcium carbonate surfaces in water depends on the concentration of calcium carbonate as well as ionic impurities in the water (Siffert and Fimbel, 1984). Vanerek et al. (2000) compare the electrophoretic mobilities of precipitated calcium carbonate (PCC) and ground calcium carbonate (GCC) at low (30 ppm) and high (1000 ppm) solids concentrations. In distilled water, the surface charge changes from negative to positive with increasing solids concentration. The impurities found in tap water are enough to affect the surface charge by maintaining a negative value at both low and high solids concentration. Since ionic impurities may also be found in distilled water, increasing the carbonate surface area with increasing solids concentration reduces the concentration of the excess ions per unit area solids. The negative surface charge measured at low calcium carbonate concentrations is likely due to the low water quality. Hence, calcium carbonate has a positive surface charge that may appear negative in the presence of impurities.

The second adsorption mechanism of NaPAA on calcium carbonate surfaces assumes that the surface calcium ions act as Lewis acids which provide binding sites for the polyacrylate carboxylate ions (Sanders, 1991).



(a)



(b)

Figure 5.3 Hypothesized surface interactions of the polyacrylate molecule with (a) protonated aluminol and silanol edge groups of kaolinite and (b) surface calciums of CaCO_3 .

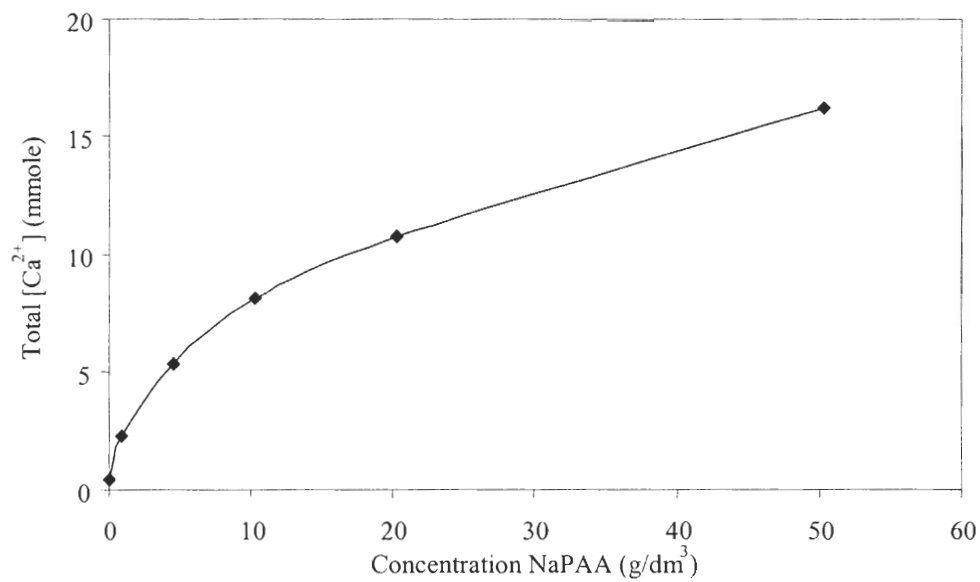


Figure 5.4 Solubility of CaCO_3 in the presence of sodium polyacrylate. The solids volume fraction is 0.02 and the molecular weight of the sodium polyacrylate is 2000 g/mole (data points from Järnström, 1993).

As shown in Figure 5.4, the presence of NaPAA tends to promote dissolution of the calcium carbonate (Järnström, 1993). The total number of Ca^{2+} ions increases as the concentration of sodium polyacrylate increases. These excess ions in solution bind to the polyacrylate molecules and reduce the number of available carboxylate groups for surface adsorption. The polyacrylate molecules then become less effective as dispersing agents, and a greater concentration of NaPAA is required to disperse the particles.

5.2.3 Influence of Calcium Chloride (CaCl_2)

The introduction of calcium ions to a kaolinite-NaPAA system promotes adsorption of polyacrylate by two mechanisms. First, Ca^{2+} ions enhance the adsorption of polyacrylate molecules through electrostatic attraction onto positively charged surface sites, such as kaolinite broken bonds sites. Adsorbed Ca^{2+} polyacrylate complexes interact with Ca^{2+} polyacrylate complexes in solution to form a thicker layer of bound molecules (Ström et al., 1995). Second, calcium ions induce polyacrylate binding onto net negative surfaces. For example, there is very little adsorption of NaPAA onto a negatively charged mica surfaces, however a layer of polyacrylate binds to the mica surface in the presence of calcium chloride (Berg et al., 1993). Järnström and Stenius (1990) find that the polyacrylate binds to both the edge and basal planes of kaolinite particles in a CaCl_2 electrolyte.

Due to its ionic nature, the polyacrylate binds to the positive sites on both kaolinite and calcium carbonate surfaces. However, by altering the pore fluid ionic concentration and careful selection of the appropriate counterion, the effects of the polymer may be modified or even reversed (Dahlvik et al., 1995; Schweins and Huber, 2001). Hence, the

suspension stability may be either enhanced or diminished, depending on the electrolyte conditions.

Clay particle flocculation is observed in previously dispersed suspensions after the addition of calcium chloride. It is inferred that the Ca^{2+} ions adsorb onto the polyacrylate molecules already bound to the clay surfaces and form Ca^{2+} polyacrylate complexes. The complexes on one particle surface may interact with complexes on another particle through Ca^{2+} ion bridging (Berg et al., 1993). Calcium-induced particle associations in kaolinite systems previously dispersed with sodium polyacrylate may either be edge-to-face flocculation or FF aggregation, depending on the electrolyte concentration. Edge-to-face associations are dominant at low CaCl_2 concentrations due to the limited adsorption of polyacrylate at the particle edges (Dahlvik et al., 1995). At high CaCl_2 concentrations, face-to-face associations dominate due to polyacrylate adsorption on the basal planes and subsequent interactions between Ca^{2+} polyacrylate complexes on the particle faces (Stenius et al., 1990).

Limited structure formation is observed with the addition of CaCl_2 in calcium carbonate suspensions initially dispersed with sodium polyacrylate (Dahlvik et al., 1995).

5.3 Materials and Procedures

5.3.1 Materials

The minerals used in the sedimentation tests include Wilklays RP2 and SA1, Premier, ground calcium carbonate, GCC #12 White, and precipitated calcium carbonate, PCC Rhombic. Their sources and properties are found in Chapter 3.

The minerals are dispersed using the sodium polyacrylate designated Colloid 211, the properties of which are listed in Table 3.6.

5.3.2 Sedimentation

The solids volume fraction for all suspensions is $\phi=0.02$, so the total mass of each mineral varies according to its specific gravity.

Suspensions containing sodium polyacrylate are prepared according to Section 3.2.2, except that 10 mL of deionized water mixed with 50 μL of Colloid 211 is added to the suspension after the appropriate mineral mass is added to the cylinder. Since Premier clay is pretreated with NaPAA, no Colloid 211 is added to the Premier suspension.

Suspensions with NaPAA and calcium chloride are prepared as suspensions with NaPAA. The small volume of concentrated CaCl_2 solution is added to the suspension after the diluted Colloid 211 so that the final pore fluid salt concentration is 0.002 mole/liter (stoichiometric ionic strength $I=2.4\times 10^{-2}$ mol/L). The CaCl_2 concentration is determined by a critical coagulation, or flocculation, test. The test is performed by varying the calcium chloride concentration in Premier clay slurries prepared at the same solids content as the sedimentation studies. The chosen CaCl_2 concentration is the one that renders a stable suspension after 24 hours. Suspension and settlement and heights are recorded for 42 days.

5.3.3 Viscosity

Single mineral suspensions are prepared for rheological studies according to Section 3.2.3 at a solids volume fraction of $\phi=0.07$. The NaPAA suspensions are prepared by first adding approximately 200 mL of deionized water to the pre-measured dry mineral mass and mixing well for several hours on a Corning stirrer. A dosage of 50 μL NaPAA per 2.5 g solids is diluted in 100 mL of deionized water and added to the suspension, mixed, and followed by enough deionized water for a 500-mL total liquid volume.

Suspensions containing both NaPAA and CaCl_2 are prepared by mixing 200 mL of deionized water with the proper mineral mass in a 600 mL beaker and stirring for several hours. NaPAA, at the same dosage as stated above, diluted in 100 mL of deionized water is then introduced to the suspension and mixed. Enough deionized water is added to the suspension for a total volume of 450 mL. The suspension is mixed for eight hours, after which a small volume of a high concentration CaCl_2 solution is introduced to achieve a 0.002 M CaCl_2 concentration in the pore fluid. The suspension is brought to a total volume of 500 mL with deionized water and mixed for 8 more hours.

5.3.4 Liquid Limit

The kaolinite Premier is not tested due to its inability to be thoroughly mixed at a moisture content sufficient for hydrating the clay without going over the liquid limit (note: a drying test is not attempted). Three different pore fluid compositions are used to prepare the soil specimens for liquid limit measurements. In the first series, the pore fluid contains no additives, i.e., the pore fluid is deionized water. In the second series, the pore fluid contains NaPAA in the form of 0.25 mL Colloid 211 per 100g of solids diluted in the first 60 mL of deionized water mixed with the solids. Higher moisture contents are achieved by adding deionized water. In the third series, the pore fluid contains both NaPAA and CaCl_2 . The same dosage of NaPAA as in the second series is diluted in 50 mL of 0.002 M CaCl_2 and mixed with the solids. The moisture contents are increased for each measurement point with additional volumes of 0.002 M CaCl_2 solution.

5.4 Results

5.4.1 Sedimentation

Table 5.2 lists the observed sedimentation response of all the tested suspensions, while Table 5.3 lists the variation in pore fluid pH of the given suspensions. The addition of NaPAA influences the RP2 kaolinite settlement from flocculation-sedimentation to dispersed-sedimentation. However, NaPAA seems to have little effect on the observed behavior of the remaining mineral suspensions in that the sedimentation appearance is dispersed both with and without NaPAA. Calcium chloride increases the flocculation tendency in SA1, Premier, and GCC suspensions, but no observable change is seen for either the RP2 or the PCC suspensions.

The influence of NaAA and NaPAA plus CaCl_2 becomes increasingly evident in comparing the induction periods (as discussed in Chapter 3). The extent of the induction periods provides a measure of relative suspension structures. In flocculated systems, the induction time increases with increasing particle interactions (Tiller and Khatib, 1984), while in dispersed systems, the induction time increases with increasing stability. The plot of induction time with the suspension fluid composition for the tested mineral suspensions is shown in Figure 5.5. While each point represents a single test, the overall responses are consistent within the given mineral groups. The untreated kaolinite SA1 has a natural tendency toward dispersive behavior that is evident with the relatively large induction time. The increase in induction time for the RP2, SA1, GCC, and PCC suspensions corresponds to the increased level of particle dispersion-stabilization with the addition of sodium polyacrylate as compared to the minerals without additives. The RP2, GCC, and PCC suspensions experience a significant increase in induction period from

Table 5.2 Observed Sedimentation Behavior of Mineral Suspensions

| Mineral | Observed Sedimentation Behavior | | |
|---------|---------------------------------|-----------|---------------------------|
| | No Additives | NaPAA | NaPAA + CaCl ₂ |
| RP2 | Flocculation | Dispersed | Dispersed |
| SA1 | Dispersed | Dispersed | Mixed-Mode |
| Premier | N/A | Dispersed | Mixed-Mode |
| GCC | Dispersed | Dispersed | Mixed-Mode |
| PCC | Dispersed | Dispersed | Dispersed |

Table 5.3 Mineral Suspensions pH in deionized water, with NaPAA and with NaPAA plus CaCl₂.

| Mineral | Deionized Water | NaPAA | NaPAA + CaCl ₂ |
|---------|-----------------|-------|---------------------------|
| RP2 | 4.66 | 6.18 | 5.27 |
| SA1 | 6.50 | 6.51 | 6.55 |
| Premier | N/A | 6.39 | 5.87 |
| GCC | 8.76 | 9.39 | 7.72 |
| PCC | 9.87 | 8.96 | 7.87 |

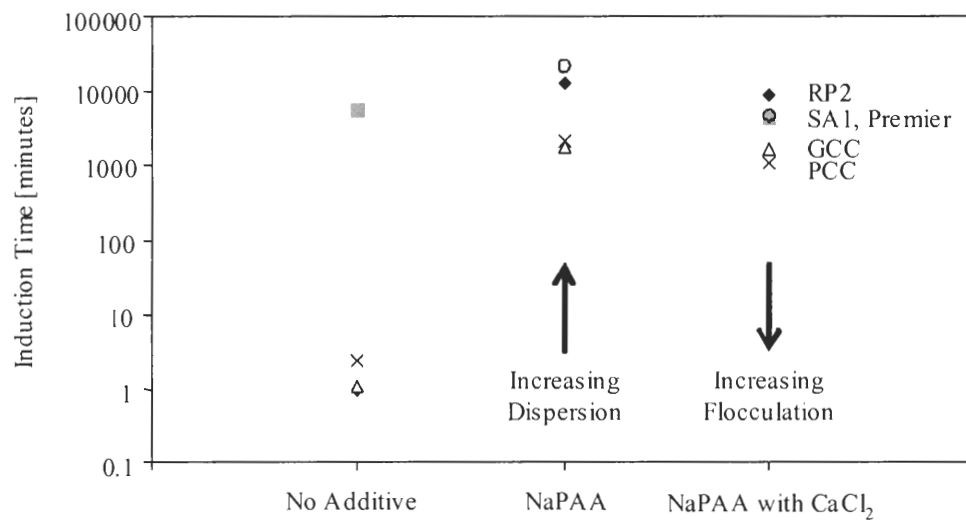


Figure 5.5 Induction periods of mineral suspensions (solids volume fraction 0.02). Cases: without additives, with sodium polyacrylate, and with sodium polyacrylate plus 0.002 M calcium chloride.

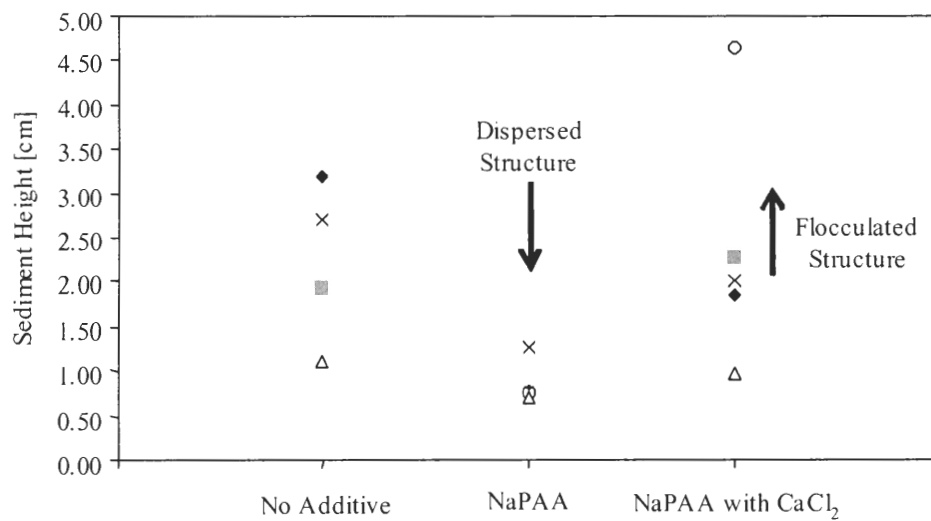


Figure 5.6 Comparison of mineral suspension sediment heights at approximately 31000 minutes. Cases: without additives, with sodium polyacrylate, and with sodium polyacrylate plus 0.002 M calcium chloride.

minutes to days. The RP2 kaolin suspension has the maximum observed percentage increase in induction period, increasing by more than 8 days in the presence of NaPAA.

All tested mineral suspensions show a decrease in induction time after the addition of CaCl_2 . The greatest impact is observed for SA1 and Premier kaolins, and the least impact is seen in GCC. However, the PCC suspension shows a much greater response to the added electrolyte.

Figure 5.6 summarizes the sedimentation heights observed 31000 minutes (~22 days) after the initiation of each test. The general trend is increasing dispersed structure with the addition of NaPAA and increasing flocculated structure in the presence of calcium chloride, in agreement with induction times. The RP2 kaolin suspension has the greatest response to NaPAA. The GCC sedimentation height decreases the least with the addition of NaPAA but is reduced by 36% compared to the untreated GCC suspension.

The level of flocculation for all the tested suspensions is greatly enhanced in the presence of CaCl_2 . The Premier clay suspension settlement shows the most significant increase in height with the addition of Ca^{2+} ions. Of the two carbonates, the PCC again has a greater response to the CaCl_2 .

5.4.2 Viscosity

Viscosity measurements at 100 RPM for all the suspensions are shown in Figure 5.7. Without any additives, only the RP2 and PCC suspensions have measurable resistance to shear across the applied range of spindle rotational speeds. In the presence of NaPAA, without and with CaCl_2 , the only measurable point for all suspensions is at 100 RPM. Hence, viscosity comparisons are made at 100 RPM for all suspensions.

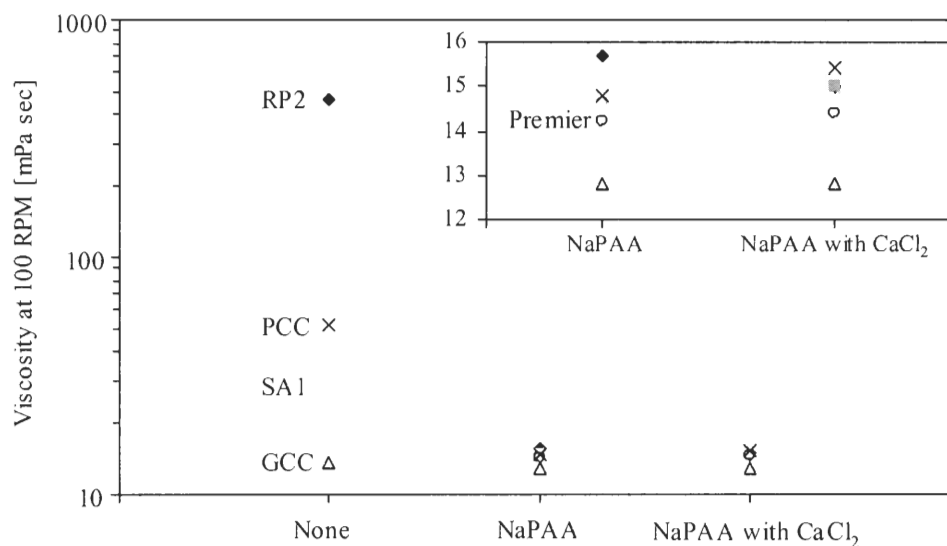


Figure 5.7 Comparison of viscosity measurements at 100 RPM for mineral suspensions with 0.07 solids volume fraction. Cases: without additives, with sodium polyacrylate, and with sodium polyacrylate plus 0.002 M calcium chloride. The viscosity of the RP2 kaolin suspension without additives is high so it is measured with Spindle #3. All other suspension viscosities are measured with Spindle #1.

Without any additives, the kaolin RP2 has the highest level of flocculation among the minerals tested. However, the sodium polyacrylate effectively reduces the RP2 suspension viscosity from 460 to 15.7 mPa·sec at 100 RPM. NaPAA also increases the level of dispersion for both the SA1 and PCC mineral suspensions, although the effect is less significant than for the RP2 case. The applied dosage of NaPAA has almost no effect on the viscosity of the GCC suspension.

For all the tested suspensions, the CaCl_2 does not increase the level of measurable flocculation in the presence of 0.002 M CaCl_2 .

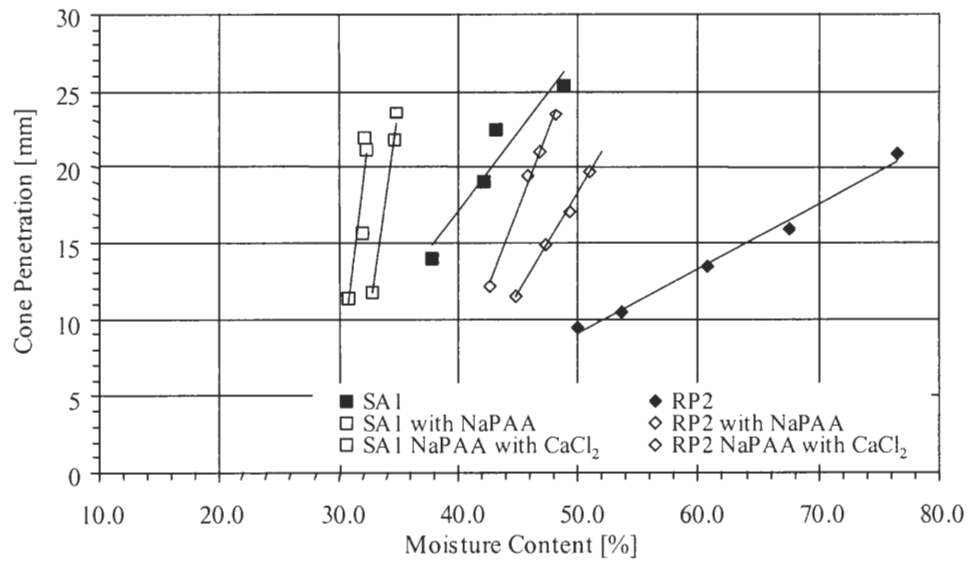
5.4.3 Liquid Limit

Figures 5.8, 5.9 and 5.10 show the fall cone penetration lines, liquid limits and penetration line slopes, respectively, of single tests. These figures compare the liquid limits of each mineral at three pore fluid conditions: no additives (deionized water), with NaPAA and with NaPAA plus CaCl_2 . The kaolin clays RP2 and SA1, as well as the PCC experience a significant reduction in liquid limit at the applied dosage of NaPAA. The largest increase in dispersion is again observed in the RP2 kaolin case. Also, the GCC again shows little response to the sodium polyacrylate.

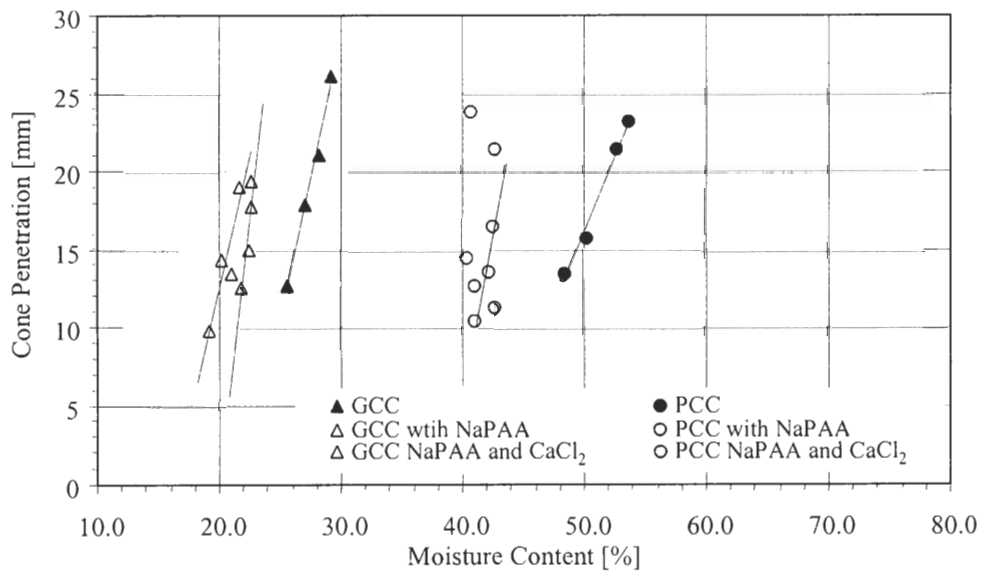
The addition of CaCl_2 has only a slight effect on the liquid limits of the tested materials compared to the NaPAA cases. Calcium chloride has almost no effect on the GCC mixture.

5.5 Discussion

The scope of this study includes four parameter categories including two mineral types, five unique materials, variation in particle size, and variation in particle shape. In



(a)



(b)

Figure 5.8 Fall cone penetration lines for (a) kaolins SA1 and RP2 and (b) GCC and PCC. Cases: without additives, with sodium polyacrylate, and with sodium polyacrylate plus 0.002 M calcium chloride.

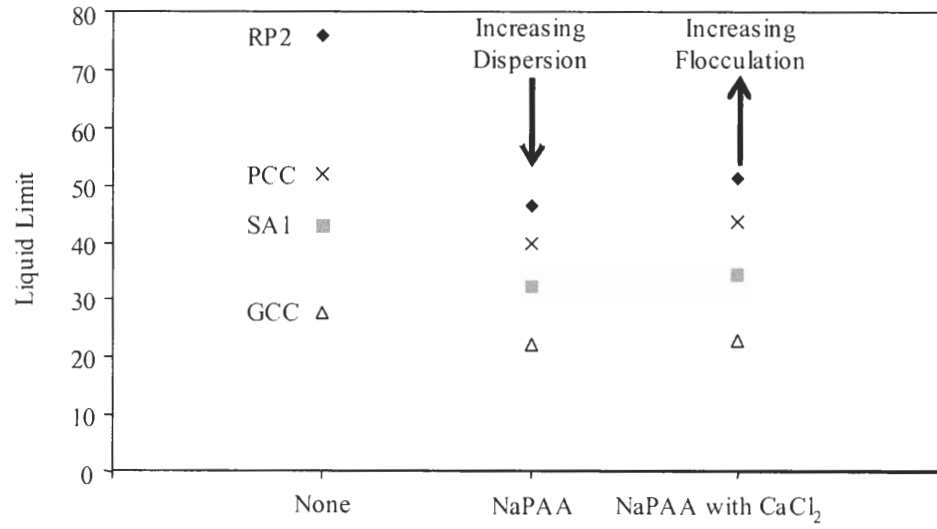


Figure 5.9 Liquid limits comparison. Cases: without additives, with sodium polyacrylate, and with sodium polyacrylate plus 0.002 M calcium chloride. The liquid limits for the Premier case are not measurable.

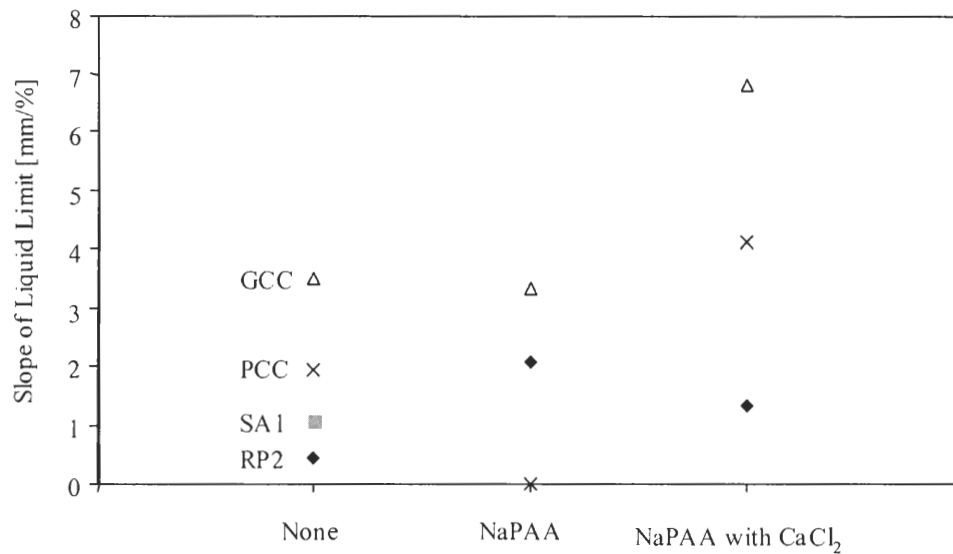


Figure 5.10 Slopes of the kaolin and calcium carbonate fall cone liquid limit lines.

addition, variability may exist for the water-solids, NaPAA-solids, and Ca^{2+} -NaPAA or Ca^{2+} -solids ratios of each material, depending on the test. Therefore, only selected slices of this Nth dimensional space are explored, in particular:

- Low solids content suspensions to understand initial free fabric formation
- Intermediate solids content (viscosity) in relation to industrial applications subjected to high shear
- High solids content (liquid limit) in relation to engineering applications

Table 5.4 summarizes the key parameter results for all sedimentation, viscosity, and fall cone tests. Global trends include:

- NaPAA induces dispersion at all solids contents for all minerals tested
- CaCl_2 has some measurable flocculation capability in the presence of sodium polyacrylate
- The level of response to NaPAA and NaPAA with CaCl_2 varies for each material, even within the same mineral group.

5.5.1 Kaolinite

NaPAA. Generally, both RP2 and SA1 exhibit an increase in the level of dispersion in the presence of sodium polyacrylate. But, RP2 has a greater sensitivity to the addition of NaPAA than SA1 in spite of the higher specific surface of RP2 ($S_s=21.9 \text{ m}^2/\text{g}$ for RP2 vs. $S_s=13.0 \text{ m}^2/\text{g}$ for SA1 – Klein, 1999). The total edge area per gram of clay for RP2 is estimated at 4.9 m^2 compared to 1.6 m^2 for SA1 (see Mathgrams 5.1-a and b). In other words, NaPAA must cover more edge area in the RP2 case than in the SA1 case. If polyacrylate adsorption is limited to the particle edges, the positive charge density along the clay particle edges is not the same for the two clay types. The variance in NaPAA

Table 5.4 Results Summary for Sedimentation, Viscosity, and Fall Cone Tests.

| Mineral | Additive | Sedimentation (0.02 solids content) | | | | Viscosity (0.07 solids content) | Fall Cone (0.41 - 0.63 solids content) | | |
|---------|---------------------------|--|---------------|----------------------|------------------------------|------------------------------------|---|------------------|--------------|
| | | Measured pH | Observed Mode | Induction Time [min] | Final Height at 22 days [cm] | | Average Measured pH | LL Slope [mm/w%] | Liquid Limit |
| RP2 | None | 4.66 | Flocculation | 0.9 | 3.20 | 460 | 4.1 | 0.425 | 76 |
| | NaPAA | 6.18 | Accumulation | 12604 | 0.85 | 15.7 | 4.3 | 2.05 | 46 |
| | NaPAA + CaCl ₂ | 5.27 | Accumulation | 8412 | 1.85 | 15.0 | 4.4 | 1.34 | 51 |
| SA1 | None | 6.50 | Dispersed | 5440 | 1.95 | 27.7 | 6.5 | 1.03 | 43 |
| | NaPAA | 6.51 | Dispersed | 20512 | 0.90 | 14.6 | 6.4 | 6.05 | 32 |
| | NaPAA + CaCl ₂ | 6.55 | Mixed | 4380 | 2.30 | 15.0 | 6.4 | 5.61 | 34 |
| Premier | None | N/A | N/A | N/A | N/A | N/A | N/A | N/A | N/A |
| | NaPAA | 6.39 | Dispersed | 21700 | 0.75 | 14.2 | -- | -- | -- |
| | NaPAA + CaCl ₂ | 5.87 | Mixed | 4604 | 4.65 | 14.4 | -- | -- | -- |
| GCC | None | 8.76 | Dispersed | 1.0 | 1.10 | 13.6 | 8.0 | 3.50 | 28 |
| | NaPAA | 9.39 | Dispersed | 1757 | 0.70 | 12.8 | 9.0 | 3.33 | 22 |
| | NaPAA + CaCl ₂ | 7.72 | Mixed | 1664 | 0.95 | 12.8 | 9.1 | 6.76 | 23 |
| PCC | None | 9.87 | Dispersed | 2.3 | 2.70 | 51.6 | 8.3 | 1.94 | 52 |
| | NaPAA | 8.96 | Dispersed | 2061 | 1.25 | 14.8 | 9.5 | -4.51 | 40 |
| | NaPAA + CaCl ₂ | 7.87 | Dispersed | 1065 | 2.00 | 15.4 | 9.3 | 4.09 | 43 |

efficiency in dispersing the two kaolinites should then be attributed to the difference in edge positive charge density. Hence, RP2 has a higher density of positive edge sites. This observation is consistent with the clay tendency to flocculate under pure deionized water conditions (near neutral pH), while SA1 tends to remain dispersed under identical conditions. (Note: the cation exchange capacities of the two clays are not measured.)

NaPAA with CaCl₂. Stenius et al. (1990) find that some critical value of $[Ca^{2+}]_{tot}/C_{PAA}$ must be reached for flocculation to take place. $[Ca^{2+}]_{tot}$ is the total concentration of calcium ions in the suspension, including those ions associated with the dry clay in the form of excess salts, while C_{PAA} is the number of polyacrylate monomers. Below this critical value, the rheological profiles of kaolin suspensions indicate dispersed systems, irrespective of the calcium chloride concentration. Above this critical value, the suspension yield stress greatly increases, indicative of structure formation. The critical ratio $[Ca^{2+}]_{tot}/C_{PAA}$ depends not only on pH and solids content but also on the type of kaolin. For the kaolin clays Stenius et al. (1990) measure, the range of critical values varies from 0.3 to 0.35. These critical values approach the ratio $[Ca^{2+}]_{tot}/C_{PAA}$ representing PAA saturation by Ca^{2+} ions (~0.3) presented by Järnström and Stenius (1990).

An estimation of the ratio of added calcium ions to total number of polyacrylate monomers, $[Ca^{2+}]_{add}/C_{PAA}$, is calculated in Mathgram 5.2. The calculated ratio 0.25 is based on the amount of NaPAA (Colloid 211) and the molar concentration of $CaCl_2$ added to the RP2 and SA1 sedimentation suspensions. The ratio for the Premier sedimentation suspension is not calculated since the NaPAA molecular weight used by the material manufacturer is unknown. Since flocculation is observed for all three kaolin

clays, SA1, RP2, and Premier, the estimated ratio $[Ca^{2+}]_{add}/C_{PAA}$ of 0.25 represents a value above the critical value for the given solids volume fraction of $\phi=0.02$. Figure 5.11 shows the impact on fabric for SA1 in the presence of NaPAA and NaPAA with $CaCl_2$. The polymer-treated clay forms thin particle layers after freeze-drying, while the $CaCl_2$ system has an increased level of structure with visible FF and EF particle associations.

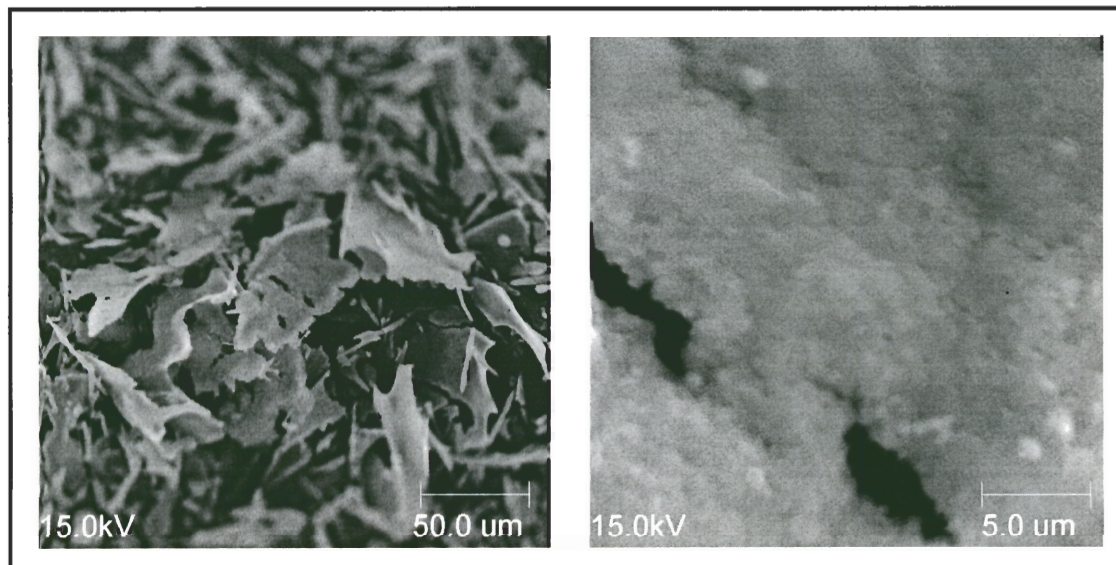
At moderate solids content, induced flocculation with $CaCl_2$ is not observed at the applied salt concentration. The dispersive behavior, even in the presence of excess Ca^{2+} ions, may be attributable to the low $[Ca^{2+}]_{tot}/C_{PAA}$ ratio. The ratio $[Ca^{2+}]_{add}/C_{PAA}$ is approximately 0.04 for the RP2 and SA1 clay systems (Mathgram 5.2), which is an order of magnitude lower than the critical value. Hence, little difference should be observed between the non- $CaCl_2$ and the $CaCl_2$ cases. The Premier clay suspension also shows no response to the added $CaCl_2$, and so it is below the critical ratio.

The liquid limit for each of the clays is little influenced by the addition of calcium chloride. The lack of response is due to the combination of low $[Ca^{2+}]_{tot}/C_{PAA}$ ratio (Mathgram 5.2), which is approximately 0.02, and hindered flocculation resulting from the high ϕ and high strain conditions (Chapter 4).

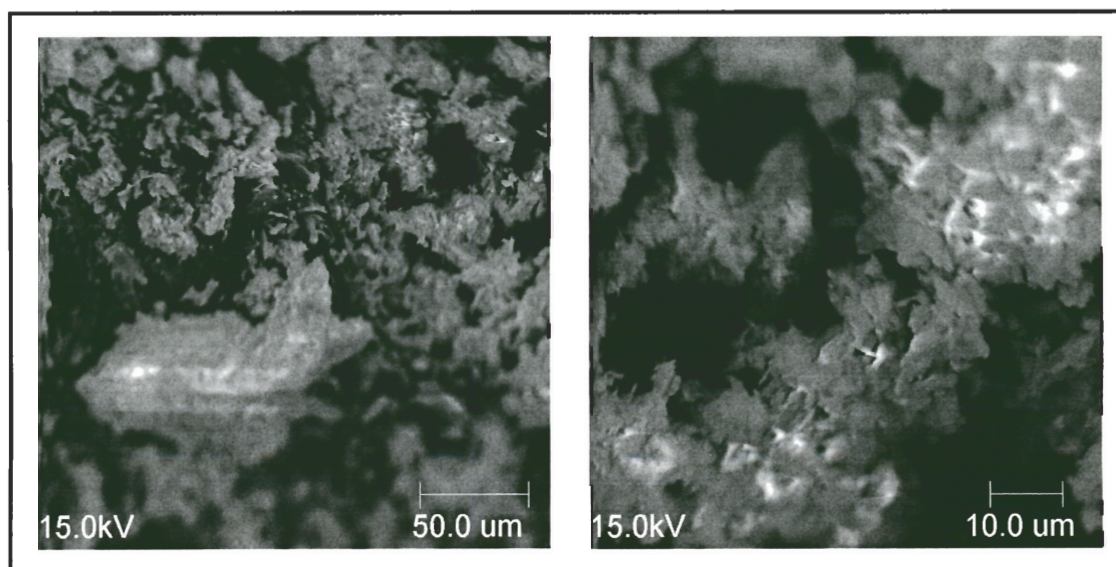
5.5.2 Calcium Carbonate

NaPAA. The NaPAA influences the behavior of the PCC more so than the GCC. The variation in behavior between the two carbonates can be attributed to the differences in particle size, S_s , and shape.

The PCC particles are much smaller, $d_{50} \approx 1 \mu m$, than the GCC particles $d_{50}=12 \mu m$ and subsequently have a much higher specific surface. Electrical forces dominate the behavior of the PCC particles, whereas the size of the GCC particles places them at the



(a)



(b)

Figure 5.11 SEM micrographs of SA1 in the presence of (a) NaPAA and (b) NaPAA with CaCl_2 .

boundary between gravitational and electrical force control. Hence, the effects of pore fluid chemistry on the carbonate particle are greater for PCC than GCC. The larger particle sizes and wider grain size distribution have a greater impact on GCC suspension behavior and resulting fabric than the NaPAA.

Particle shape influences the fabric of the free-formed sediments. Even in the presence of NaPAA, the needle-like PCC particles have a greater tendency to form a more open, voluminous structure than the more blocky GCC particles. This is consistent with Hagemeyer's (1960) findings comparing sediment volumes of needle-like and rhombic (blocky) carbonates with similar sizes.

NaPAA with CaCl₂. The addition of CaCl₂ has a greater impact on the behavior of the PCC than on GCC, paralleling the influence of NaPAA alone. The response to CaCl₂ also decreases with increasing solids content. Only slight increases in liquid limit compared to the NaPAA cases are observed. The estimated $[Ca^{2+}]_{tot}/C_{PAA}$ ratios, not including the Ca²⁺ ions dissociated from the carbonate itself, are also quite low, ~0.013 for the GCC and ~0.02 for the PCC.

5.6 Conclusions

Fabric formed from single minerals can be controlled with a polymer and added salts. The efficiency of the polymer NaPAA is mineral dependant. In kaolinite particle systems, the efficiency is related to the edge surface charge. The higher the positive charge density, the greater the dispersive strength of NaPAA. The polyacrylate molecules have a stronger interaction with the RP2 clay particles compared to the SA1 clay particles.

In the presence of calcium chloride, the ratio $[Ca^{2+}]_{tot}/C_{PAA}$ determines the level of flocculation within the clay suspensions. There exists a critical ratio above which flocculation takes place. Of the three kaolin clays at low solids content, calcium chloride has the greatest impact on the Premier kaolin. Premier particles floc in an open voluminous fabric at the test $CaCl_2$ concentration.

NaPAA and NaPAA in combination with $CaCl_2$ have little influence over the final fabric of the carbonate GCC. Instead, the behavior over the given range of solids content depends on the particle size (gravitational forces), particle size gradation and particle shape. On the other hand, the applied dosage of NaPAA disperses the smaller PCC particles over the tested range of solids content. However, the final fabric at low solids content is in part attributable to the prismatic shape of the PCC particles.

Mathgram 5.1 (a). Estimated RP2 Particle Edge Area

Material - Wilkinson Kaolin Clay, RP2

Mean Particle Size (manufacturer's data):

$$d_{50} := 0.36 \cdot 10^{-6} \cdot \text{m}$$

Specific Gravity:

$$G_s := 2.6$$

Specific Surface, measured by K. Klein:

$$S_s := 21.9 \frac{\text{m}^2}{\text{gm}}$$

Unit Weight of Water:

$$\gamma_w := 9.8 \cdot 10^3 \cdot \frac{\text{N}}{\text{m}^3}$$

Particle Density:

$$\rho := \frac{G_s \cdot \gamma_w}{g}$$

Specific Surface of an idealized kaolinite particle:

$$S_a = \frac{8}{\sqrt{3} \cdot d_{50} \cdot \rho} + \frac{2}{t \cdot \rho}$$

Particle thickness based on specific surface:

$$t := -6 \cdot \frac{d_{50}}{\left(-3 \cdot S_s \cdot d_{50} \cdot \rho + 8 \cdot 3^{\frac{1}{2}} \right)}$$

$$t = 4.538 \times 10^{-8} \text{ m}$$

Percentage of surface area attributed to the edges:

$$\text{EdgeArea} := \frac{t}{t + \frac{\sqrt{3}}{4} \cdot d_{50}} \cdot 100$$

$$\text{EdgeArea} = 22.548$$

Amount of Edge area per gram:

$$\text{EA}_g := S_s \cdot \frac{\text{EdgeArea}}{100}$$

$$\text{EA}_g = 4.938 \text{ m}^2 \frac{1}{\text{gm}}$$

Mathgram 5.1 (b). Estimated SA1 Particle Edge Area

Material - Wilkinson Kaolin Clay, SA1

Mean Particle Size (manufacturer's data):

$$d_{50} := 1.1 \cdot 10^{-6} \cdot \text{m}$$

Specific Gravity:

$$G_s := 2.6$$

Specific Surface, measured by Klein (1999):

$$S_s := 13.0 \frac{\text{m}^2}{\text{gm}}$$

Unit Weight of Water:

$$\gamma_w := 9.8 \cdot 10^3 \cdot \frac{\text{N}}{\text{m}^3}$$

Particle Density:

$$\rho := \frac{G_s \cdot \gamma_w}{g}$$

Specific Surface of an idealized kaolinite particle:

$$S_a = \frac{8}{\sqrt{3} \cdot d_{50} \cdot \rho} + \frac{2}{t \cdot \rho}$$

Particle thickness based on specific surface:

$$t := -6 \cdot \frac{d_{50}}{\left(-3 \cdot S_s \cdot d_{50} \cdot \rho + 8 \cdot 3^{\frac{1}{2}} \right)}$$

$$t = 6.762 \times 10^{-8} \text{ m}$$

Percentage of surface area attributed to the edges:

$$\text{EdgeArea} := \frac{t}{t + \frac{\sqrt{3}}{4} \cdot d_{50}} \cdot 100$$

$$\text{EdgeArea} = 12.431$$

Amount of Edge area per gram:

$$\text{EA}_g := S_s \cdot \frac{\text{EdgeArea}}{100}$$

$$\text{EA}_g = 1.616 \text{ m}^2 \frac{1}{\text{gm}}$$

Mathgram 5.2. $[\text{Ca}^{2+}]_{\text{add}}/\text{C}_{\text{PAA}}$ Ratios

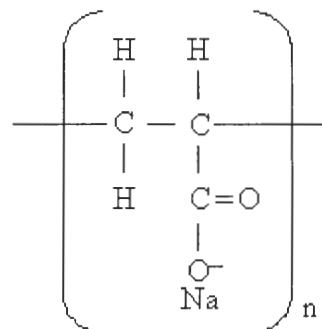
Sodium Polyacrylate, $\text{CH}_2\text{CH}(\text{COONa})$

Approximate Molecular Weight and density, manufacturer's data:

Colloid 211 -- 3400 g/mole

$$\text{MW} := 3400 \frac{\text{gm}}{\text{mole}}$$

$$\rho_{211} := 1.30 \frac{\text{gm}}{\text{mL}}$$



Individual Atom Molecular Weights

$$\text{H} := 1.007947 \frac{\text{gm}}{\text{mole}}$$

$$\text{C} := 12.01078 \frac{\text{gm}}{\text{mole}}$$

$$\text{O} := 15.99943 \frac{\text{gm}}{\text{mole}}$$

$$\text{Na} := 22.9897702 \frac{\text{gm}}{\text{mole}}$$

Equation Based on Chemical Formula

$$n \cdot (3 \cdot \text{C} + 3 \cdot \text{H} + 2 \cdot \text{O} + \text{Na}) + 2 \cdot n \cdot \text{H} = \text{MW}$$

Approximate Number of Monomers Per Molecule, n:

$$n_{\text{monomer}} := \frac{\text{MW}}{(3 \cdot \text{C} + 5 \cdot \text{H} + 2 \cdot \text{O} + \text{Na})} \quad \boxed{n_{\text{monomer}} = 35.394}$$

Approximate Number of NaPAA Molecules Per mL Colloid 211, $N_{\text{molecules}}$:

$$N_{\text{av}} := 6.022 \cdot 10^{23} \cdot \frac{1}{\text{mole}}$$

$$N_{\text{molecules}} := N_{\text{av}} \cdot \frac{1}{\text{MW}} \cdot \rho_{211} \quad N_{\text{molecules}} = 2.303 \times 10^{20} \frac{1}{\text{mL}}$$

RP2 - Fall Cone

Initial Solution: 0.75 mL Colloid 211 in 50 mL 0.002 M CaCl_2

$i := 0..4$

$$\text{Total}_{\text{monomers}}_0 := N_{\text{molecules}} \cdot 0.75 \text{ mL} \cdot n_{\text{monomer}}$$

$$\text{Total}_{\text{monomers}}_0 = 6.112 \times 10^{21}$$

$$\text{CaCl}_2 \text{Vol} := \begin{pmatrix} 50 \\ 63 \\ 9 \\ 7 \\ 5 \end{pmatrix} \cdot \text{mL} \quad \text{CaCl}_2 \text{Concen} := 0.002 \frac{\text{mole}}{\text{L}}$$

There is one mole of Ca^{2+} ions for every mole CaCl_2

$$\text{Calons}_i := \text{CaCl}_2 \text{Vol}_i \cdot \text{CaCl}_2 \text{Concen} \cdot N_{\text{av}} \quad \text{Calons} = \begin{pmatrix} 6.022 \times 10^{19} \\ 7.588 \times 10^{19} \\ 1.084 \times 10^{19} \\ 8.431 \times 10^{18} \\ 6.022 \times 10^{18} \end{pmatrix}$$

$$\text{Total}_{\text{monomers}}_{i+1} := \text{Total}_{\text{monomers}}_i - \text{Calons}_i$$

$$\text{CummCalons}_{i+1} := \text{CummCalons}_i + \text{Calons}_i$$

$$\text{Total}_{\text{monomers}} = \begin{pmatrix} 6.112 \times 10^{21} \\ 6.052 \times 10^{21} \\ 5.976 \times 10^{21} \\ 5.965 \times 10^{21} \\ 5.957 \times 10^{21} \\ 5.951 \times 10^{21} \end{pmatrix} \quad \text{CummCalons} = \begin{pmatrix} 0 \\ 6.022 \times 10^{19} \\ 1.361 \times 10^{20} \\ 1.469 \times 10^{20} \\ 1.554 \times 10^{20} \\ 1.614 \times 10^{20} \end{pmatrix}$$

$$\text{Ratio}_i := \frac{\text{CummCalons}_{i+1}}{\text{Total}_{\text{monomers}}_0} \quad \text{Ratio} = \begin{pmatrix} 9.852 \times 10^{-3} \\ 0.022 \\ 0.024 \\ 0.025 \\ 0.026 \end{pmatrix}$$

SA1 - Fall Cone

Initial Solution: 0.75 mL Colloid 211 in 50 mL 0.002 M CaCl_2

$$i := 0..4$$

$$\text{Total}_{\text{monomers}}_0 := N_{\text{molecules}} \cdot 0.75 \text{ mL} \cdot n_{\text{monomer}}$$

$$\text{Total}_{\text{monomers}}_0 = 6.112 \times 10^{21}$$

$$\text{CaCl}_2 \text{Vol} := \begin{pmatrix} 50 \\ 45 \\ 5 \\ 2 \\ 2.5 \end{pmatrix} \cdot \text{mL} \quad \text{CaCl}_2 \text{Concen} := 0.002 \frac{\text{mole}}{\text{L}}$$

There is one mole of Ca^{2+} ions for every mole CaCl_2

$$\text{Calons}_i := \text{CaCl}_2 \text{Vol}_i \cdot \text{CaCl}_2 \text{Concen} \cdot N_{\text{av}} \quad \text{Calons} = \begin{pmatrix} 6.022 \times 10^{19} \\ 5.42 \times 10^{19} \\ 6.022 \times 10^{18} \\ 2.409 \times 10^{18} \\ 3.011 \times 10^{18} \end{pmatrix}$$

$$\text{Total}_{\text{monomers}}_{i+1} := \text{Total}_{\text{monomers}}_i - \text{Calons}_i$$

$$\text{CummCalons}_{i+1} := \text{CummCalons}_i + \text{Calons}_i$$

$$\text{Total}_{\text{monomers}} = \begin{pmatrix} 6.112 \times 10^{21} \\ 6.052 \times 10^{21} \\ 5.998 \times 10^{21} \\ 5.992 \times 10^{21} \\ 5.989 \times 10^{21} \\ 5.986 \times 10^{21} \end{pmatrix}$$

$$\text{CummCalons} = \begin{pmatrix} 0 \\ 6.022 \times 10^{19} \\ 1.144 \times 10^{20} \\ 1.204 \times 10^{20} \\ 1.228 \times 10^{20} \\ 1.259 \times 10^{20} \end{pmatrix}$$

$$\text{Ratio}_i := \frac{\text{CummCalons}_{i+1}}{\text{Total}_{\text{monomers}}_0}$$

$$\text{Ratio} = \begin{pmatrix} 9.852 \times 10^{-3} \\ 0.019 \\ 0.02 \\ 0.02 \\ 0.021 \end{pmatrix}$$

GCC - Fall Cone

Initial Solution: 0.875 mL Colloid 211 in 50 mL 0.002 M CaCl_2

$$i := 0..4$$

$$\text{Total}_{\text{monomers}}_0 := N_{\text{molecules}} \cdot 0.875 \text{ mL} \cdot n_{\text{monomer}}$$

$$\text{Total}_{\text{monomers}}_0 = 7.131 \times 10^{21}$$

$$\text{CaCl}_2 \text{Vol} := \begin{pmatrix} 50 \\ 25 \\ 4 \\ 3 \\ 2 \end{pmatrix} \cdot \text{mL} \quad \text{CaCl}_2 \text{Concen} := 0.002 \frac{\text{mole}}{\text{L}}$$

There is one mole of Ca^{2+} ions for every mole CaCl_2

$$\text{Calons}_i := \text{CaCl}_2 \text{Vol}_i \cdot \text{CaCl}_2 \text{Concen} \cdot N_{\text{av}}$$

$$\text{Calons} = \begin{pmatrix} 6.022 \times 10^{19} \\ 3.011 \times 10^{19} \\ 4.818 \times 10^{18} \\ 3.613 \times 10^{18} \\ 2.409 \times 10^{18} \end{pmatrix}$$

$$\text{Total}_{\text{monomers}}_{i+1} := \text{Total}_{\text{monomers}}_i - \text{Calons}_i$$

$$\text{CummCalons}_{i+1} := \text{CummCalons}_i + \text{Calons}_i$$

$$\text{Total}_{\text{monomers}} = \begin{pmatrix} 7.131 \times 10^{21} \\ 7.071 \times 10^{21} \\ 7.041 \times 10^{21} \\ 7.036 \times 10^{21} \\ 7.032 \times 10^{21} \\ 7.03 \times 10^{21} \end{pmatrix}$$

$$\text{CummCalons} = \begin{pmatrix} 0 \\ 6.022 \times 10^{19} \\ 9.033 \times 10^{19} \\ 9.515 \times 10^{19} \\ 9.876 \times 10^{19} \\ 1.012 \times 10^{20} \end{pmatrix}$$

$$\text{Ratio}_i := \frac{\text{CummCalons}_{i+1}}{\text{Total}_{\text{monomers}}_0}$$

$$\text{Ratio} = \begin{pmatrix} 8.445 \times 10^{-3} \\ 0.013 \\ 0.013 \\ 0.014 \\ 0.014 \end{pmatrix}$$

PCC - Fall Cone

Initial Solution: 0.875 mL Colloid 211 in 50 mL 0.002 M CaCl_2

$$i := 0..4$$

$$\text{Total}_{\text{monomers}_0} := N_{\text{molecules}} \cdot 0.875 \text{ mL} \cdot n_{\text{monomer}}$$

$$\text{Total}_{\text{monomers}_0} = 7.131 \times 10^{21}$$

$$\text{CaCl}_2 \text{Vol} := \begin{pmatrix} 60 \\ 72 \\ 13 \\ 4 \\ 1.5 \end{pmatrix} \cdot \text{mL} \quad \text{CaCl}_2 \text{Concen} := 0.002 \frac{\text{mole}}{\text{L}}$$

There is one mole of Ca^{2+} ions for every mole CaCl_2

$$\text{Calons}_i := \text{CaCl}_2 \text{Vol}_i \cdot \text{CaCl}_2 \text{Concen} \cdot N_{\text{av}} \quad \text{Calons} = \begin{pmatrix} 7.226 \times 10^{19} \\ 8.672 \times 10^{19} \\ 1.566 \times 10^{19} \\ 4.818 \times 10^{18} \\ 1.807 \times 10^{18} \end{pmatrix}$$

$$\text{Total}_{\text{monomers}_{i+1}} := \text{Total}_{\text{monomers}_i} - \text{Calons}_i$$

$$\text{CummCalons}_{i+1} := \text{CummCalons}_i + \text{Calons}_i$$

$$\text{Total}_{\text{monomers}} = \begin{pmatrix} 7.131 \times 10^{21} \\ 7.059 \times 10^{21} \\ 6.972 \times 10^{21} \\ 6.956 \times 10^{21} \\ 6.951 \times 10^{21} \\ 6.95 \times 10^{21} \end{pmatrix} \quad \text{CummCalons} = \begin{pmatrix} 0 \\ 7.226 \times 10^{19} \\ 1.59 \times 10^{20} \\ 1.746 \times 10^{20} \\ 1.795 \times 10^{20} \\ 1.813 \times 10^{20} \end{pmatrix}$$

$$\text{Ratio}_i := \frac{\text{CummCalons}_{i+1}}{\text{Total}_{\text{monomers}_0}} \quad \text{Ratio} = \begin{pmatrix} 0.01 \\ 0.022 \\ 0.024 \\ 0.025 \\ 0.025 \end{pmatrix}$$

Viscosity

Initial Solution: 1.87 (RP2 and SA1) or 1.951mL (GCC and PCC) Colloid 211 in 464 mL 0.002M CaCl_2

$$j := 0..1$$

$$n_{\text{monomer}} = 35.394$$

Total number of NaPAA monomers (potential binding sites for Ca^{2+} ions)

$$\text{Vol211} := \left(\frac{1.87}{1.951} \right) \cdot \text{mL}$$

$$T_{\text{monomers}_j} := N_{\text{molecules}} \cdot \text{Vol211}_j \cdot n_{\text{monomer}}$$

$$T_{\text{monomers}} = \begin{pmatrix} 1.524 \times 10^{22} \\ 1.59 \times 10^{22} \end{pmatrix}$$

Volume of 0.002M CaCl_2 solution added to mineral solids:

$$\text{CaCl2Vol} := 464 \text{ mL}$$

$$\text{CaCl2Concen} := 0.002 \frac{\text{mole}}{\text{L}}$$

There is one mole of Ca^{2+} ions for every mole CaCl_2

$$\text{Calons} := \text{CaCl2Vol} \cdot \text{CaCl2Concen} \cdot N_{\text{av}}$$

$$\text{Calons} = 5.588 \times 10^{20}$$

Ratio of Ca^{2+} ions to total number of COO^- sites (potential binding sites)

$$R_j := \frac{\text{Calons}}{T_{\text{monomers}_j}}$$

$$R = \begin{pmatrix} 0.037 \\ 0.035 \end{pmatrix}$$

Sedimentation

Initial Solution: 50 μ L Colloid 211 in 84.49 mL 0.002M CaCl_2

$$n_{\text{monomer}} = 35.394$$

Total number of NaPAA monomers (potential binding sites for Ca^{2+} ions)

$$\text{Vol211} := 0.05 \text{ mL}$$

$$T_{\text{monomers}} := N_{\text{molecules}} \cdot \text{Vol211} \cdot n_{\text{monomer}}$$

$$T_{\text{monomers}} = 4.075 \times 10^{20}$$

Volume of 0.002M CaCl_2 solution added to mineral solids:

$$\text{CaCl}_2 \text{Vol} := 84.49 \text{ mL}$$

$$\text{CaCl}_2 \text{Concen} := 0.002 \frac{\text{mole}}{\text{L}}$$

There is one mole of Ca^{2+} ions for every mole CaCl_2

$$\text{Calons} := \text{CaCl}_2 \text{Vol} \cdot \text{CaCl}_2 \text{Concen} \cdot N_{\text{av}}$$

$$\text{Calons} = 1.018 \times 10^{20}$$

Ratio of Ca^{2+} ions to total number of COO^- sites (potential binding sites)

$$R := \frac{\text{Calons}}{T_{\text{monomers}}}$$

$$R = 0.25$$

CHAPTER 6

TWO-MINERAL MIXTURES WITHOUT POLYMER

Previous chapters address fabric formation and implications in single-mineral systems. The study of mineral mixtures requires a detailed understanding of chemical interactions and ensuing fabric formation. This knowledge is relevant to many soil environments and the possible development of engineered soil fabrics. The study of mixed mineral systems without additives is undertaken herein. Chapter 7 extends this investigation to the case of mixtures with polymers. The purpose of this chapter is to study kaolinite-calcium carbonate mixtures across a range of applied strain conditions to determine the governing mechanisms affecting fabric formation. The choice of mixture components reflects the distinct pH dependency in kaolin and calcium carbonate. This study will address differences in particle shape, size, mineralogy, and relative masses in addition to the mixtures response to various strain levels.

6.1 Introduction

6.1.1 Mineral Mixtures

Many studies have addressed mixtures of coarse-and-fine grains. The strength, index properties and other characteristics of clayey soils can be altered by the addition of sands. For example, the compressive strength of a clay is improved and the liquid limit is decreased with increasing sand percentage (Leelanitkul, 1989). Properties such as compressional wave velocity and porosity are also influenced by the relative proportions in sand-clay mixtures. Marion et al. (1992) find that for Ottawa sand-kaolinite mixtures a minimum porosity is reached in the range of 20 to 40 percent clay by weight. A

maximum P-wave velocity is measured at 40% clay content, and it is higher than that of pure sand or pure clay. The influence of specific surface on the liquid limit of mineral mixtures is observed by Vipulanandan and Leung (1991). Replacing 40 percent of a kaolin clay by weight with sand reduces the liquid limit from 57% for the pure kaolin clay to 47% for the mixture. At 30/70 kaolin/sand, the liquid limit is further reduced to 33%. But, adding just 6% bentonite to the 30/70 mixture increases the liquid limit to 61%.

Clay-sand mixtures are also important in the study of particle detachment and erodibility. Bradford and Blanchar (1999) conduct mini-flume tests on clay-sand mixtures and find erodibility decreases with increasing clay content and increases with decreasing ionic concentration for Ca-illite and Ca-montmorillonite. Changing the pore fluid ionic concentration had no effect on the erodibility of either Ca-kaolinite or Na-montmorillonite. Ca-clay forms (montmorillonite, kaolinite, illite) were more erodible than their Na- forms.

Mixtures of two different fine-grained minerals are equally intriguing. The rheological properties of clay suspensions are particularly sensitive to the presence of other clay minerals. For example, adding montmorillonite to kaolinite suspensions (moderate solids content) alters the flow behavior by electrostatically linking with the kaolin particles to form associations and/or decreasing the freely flowing fluid volume by adsorbing water molecules from the pore fluid (Keren, 1989). The rheological behavior of palygorskite suspensions also depends on the added concentration of montmorillonite (Neaman and Singer, 2000): a small percentage of montmorillonite (<10% by weight) increases the number of particle interactions, whereas a larger percentage (10 to 20%)

decreases the plastic viscosity and Bingham yield value. A very high percentage of montmorillonite (20 to 40%) results in constant viscosity values.

Other minerals may be added to clays to alter their properties. Since the liquid limit of a clay material is proportional to the total specific surface (Muhunthan, 1991), the liquid limit can be increased just by adding a high specific surface clay such as bentonite (Ahmad et al., 2000). Using rheological measurements of montmorillonite-coal mixtures, de Kretser et al. (1998) determine that the presence of finely ground coal particles reduces the montmorillonite suspension thixotropic tendencies by reducing the degree of platelet particle orientation. The liquid limit of London clay can be increased with only 1% lime by weight, although additional lime decreases the liquid limit (lime has a much greater effect on the plastic limit of montmorillonitic soils than on kaolinitic clays – Bell and Coulthard, 1990). Pamukcu et al. (1990) study mixtures of flyash and kaolin and observe that flyash can increase kaolinite shear modulus (up to 20% flyash) and coefficient of permeability (up to 10% flyash). The shear modulus and coefficient of permeability both decrease with additional flyash.

Some of these mixtures promote important chemical reactions. Chu and Kao (1993) determine the optimum mixture of a low plasticity clay, slag and flyash for soil improvement. The flyash used has a low CaO content, so when added to the clay alone no increase in the unconfined compressive strength is observed. Adding slag, a high CaO-containing material, to the mixture increases the pozzolanic reaction and induces an increase in the unconfined compressive strength with time.

Mineral mixtures are extensively used in paper coatings. A paper coating suspension contains pigments, binders, and other additives (Andersson, 1993). Kaolin

clay and calcium carbonate are two of the most widely-used pigments. Pigment mixtures are chosen to enhance certain optical properties of the coated paper including brightness, whiteness, smoothness, gloss, opacity, and ink receptivity. Table 6.1 defines select optical properties, their measurement techniques and the controlling factors for each. The quality of these properties depends on the relative refractive indices of the coating components, the number of optical interfaces, light scattering capability, final pore volume, size and distribution, particle shape, size distribution, aspect ratio, and packing (Scott, 1996; Hagemeyer, 1984). Table 6.2 lists some typical characteristics of kaolin clays and calcium carbonates as coating materials.

6.1.2 Particle Shape

A key element influencing the final fabric of mineral mixtures is particle shape. Hagemeyer (1960) studies the effects of particle shape on mixtures of platy and needle-like particles. By measuring centrifuged sediment volumes and viscosity of kaolinite-calcium carbonate blends with dispersants, Hagemeyer finds that: (1) particle shape affects the final fabric and (2) the trend in sediment volume parallels the trend in viscosity, that is, both the sediment volume and the viscosity peak with a slight addition (20% of total solids) of needle-like carbonate particles and then decrease with additional carbonate. But, Huber and Weigl (1972) measure the same trend in relative sediment volume of dispersant-treated kaolin and *ground* calcium carbonate mixtures. This suggests that more than particle shape accounts for the general appearance of a maximum at the 20/80 carbonate/clay ratio. Without the dispersant, Huber and Weigl (1972) find a general decrease in relative sediment volume with increasing carbonate percentage. Yuan and Murray (1997) find similar results in that they observe a viscosity peak at a low

Table 6.1 Typical Measured Optical Coating Properties

| Optical Property | Definition | Measurement Technique(s) | Controlling Factors |
|--------------------------|---|--|--|
| Brightness | Reflectivity of paper surface. Reflectance of light in the range of 400-500 nm, with the receptor sensitivity peaked at 457 nm (blue light), by white or nearly white paper under standard conditions ^a . | <ul style="list-style-type: none"> A reflectance factor is determined with either directional or diffuse lighting methods (centered at 457 nm wavelength) and measuring the percentage of reflected light between 400 and 500 nm^{a,b}. | <ul style="list-style-type: none"> Relative refractive indices/light scattering coefficients of coating components^c Pore volume/size^d Degree of uniformity of distribution of air-filled pores^d |
| Whiteness | Paper color deviation from neutral (i.e., amount of red or green reflectance). Degree to which surface equally reflects all wavelengths in visible spectrum ^a . | <ul style="list-style-type: none"> The reflectance of paper across the visible spectrum (400 to 700 nm) is measured, and a tint deviation factor is calculated^a. Specific methodologies include CIE Whiteness, Hunter Whiteness, Stensby Whiteness, Ganz Whiteness^e. | <ul style="list-style-type: none"> Relative refractive indices of coating constituents^c Presence or lack of iron or other metals^d Degree of uniformity of distribution of air-filled pores^d |
| Smoothness/ Roughness | Paper surface topography and the degree of planar surface structure ^a . | <ul style="list-style-type: none"> Air leak method. The rate of air flow between the paper surface and a polished metering land is measured. Since air flows between two parallel surfaces at a rate proportional to their separation distance (cubed), the measured flow provides a means of estimating the average separation distance, and hence, the deviation from the ideal planar surface^f. | <ul style="list-style-type: none"> Particle orientation – particles should be parallel at the coating surface to create a smoother finish^d Particle shape and size – need fine, thin, small-diameter particles for high smoothness^d Particle size distribution – need uniform psd^d Gloss – smoothness improves with gloss in a nonlinear relationship^d |

Table 6.1 (cont'd)


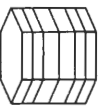


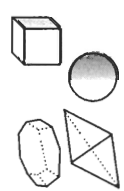
| Optical Property | Definition | Measurement Technique(s) | Controlling Factors |
|------------------|---|--|--|
| Gloss | <p>Surface luster. When reflection angle of light equals the incidence angle, the light reflects specularly. Gloss is the amount of specular reflectance from the surface at a given angle^a.</p> | <ul style="list-style-type: none"> 75° specular gloss method – used for low- to high-gloss papers; incident and capture angles are 75° from the plane normal to the paper surface. Light from a lamp is condensed to illuminate a paper sample at an angle 15° from the plane of the paper. A light detector is used to capture and measure the intensity of light reflected from the paper surface. Measurements are reported as gloss units^a. 20° specular gloss method – used for very high-gloss papers^a. Goniophotometry – measurement of the distribution of reflected light intensity with high angular resolution; the narrower the distribution, the glossier the surface^e. | <ul style="list-style-type: none"> Aspect ratio – need thin kaolin platelets for high gloss. Stacked particles/booklets decrease gloss^d. Particle size distribution – need uniform psd^d. Pore volume – need large pore volume for high specular reflectance^d. Amount of ultrafines (< 0.2µm) – may increase or decrease gloss depending on percentage^h. |

Table 6.1 (cont'd)

| Optical Property | Definition | Measurement Technique(s) | Controlling Factors |
|------------------|---|--|---|
| Opacity | Ability of paper to block the passage of light. Opacity is the reciprocal of the amount of transmitted light ^a . | <ul style="list-style-type: none"> A reflectance factor ratio is determined by first measuring the reflectance with a device whose sensitivity corresponds to the response of a healthy eye, i.e. at light wavelengths 400-700 nm centered at 557 nm. A second reflectance factor is then measured using a single sheet against a black backing^a. The contrast ratio is the ratio of the reflectance of a single sheet measured against a black backing and the measured reflectance of the same sheet using a backing with a reflectance of 89%^a. | <ul style="list-style-type: none"> Particle packing (size, shape, distribution)^d Particle Structuring (pore volume/size)ⁱ Refractive indices of individual coating components^c Difference in refractive indices of components, including air, forming an optical interface^c. Number of optical interfaces. Light scatter increases with greater differences in refractive indices and increasing number of optical interfaces^c. |

^aLevlin and Söderhjelm (1999), ^bConners and Banerjee (1995), ^cScott (1996), ^dHagemeyer (1984), ^eBranston. (1999), ^fTesting Machines (2002), ^gWygant, et al. (1998), ^hMalla, et al. (1999), ⁱRiggin (1999).

Table 6.2 Properties of Select Kaolin and Calcium Carbonate Pigments

| Material | Particle Shape ^{a,b} | Average Particle Size μm | Refractive Index | Scattering Coefficient cm^2/g | Brightness s % | Surface Area m^2/g | IEP |
|--|---|---|---------------------|---|----------------------|--|---|
| Kaolin $G_s=2.62^c$ |  pseudo-hexagonal platelets | 0.2 – 2.0 diameter, 0.05 – 0.2 thickness $S_s=10 - 25 \text{ m}^2/\text{g}$ | 1.57 | 1100 – 1200 | 78 – 90 | 10 – 25 | ~ 7.2 (edge) ^d ~ 4 (face/ particle) ^d |
| |  stacks/booklets | 0.5 – 10 thickness | | | | | |
| Calcined Clay $G_s=2.6^b$ |  bulky, porous aggregated kaolin plates | 0.7 – 1.5 $S_s=15 - 25 \text{ m}^2/\text{g}$ | 1.56 | 2600 – 3000 | 90 – 95 | 15 – 25 | |
| Natural/ Ground CaCO_3 $G_s=2.6 - 2.8^b$ |  hexagonal-scalenohedral | 0.7 – 3.0 $S_s=2 - 12 \text{ m}^2/\text{g}$ | 1.59 | 1400 – 1700 | 80 – 95 | 2 – 12 | 8.5, 10.8 ^e |
| Precipitated CaCO_3 $G_s=2.71^b$ |  scalenohedral prismatic/rhombic spherical, cubic | 0.3 – 3.0 $S_s=5 - 25 \text{ m}^2/\text{g}$ | 1.59 | 2200 – 2700 | 96 – 100 | 5 – 25 | pCa=4.4 ^f |

After Scott (1996) with additional information from ^aAndersson (1993), ^bHagemeyer (1997), ^cHagemeyer (1984), ^dSantamarina et al. (2001), ^eLangmuir (1997), ^fSanders (1991).

percentage of spherical particles in mixtures of spherical halloysite and platy kaolinite dispersed with sodium hexametaphosphate.

6.1.3 Size

In addition to shape, the relative sizes of particles in mixtures affect the overall behavior of mineral suspensions. Alinec and Lepoutre (1983b) illustrate that high-solids dispersed suspensions of clay or latex particles of like shape (platy or spherical) but different sizes exhibit a viscosity minimum at a particular mixing ratio (Figure 6.1). Blends of platy and spherical particles (clay and latex) at low shear exhibited a general viscosity increase with decreasing spherical particle diameter. Depending on the relative size of the spherical particles, either the viscosity increased, reached a maximum, then decreased as the fraction of spherical particles increased ($d_{\text{esd}}:d=7$ and 2 clay:latex), or the viscosity decreased with increasing latex content ($d_{\text{esd}}:d=1.4$ clay:latex). Tari et al. (1998) show similar behaviors for mixtures of fine silica sand and kaolin: viscosity decreases and shear thinning takes place with increasing percentages of silica sand.

6.2 Materials and Procedures

6.2.1 Materials

Mineral mixtures are prepared with two kaolin clays, Wilklay SA1 and Wilklay RP2, and two calcium carbonates, GCC #12 White (ground) and PCC Rhombic (precipitated). The properties of these materials are presented in Chapter 3.

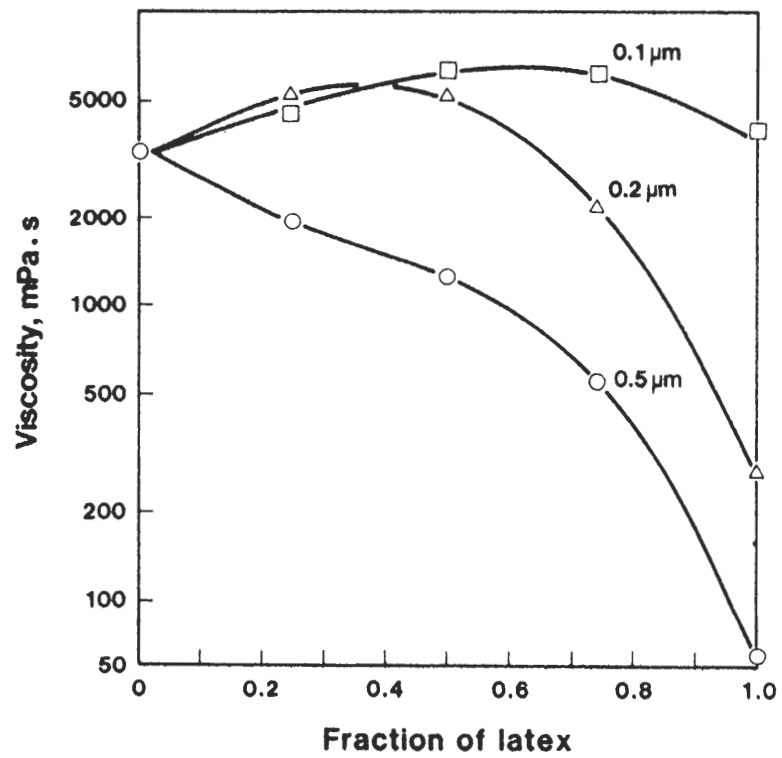


Figure 6.1 Viscosity of dispersed kaolinite-latex sphere mixtures. The clay mean equivalent spherical diameter $d_{esd}=0.7\mu\text{m}$. Sphere diameters are 0.1, 0.2 and $0.5\mu\text{m}$, and total solids volume content $\phi=0.55$ (Aline and Lepoutre, 1983a and b).

6.2.2 Sedimentation

Two mixture series of sedimentation tests are performed: (1) RP2 and GCC and (2) SA1 and GCC.

RP2 and GCC. Wilklay RP-2 and GCC #12 White are mixed together in proportions of 0:100, 10:90, 20:80, 30:70, 40:60, 50:50, 60:40, 70:30, 80:20, 90:10, and 0:100 clay:carbonate by mass. The total mass of solids in each mixture is 5 g, and the final solids content in each suspension is approximately 0.02.

SA1 and GCC. The same procedures are followed to prepare Wilklay SA1 and GCC #12 White mixtures, but a reduced sequence is used: 100, 75:25, 50:50, 25:75, and 0:100% clay:carbonate by mass.

6.2.3 Viscosity

Suspensions are prepared with kaolinite SA1 to PCC mass ratios of 0:100, 25:75, 50:50, 75:25, and 100:0%.

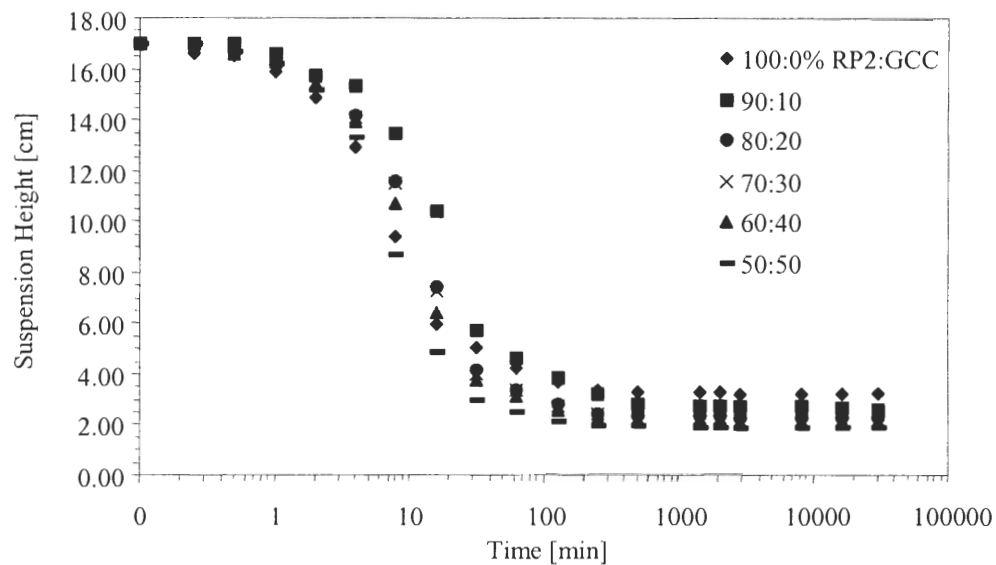
6.2.4 Liquid Limit

Kaolinite SA1 and PCC are mixed together at 0, 20, 40, 60, and 100% clay by mass.

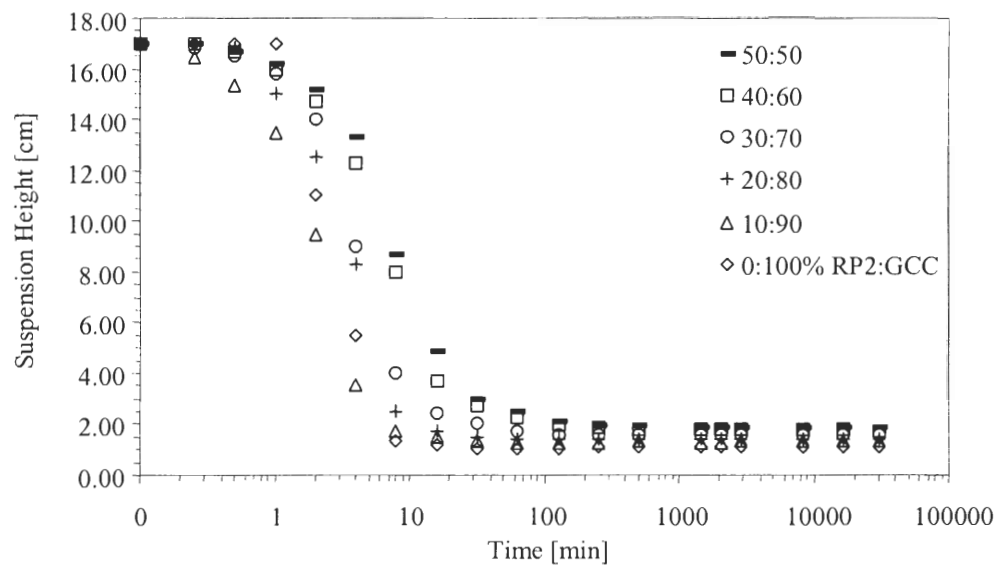
6.3 Experimental Results

6.3.1 Sedimentation Tests

Mixtures of RP2 and GCC. The RP2-GCC sedimentation curves are presented in Figure 6.2, and the observed sedimentation behavior for each suspension is summarized in Table 6.3. The observed sedimentation behavior of all suspensions containing GCC is mixed-mode, with most of the settling characteristics consistent with flocculation



(a)



(b)

Figure 6.2 Sedimentation curves at 21 days for RP-2-GCC mixtures (a) 100% RP2 through 50% RP2 and (b) 50% RP2 through 100% GCC by mass.

Table 6.3 Observed Sedimentation Behavior for RP2-GCC Mixtures

| Suspension RP2:GCC | Observed Characteristics During Settlement | | | | Sedimentation Type |
|-----------------------|--|---|---------------------------------------|--|-----------------------|
| | Suspension-Supernatant Boundary | Supernatant | Suspension | Settlement Type | |
| 100:0 (100% RP2) | Sharp | Clear | Heterogeneous, yet dense structure | Slow consolidation | Flocculation |
| 90:10 | Slightly indistinct | Initially, few fines visible, clear after 24 hours | Heterogeneous, yet dense structure | Slow consolidation | Mixed-Mode |
| 80:20 | Slightly indistinct; boundary clear at 30 minutes | Initially, fines visible, clear after 24 hours | Heterogeneous, yet dense structure | Slow consolidation | Mixed-Mode |
| 70:30 | Indistinct, boundary clear at 30 minutes | Fines content greater than in 80:20, clear after 24 hours | Heterogeneous, yet dense structure | Slow consolidation | Mixed-Mode |
| 60:40 | Indistinct, boundary clear at 30 minutes | Fines content greater than 70:30, clear after 24 hours | Heterogeneous, yet dense structure | Slow consolidation | Mixed-Mode |
| 50:50 | Indistinct, boundary clear at 30 minutes | Fines content greater than 60:40, clear after 24 hours | Heterogeneous, yet dense structure | Slow consolidation | Mixed-Mode |
| 40:60 | Indistinct, boundary clear at 30 minutes | Fines content greater than 50:50, clear after 24 hours | Heterogeneous, yet dense structure | Slow consolidation | Mixed-Mode |
| 30:70 | Completely indistinguishable, boundary clear at 30 minutes | Fines content greater than 40:60, clear after 24 hours | Heterogeneous, yet dense structure | Slow consolidation | Mixed-Mode |
| 20:80 | Completely indistinguishable, boundary clear at 30 minutes | Fines content greater than 40:60, clear after 24 hours | Heterogeneous, yet dense structure | Slow consolidation | Mixed-Mode |
| 10:90 | Completely indistinguishable, boundary clear at 30 minutes | Fines content greater than 40:60, clear after 24 hours | Heterogeneous, yet dense structure | Slow consolidation | Mixed-Mode |
| 0:100 (100% GCC) | Indistinct | Very cloudy, clear after 24 hours | Increasing density from top to bottom | Sediment accumulation at cylinder bottom | Dispersed |

sedimentation. Only the 100% clay suspension exhibited true flocculation sedimentation, i.e. a sharp supernatant-suspension boundary (no observable fines in the supernatant) and a uniform density suspension that slowly consolidates to the final sedimentation height. No mineral segregation is observed for any of the suspensions. With increasing mass of GCC, the observed sedimentation behavior becomes more dispersed, although none of the mixtures displayed truly dispersed settlement conditions, the supernatant-suspension boundary became less distinct, and more fines remained in suspension as most particles settled. The bulk suspensions for all mixtures settled as the 100% clay suspension, that is, slow consolidation. In addition, each suspension had a uniform appearance and within 24 hours, no suspended fines were visible in any of the suspensions.

The initial settlement velocity α is a measure of the degree of particle associations just before the particles, flocs or aggregates begin to settle, and provides some insight into the suspension state of dispersion (Chapter 4). Figure 6.3 plots α for each of the RP2-GCC suspensions. Overall, the initial settling velocity tends to decrease with increasing clay mass percentage. The settlement velocity then indicates an increasingly flocculated behavior with increasing relative clay mass.

The sedimentation height also suggests the state of dispersion (Chapter 3). The sedimentation heights 24 hours after test initiation presented in Figure 6.4 (no visible particles remain in suspension) show the increasing sediment height with increasing clay mass percentage. The comparison between 100% carbonate and 100% clay sediment heights is consistent with the observed flocculation behavior of the clay suspension and the dispersive behavior of the GCC.

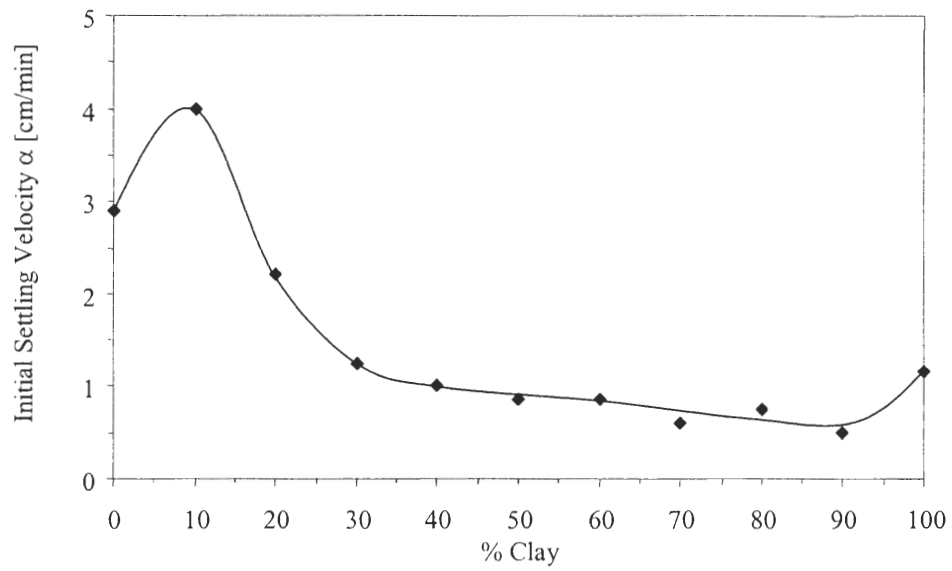


Figure 6.3 Mixture Suspensions – RP2-GCC Initial Settling Velocity α .

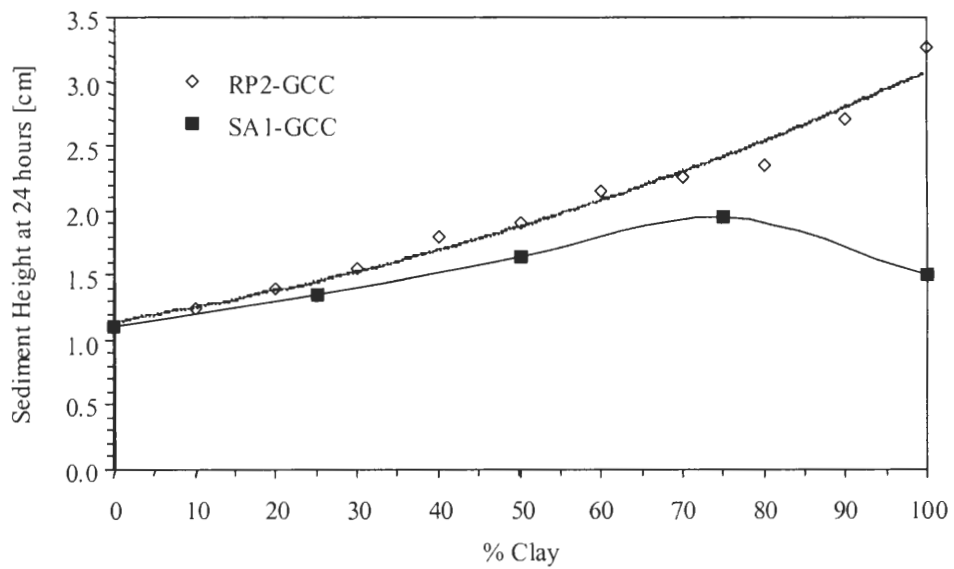


Figure 6.4 Sediment heights for RP2-GCC and SA1-GCC mixtures at 24 hours.

At relative masses greater than just a few percent, calcium carbonate dissolution dominates the pore fluid pH by consuming H^+ according to the reaction (Bohn et al., 1985)



Figure 6.5 plots the measured supernatant pH for all RP2-GCC suspensions. Without any added clay, the measured supernatant pH is 8.09 and changes very little from 10 to 90% clay (pH = 7.88 to 7.55). The self-buffering pH of kaolinite RP2 is pH=4.4.

Mixtures of SA1 and GCC. The observed sedimentation behavior of the SA1-GCC mixtures is significantly different than that of the RP2-GCC mixtures (Figure 6.6). All of the suspensions in this series exhibit primarily dispersed sedimentation behavior. In particular, the 100% SA1 suspension exhibits all major characteristics of dispersed settlement including minimal particle interactions (as evident by the suspension homogeneous milky appearance), the suspension density increases from the top to bottom without a clear suspension-supernatant boundary, and there is a clear sediment build-up at the bottom of the cylinder. Decreasing the clay content has little effect on the observed behavior except that the induction time decreases. No mineral segregation is observed in the sediment for any of the mixtures.

The length of the induction period of kaolinite slurries has been associated with the degree of particle associations in that the greater the flow unit density, the longer the induction period, particularly with increasing ionic concentration and increasing counterion valence (Klein, 1999). But, for a completely dispersed system, the induction period will also be relatively long due to interparticle repulsion. Due to the extended

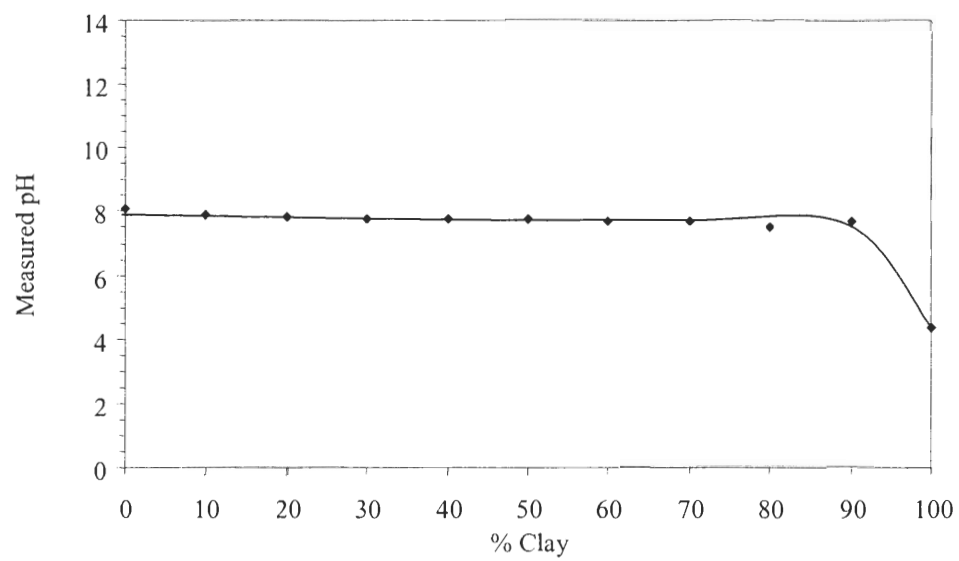
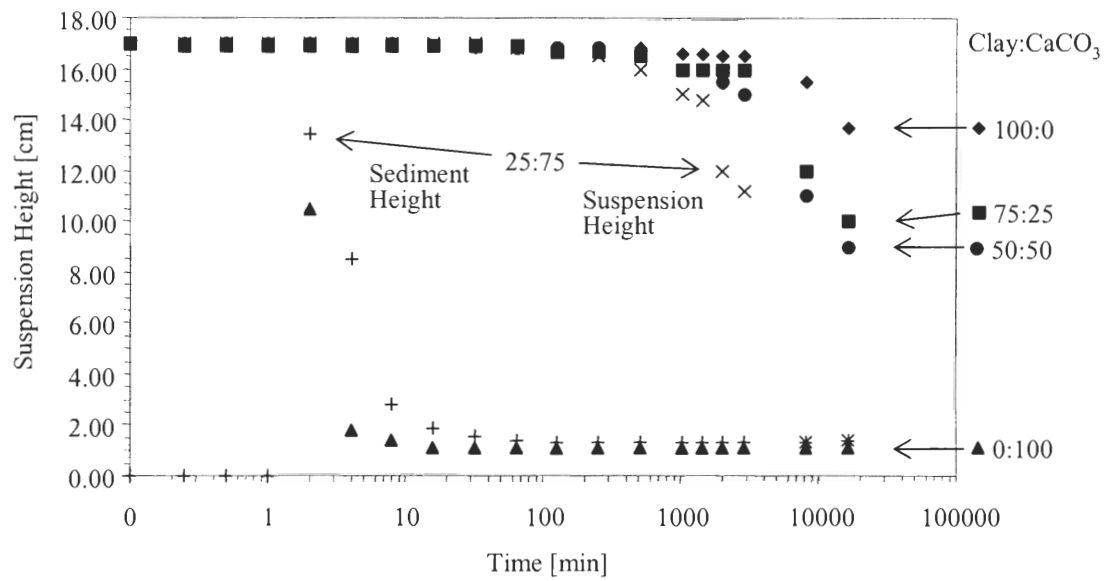
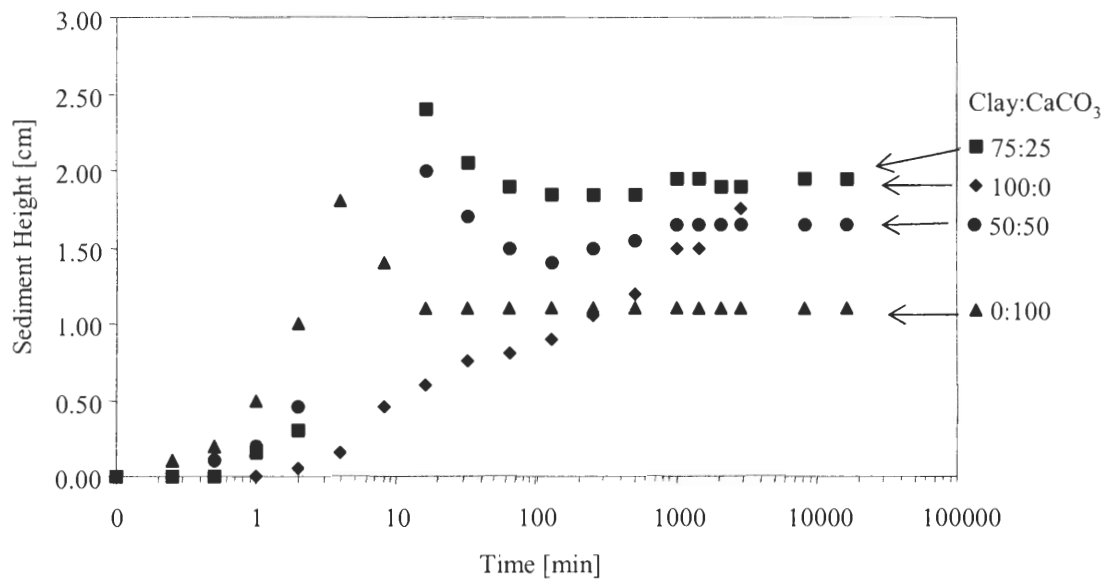


Figure 6.5 Supernatant pH of RP2 Kaolinite -GCC Mixtures.



(a)



(b)

Figure 6.6 Sedimentation curves at 11.4 days for SA1-GCC mixtures. (a) Suspension height and (b) sediment height.

induction periods of the SA1-GCC series, the settlement velocity for most of the suspensions is not evident.

The 100% SA1 kaolin slurry remains dispersed at the self-buffered pH of 6.5. With increasing GCC content, the induction time decreases indicating an increase in the level of flocculation.

The sedimentation height of the SA1-GCC mixture series at 24 hours is shown in Figure 6.4. Even though the suspensions have not completely settled at this time, the trend is similar to the RP2-GCC mixtures: the 24-hour sediment height increases with increasing kaolin content. Note that a relatively low sediment height is expected for the 100% kaolin suspension (as compared to the same suspension at flocculation pH and ionic concentration).

6.3.2 Rheological Tests

Viscosity measurements for the SA1-PCC mixtures are shown in Figure 6.7. The viscosity measurements of the 100% kaolinite suspension at 50, 60, and 100 RPM is approximately constant ($\mu \approx 28 \text{ mP}\cdot\text{s}$) and suggests the suspension is fairly dispersed. The remaining suspensions are shear thinning, i.e. their measured viscosity decreases with increasing shear rate. This means that the suspensions hold at least some flocculated structure that brakes down with increasing strain brought about by the rotating spindle. Data points for each suspension tested here fall along near-parallel lines on the log-log plot. The vertical position of each line gives an indication of the relative state of dispersion. The number of particle associations increases in the order of 100, 75, 50, 0, and 25% of SA1 kaolin.

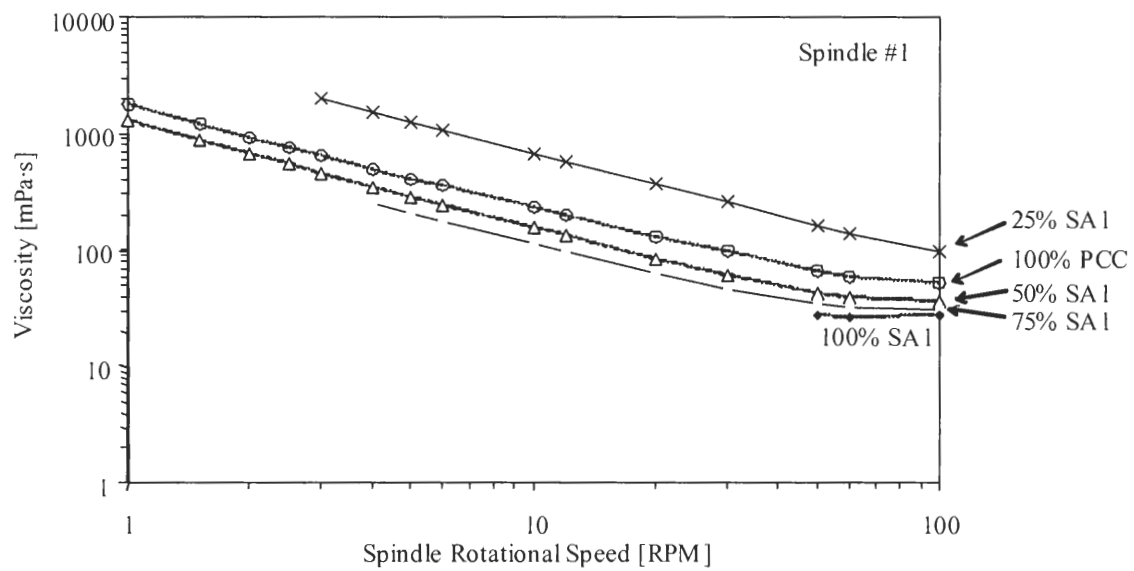


Figure 6.7 Viscosity measurements of SA1-PCC mixtures.

6.3.3 Liquid Limit

The liquid limits for the given SA1-GCC mineral mixtures are shown in Figure 6.8. The liquid limit increases with increasing clay content from 20 to 100% kaolinite. This finding is consistent with that of Arkin and Michaeli (1989) who test mixtures of untreated chalk and kaolinite.

The slopes of the liquid limit lines for the tested mixtures are also plotted in Figure 6.8. As the clay content increases from 20 to 100%, the slope decreases. The relative trend (increasing liquid limit corresponding to decreasing slope) is consistent with the trend observed in Chapter 3.

6.4 Discussion

6.4.1 Sedimentation

RP2 and GCC. While the kaolin has some buffering capacity (towards pH ~ 4.4), the presence of CaCO₃ has a controlling effect on pH (Figure 6.5). Any decrease in pH caused by the presence/dissolution of the clay mineral only enhances the CaCO₃ dissolution and thereby again increasing the solution pH.

At a solution pH above the edge isoelectric point, kaolin particles tend to remain dispersed having a net negative charge along both the basal and edge planes. For the pH conditions presented in Figure 6.5, the RP2 kaolin particles tend toward a dispersive behavior (refer to Chapter 4). However, the negatively-charged kaolin particles most likely interact with the positive surface sites of the GCC particles. With a small introduction of kaolinite (10%), and considering the mutual attraction between the two mineral types, the kaolin particles are quickly bound to the carbonate surfaces. The

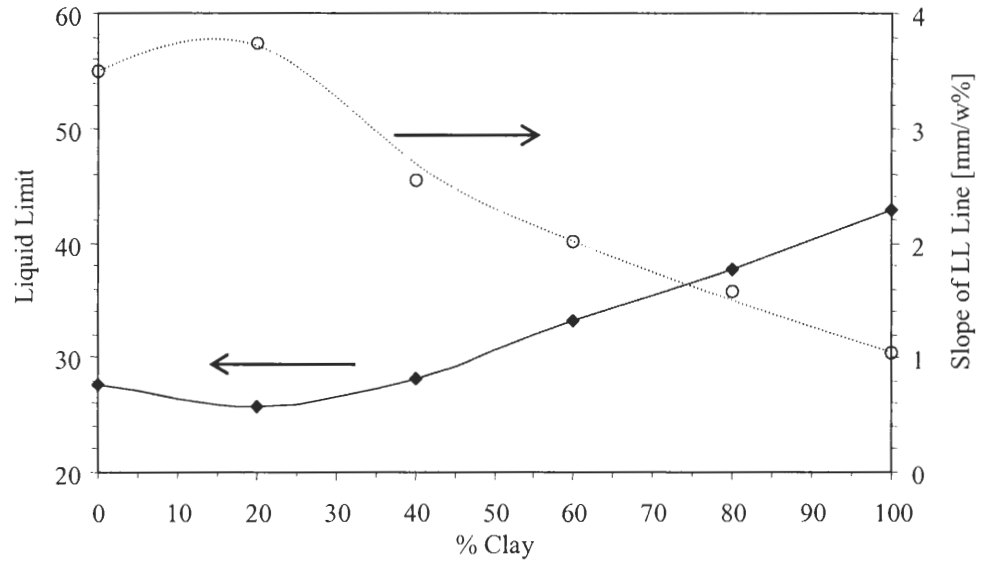


Figure 6.8 Liquid limits for SA-1-GCC mixtures and sensitivity to moisture

intermineral association produces a larger flow unit and so settles in a more open, voluminous structure. The greater the clay content, the larger the flow units and final sediment height. This hypothesis is consistent with the observed trend in settling velocity. But, at 100% clay content, the solution pH is ~ 4.4 and the particles in this case have more likely flocculated in a very open EF configuration.

SA1 and GCC. The electrostatic interactions between the positive GCC particle surfaces and the negatively-charged kaolinite particles (Figure 6.9) result in an increasingly flocculated system as indicated by the decreasing induction time as well as increasing sediment height.

6.4.2 Rheology

SA1 and PCC. Recall from Chapter 3 that the SA1 $d_{50}=1.1\ \mu\text{m}$ and PCC $d_{50}=1\ \mu\text{m}$. The mineral mixture with the largest measured viscosity is the suspension containing 25% SA1 kaolin. This is consistent with observations made by Alinec and Lepoutre (1983b) for clay- CaCO_3 mixtures (the two minerals having similar equivalent spherical diameters), at both a $\phi=0.50$ and $\phi=0.55$ total solids volume content. The high solids content is due to the presence of a dispersant. Their findings include: (1) the 100% carbonate suspension had the lowest viscosity, (2) the maximum measured viscosity is at the 50:50 carbonate:clay blend and not at endpoints (either 100% carbonate or 100% clay). Hence, for similarly-sized particles mixing the two minerals at some critical ratio creates a greater degree of structure than in either of the single mineral cases.

As in the sedimentation cases, the presence of carbonate enhances the degree of particle associations. Whereas the 100% carbonate suspension at low ϕ exhibited dispersive characteristics, at moderate solids content the suspension has almost the same

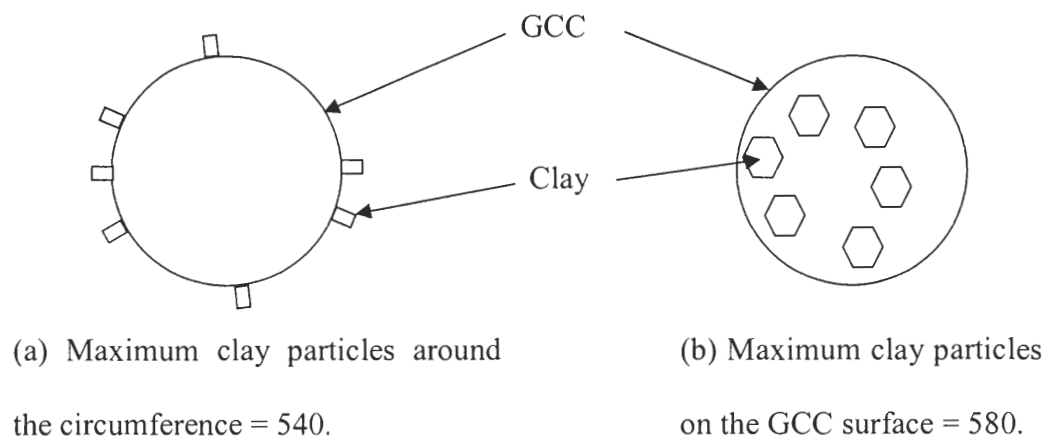


Figure 6.9 Possible particle associations between SA1 and GCC and maximum number of particle attachments: (a) clay particle edge to GCC face and (b) clay particle face to GCC face. Maximum number of particle attachments assuming clay particle thickness $t=0.07 \mu\text{m}$ (estimated from SEM micrograph), and spherical GCC shape with $d=12 \mu\text{m}$.

resistance to shear as the 25:75 clay-carbonate mixture. This is not likely due to actual flocculation of particles (as the carbonate particles have similar charge), but rather due to the shape of the particles: while the particles are elongated and may align with the fluid streamlines, their diameter (perpendicular to the long axis) is approximately one-third to one-half the particle length (Figure 3.4-b). While both particle types may align with the streamlines, the PCC diameter is thick enough to perturb the fluid streamlines more than the platy clay particles do.

6.4.3 Liquid Limit

SA1 and GCC. Given that the SA1 clay has a specific surface of $13.0 \text{ m}^2/\text{g}$ (Klein, 1999) and the GCC has a specific surface of approximately $0.2 \text{ m}^2/\text{g}$, replacing just 20% of the mass of GCC with clay (100 to 80% GCC) significantly increases the total mineral surface area. Hence, increasing the amount of added clay greatly increases the amount of surface area and therefore the amount of water necessary to coat the particles. However, the liquid limit at 100% GCC is slightly higher than at 20% kaolinite. At this clay percentage, the particles may just be primarily coating the larger carbonate particles.

Changing the relative amount of clay, and therefore the total surface area, in the mineral mixture system is only one mechanism by which the liquid limit is altered. Clay-to-clay particle aggregation stemming from dissolved Ca^{2+} ions collapsing their double layers also reduces the liquid limit. Consequently, this mechanism influences the fabric formation of clay-carbonate blends.

6.5 Conclusions

The behavior of kaolinite-calcium carbonate mineral mixtures depends on the type of kaolin, the shape of the carbonate particles and the relative solids content. At low solids content, mixtures containing the RP2 clay have the characteristics of flocculated systems, while those containing SA1 clay are more dispersed (although not *purely* dispersed) with some variation from mixture to mixture. Electrostatic interactions between the positively charged calcium carbonate surfaces and the negatively charged particles, at carbonate-induced pH conditions, are the main mechanisms for particle flocculation. The clay volume fraction at low solids content determines the number of particles associations; a voluminous fabric can be achieved with low percentages of carbonate.

The degree of particle interaction does not increase linearly with increasing clay content. In fact, at moderate ϕ flocculation of the kaolinite particles increases with increasing carbonate content, but with maximum particle interactions at some apparent clay-carbonate ratio.

At high solids content, increasing the relative mass of calcium carbonate within the soil mixture significantly reduces the surface area. The reduction in surface area along with the clay-to-clay aggregation triggered by the release of divalent cations from the carbonate surface and carbonate-clay association decrease the liquid limit.

CHAPTER 7

TWO-MINERAL MIXTURES WITH POLYMER

Previous chapters explored the interaction among mineral particles behavior in varying pore fluid environments, for single and two-mineral systems. The purpose of this chapter is to investigate the mechanisms governing the influence of sodium polyacrylate on fabric formation for kaolinite-calcium carbonate mixtures at varying solids content and strain conditions. In addition, this study will explore changes in mineral mixture fabric with sodium polyacrylate in the presence of a divalent cation within the context of varying solids concentration. As in previous chapters, assessments are based on parameters obtained from sedimentation, rheological, and liquid limit observations and measurements.

7.1 Introduction

Particle associations in mineral mixtures without additives, are a function of Coulombian attraction, double layer osmotic repulsion and van der Waals attraction. Mineral surface modification with polymers adds another dimension for controlling the interactions between particles at the microscale. The type of polymer, chain length and affinity for the mineral face or edge all influence the degree and type of particle interactions, including dispersion, flocculation, or aggregation (Sjöberg et al., 1999; Bergström et al., 1996; Mallett and Craig, 1977).

Mineral mixtures with polymers are often investigated within the context of the paper coating industry (e.g., Andersson, 1993) since the basic components of coating slurries typically include pigments (kaolin, CaCO_3 , TiO_2), binders (starch, latex), and

chemical additives (dispersants, pH modifiers). Dispersants alter the behavior of coating slurries in two significant ways. First, the preservation of individual particles without associations increases the free particle movement. Second, floc prevention results in lower viscosity due to untrapped water between the flocs. These conditions benefit the coating application process by allowing for high-speed application with a higher solids loading. The coating runnability and final structure also depend on the coating solids content (Robinson et al., 1997).

Dahlvik et al. (1995) investigate the rheological behavior of NaPAA-treated pure calcium carbonate and kaolinite-calcium carbonate suspensions with varying mixture ratios, pH, and CaCl_2 concentration. They find that the yield stress of pure CaCO_3 suspensions increases very little and plateaus at a low yield stress with increasing CaCl_2 concentration. This is attributed to weak bonds between the Ca^{2+} ions and the polyacrylate molecules. In clay-carbonate systems with constant CaCl_2 concentration, the suspensions are pH dependent between pH 7 and 8 but pH-independent between pH 9 and 10.

7.2 Materials and Procedures

7.2.1 Materials

The minerals used in this study include Premier kaolin and precipitated calcium carbonate PCC Rhombic. Their sources and properties are reported in Chapter 3.

7.2.2 Sedimentation

Premier kaolin and PCC are mixed together in proportions by mass of 100:0, 75:25, 50:50, 25:75, and 0:100 clay:carbonate and solids volume fraction $\phi=0.02$. Fifty

microliters of Colloid 211 are added to the carbonate suspension. Suspensions containing calcium chloride are prepared according to Section 5.3.2.

7.2.3 Viscosity

Suspensions are prepared with mass ratios of 100:0, 75:25, 50:50, 25:75, and 0:100 clay:carbonate. Suspensions containing CaCl_2 are prepared with an ionic concentration of 0.002 M.

7.2.4 Liquid Limit

Kaolinite Premier and PCC are mixed together at 100:0, 75:25, 50:50, 25:75, and 0:100 clay:carbonate by mass. The 100% clay specimen is not tested because it becomes fluid-like and unworkable at a moisture content sufficient for hydrating the clay (note: a drying sequence was not attempted). To study the influence of CaCl_2 , similar mixtures are hydrated with 0.002 M CaCl_2 solution prior to testing.

7.3 Results

7.3.1 Sedimentation Tests

Without CaCl_2 . The time varying suspension heights during settlement for the Premier-PCC blends are shown in Figure 7.1. With the exception of the 25:75 case, the suspensions exhibit dispersive sedimentation behavior as summarized in Table 7.1, while Table 7.2 lists the supernatant pH. One general observation made by comparing the settlement curves is the induction period decreases with increasing carbonate content. The low-solids volume fraction clay-carbonate suspensions do not exhibit zone settling, i.e. flocculation sedimentation, and therefore, the relationship between increasing

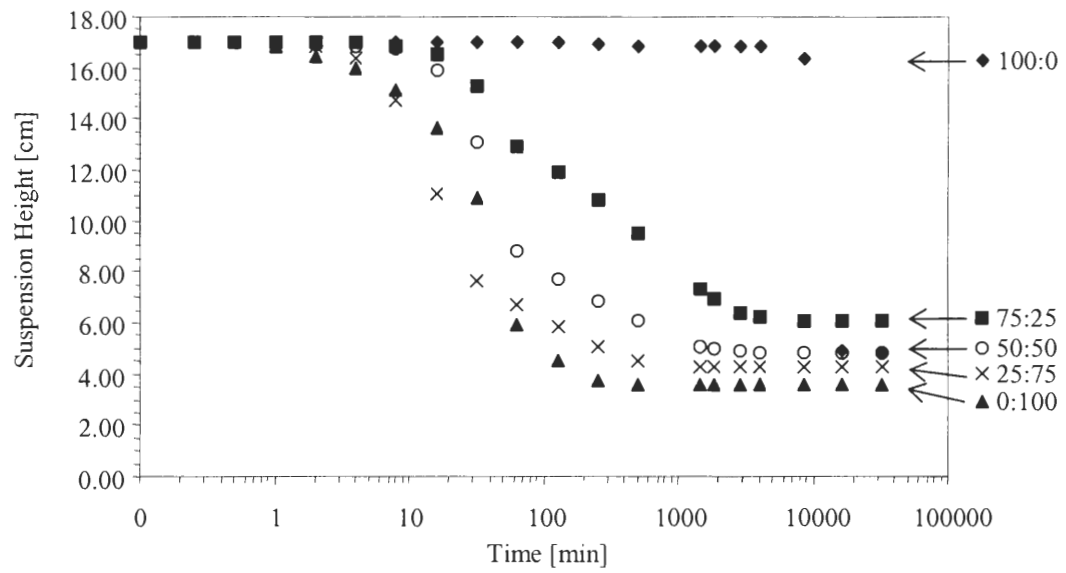


Figure 7.1 Sedimentation curves at 23 days for Premier-PCC mixtures.

Table 7.1 Observed Sedimentation Behavior for Premier-PCC Mixtures

| Suspension | Observed Characteristics During Settlement | | | | Sedimentation Type |
|-------------------|--|--|-------------|------------------------------|--------------------|
| | Suspension-Supernatant Boundary | Supernatant | Suspension | Settlement Type | |
| 100% Premier | None | Not Distinguishable | Homogeneous | Very slow sediment formation | Dispersed |
| 75:25 Premier:PCC | None | Not Distinguishable | Homogeneous | Very slow sediment formation | Dispersed |
| 50:50 Premier:PCC | None | Not Distinguishable | Homogeneous | Very slow sediment formation | Dispersed |
| 25:75 Premier:PCC | Distinct | Some suspended particles | Homogeneous | Very slow consolidation | Mixed-Mode |
| 100% PCC | Slightly indistinct | Concentration suspended particles greater than 25:75 | Homogeneous | Slow consolidation | Mixed-Mode |

Table 7.2 Supernatant pH of Premier-PCC Mixtures

| Suspension | Supernatant pH |
|-------------------|----------------|
| 100:0 Premier:PCC | 6.35 |
| 75:25 Premier:PCC | 7.44 |
| 50:50 Premier:PCC | 7.61 |
| 25:75 Premier:PCC | 8.56 |
| 0:100 Premier:PCC | 9.29 |

induction period and increasing flocculation described by Tiller and Khatib (1984) for single mineral systems does not hold. In this case, all sedimentation characteristics suggest that the induction period extends with increasing degree of particle dispersion. In a completely dispersed system and as long as the system remains stable, the particles do not interact with one another. Particle movements for dispersed particles with dimensions on the order of one micron are dominated by Brownian motion relative to gravitational forces. The random movements help keep the particles in suspension, and so the suspension height does not change. Since the 100% Premier case is the most dispersed, it has the longest induction time. In addition, at higher carbonate contents (75 and 100% PCC) the induction times are significantly less than the remaining suspensions.

The sediment height at 23 days for each suspension is shown in Figure 7.2. The overall effect of increasing PCC content is an increase in sediment height, while at lower carbonate contents sediment accumulation is hindered. Even at 23 days, the 100:0, 75:25, and 50:50 Premier:PCC systems have not settled significantly, although the opacity of the suspension component is much lower than at time zero.

All suspensions exhibit dispersed sedimentation behavior except the 25:75 clay:carbonate case that shows a mixed-mode, with more characteristics of a flocculated or aggregated system (see Table 7.1).

With CaCl_2 . The observed suspension heights with time for the Premier:PCC blends with added CaCl_2 are shown in Figure 7.3. A comparison between the sediment heights and induction times for the Premier-PCC suspensions with and without added divalent cations are presented in Figures 7.4 and 7.5. Except for the 0:100 clay:carbonate mixture, all suspensions have a reduced induction period compared to the corresponding

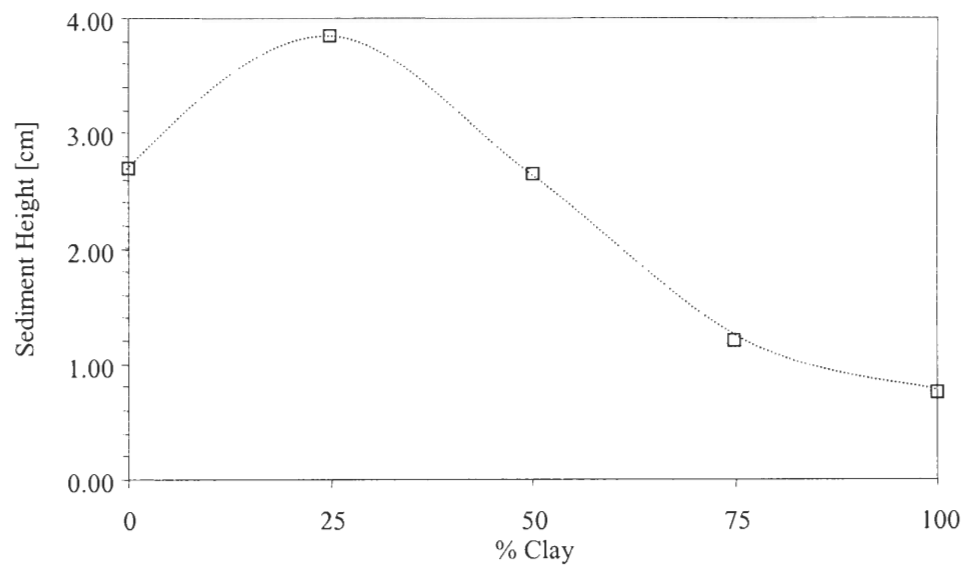


Figure 7.2 Sediment heights of Premier-PCC mixtures at 23 days.

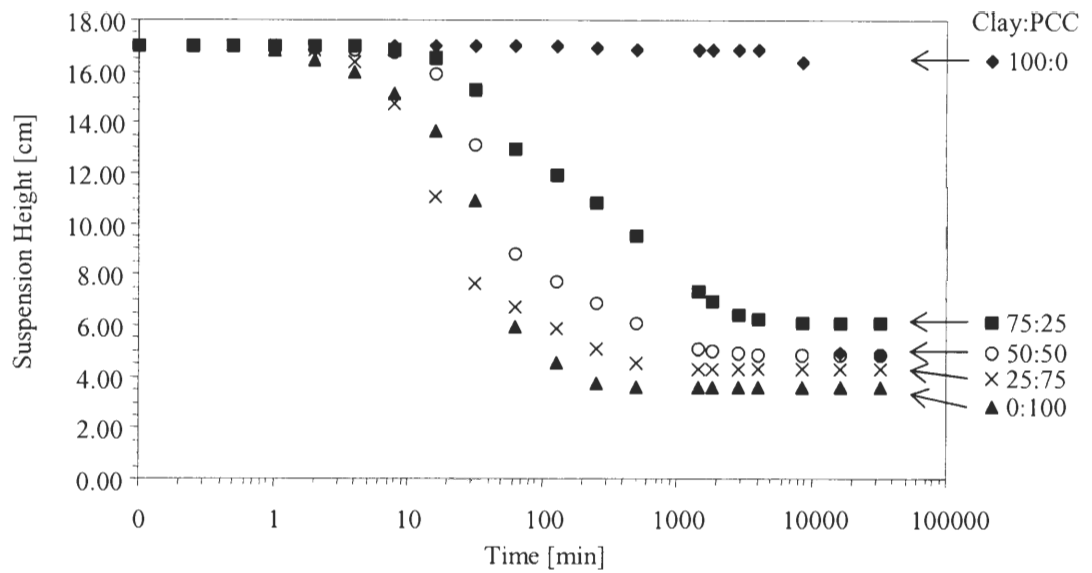


Figure 7.3 Sedimentation curves at 23 days for Premier-PCC mixtures with CaCl_2 .

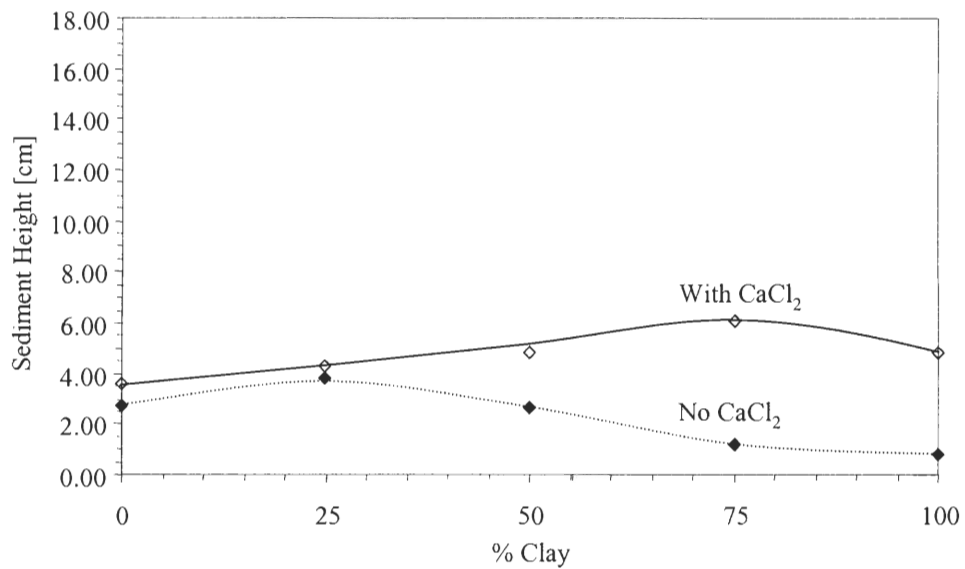


Figure 7.4 Premier-PCC sediment heights at 23 days with and without CaCl_2 .

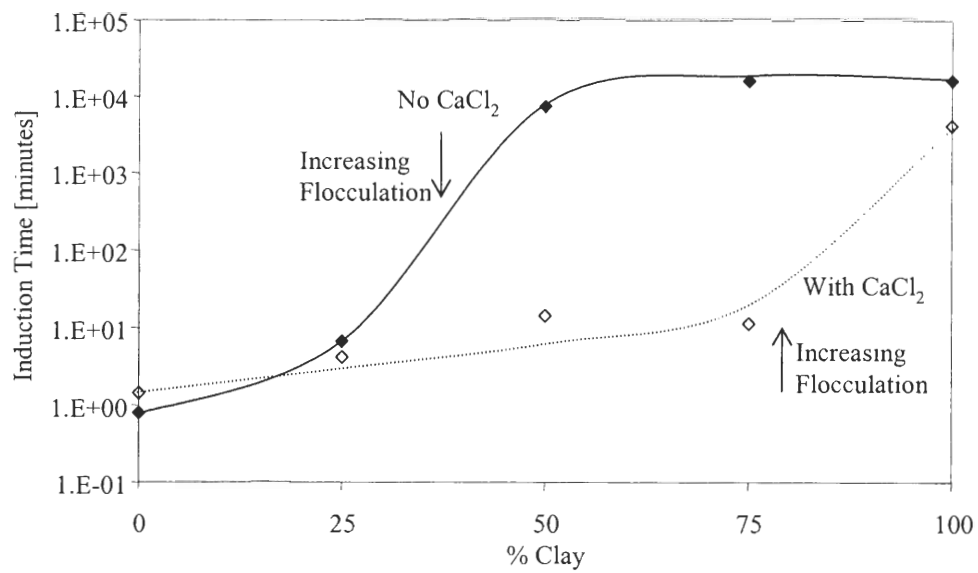


Figure 7.5 Premier-PCC suspension induction times with CaCl₂.

suspensions without CaCl_2 , and the induction times decrease with increasing carbonate content.

Tables 7.3 and 7.4 summarize the observed sedimentation behavior for the given suspensions containing calcium chloride and the supernatant pH, respectively. With increasing relative mass of PCC, the behavior changes from primarily dispersive to increasingly associative. At high clay concentrations the suspension-supernatant boundary is not immediately observed. In the presence of PCC, not only does a clear suspension-supernatant boundary develop, but the time for the boundary formation lessens with increasing carbonate content. In addition, the supernatant holds no visible particles in suspension. The clay-carbonate suspension appearance changes from milky and continuous at 100% Premier to sediment-like in the suspensions containing PCC, although no mineral segregation is observed in the final sediment. These heterogeneous suspensions settle by slow consolidation until reaching their final height. Hence, the suspensions containing PCC have characteristics consistent with flocculation or aggregation sedimentation.

The settlement mode for the 100% Premier suspension is dispersed. According to Figure 7.3 even with the added divalent cations, the 100% Premier suspension seems to maintain this behavior. Recall that the CaCl_2 concentration is chosen such that flocculation for a 100% Premier suspension occurs after 24 hours. But, the sudden appearance of a large sediment height at 2880 minutes (48 hours) suggests that the particles begin to settle prior to this measurement. Indeed, the sediment height is indistinguishable from the suspension prior to the 2880 minute mark. Both the induction period and the time to beginning of sediment accumulation are less than the

Table 7.3 Observed Sedimentation Behavior for Premier-PCC Mixtures with CaCl₂

| Suspension | Observed Characteristics During Settlement | | | | Sedimentation Type |
|-------------------|---|--|---|------------------------------|--------------------|
| | Suspension-Supernatant Boundary | Supernatant | Suspension | Settlement Type | |
| 100% Premier | None | None | Homogeneous | Very slow sediment formation | Dispersed |
| 75:25 Premier:PCC | None initially, Clear boundary at 8 minutes | Initially none, no suspended particles after 8 minutes | Heterogeneous, uniform density from top to bottom | Very slow consolidation | Flocculated |
| 50:50 Premier:PCC | None initially, Clear boundary at 2 minutes | Initially none, no suspended particles after 2 minutes | Heterogeneous, uniform density from top to bottom | Slow consolidation | Flocculated |
| 25:75 Premier:PCC | None initially, Clear boundary at 2 minutes | Initially none, no suspended particles after 2 minutes | Heterogeneous, uniform density from top to bottom | Slow consolidation | Flocculated |
| 100% PCC | Slightly indistinct | High concentration of suspended particles | Homogeneous | Slow consolidation | Mixed-Mode |

Table 7.4 Supernatant pH of Premier-PCC Mixtures with CaCl₂

| Suspension | Supernatant pH |
|-------------------|----------------|
| 100:0 Premier:PCC | 5.81 |
| 75:25 Premier:PCC | 7.75 |
| 50:50 Premier:PCC | 8.01 |
| 25:75 Premier:PCC | 7.72 |
| 0:100 Premier:PCC | 11.33 |

corresponding suspension without Ca^{2+} ions (Figure 7.1) which points to the role of Ca^{2+} ions as flocculating agents in the presence of a dispersant. The 100% Premier with CaCl_2 suspension has some observable characteristics of a dispersed system, yet it is better described as mixed-mode.

7.3.2 Viscosity

Without CaCl_2 . The measured viscosities with the applied range of spindle rotational speeds for the five Premier-PCC suspensions are shown in Figure 7.6. The viscosities of four suspensions, 100:0, 75:25, 50:50, and 0:100 Premier:PCC are below the viscometer measurable range except at 100 RPM. However, 25:75 Premier:PCC blend has measurable viscosity beginning at 5 RPM. Figure 7.7 shows a series of SEM micrographs for Premier-PCC mixtures prepared as suspensions with the same solids volume fraction as the viscosity tests.

With CaCl_2 . The viscosities of Premier-PCC suspensions with CaCl_2 are shown in Figure 7.8. The 25:75, 50:50 and 75:25 clay:carbonate suspensions exhibit shear-thinning behavior. Comparing the relative state of dispersion between the different mixtures, the suspension structure increases with increasing carbonate content, with the exception of 100% PCC. Figure 7.9 shows the mixture viscosities with and without CaCl_2 .

7.3.3 Liquid Limit

Without CaCl_2 . The liquid limit is measured for each of four cases to discern the relative state of dispersion for the given Premier-PCC mixtures at a high solids content and large applied strain relative to the sedimentation and rheological measurements. The

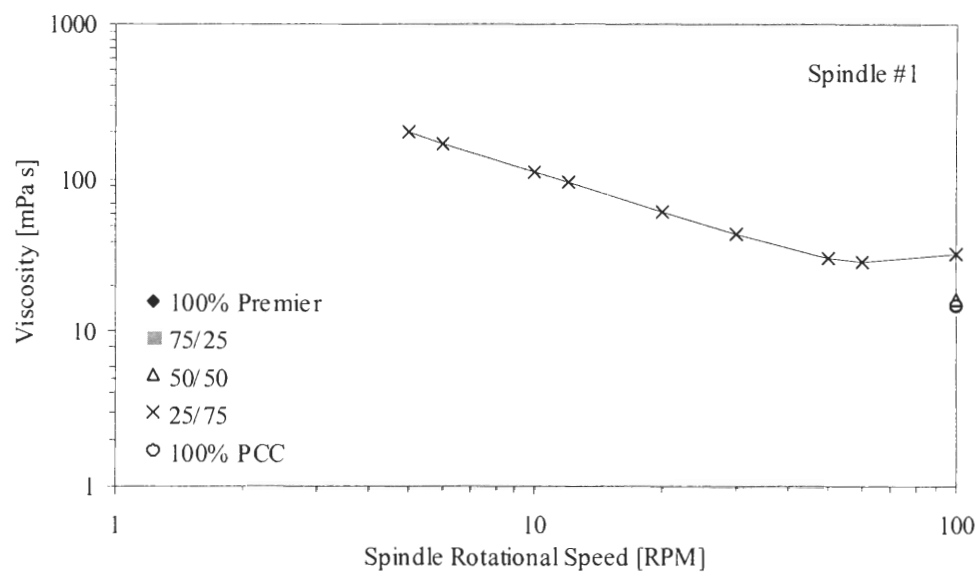
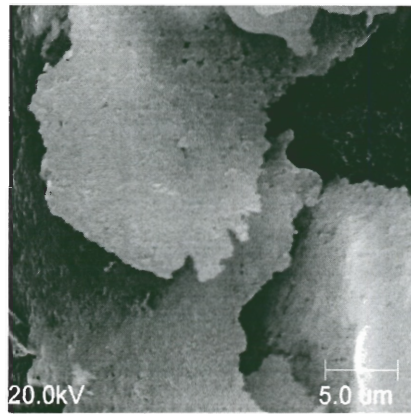
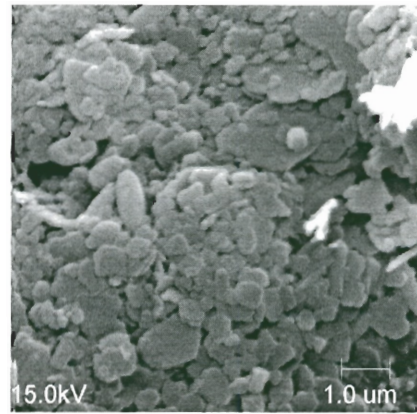


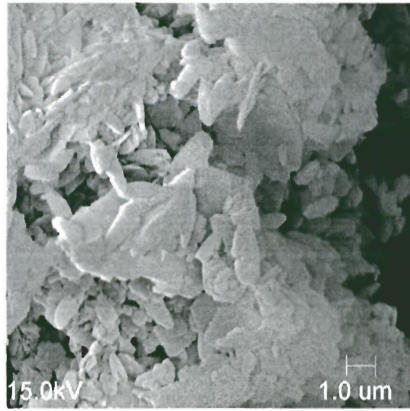
Figure 7.6 Viscosity measurements of Premier-PCC suspensions.



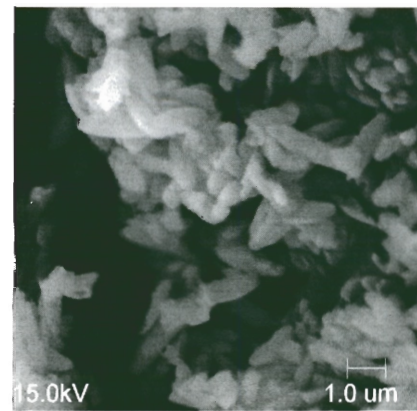
(a)



(b)



(c)



(d)

Figure 7.7 SEM micrographs for Premier-PCC mixtures prepared as suspensions with the same solids volume fraction $\phi=0.07$ as the viscosity tests: (a) 100:0, (b) 75:25, (c) 25:75 and (d) 0:100 Premier:PCC

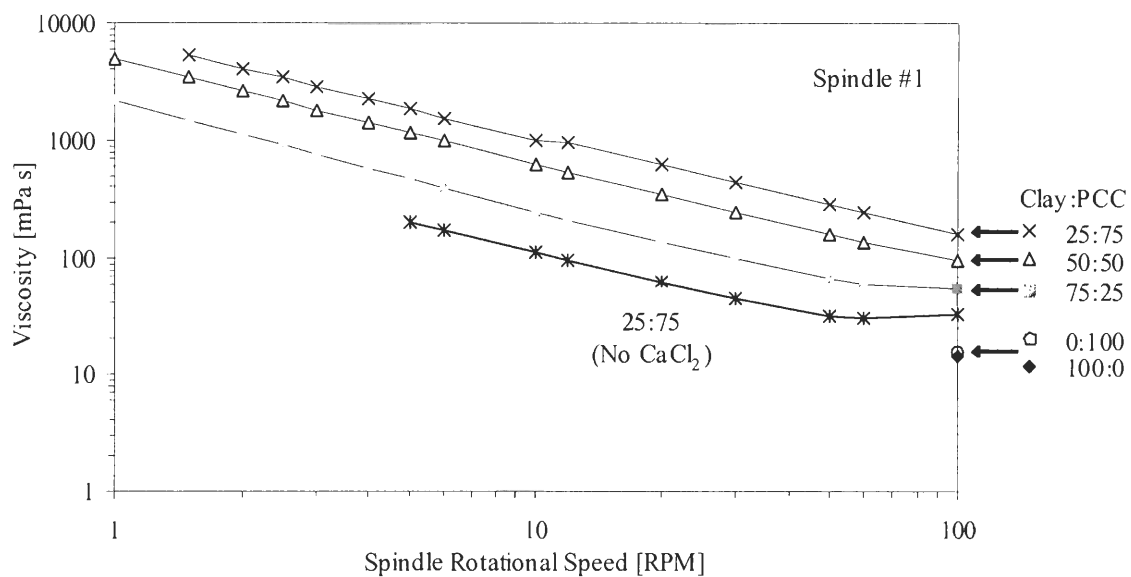


Figure 7.8 Premier-PCC suspension viscosities with CaCl₂ and 25:75 Premier-PCC

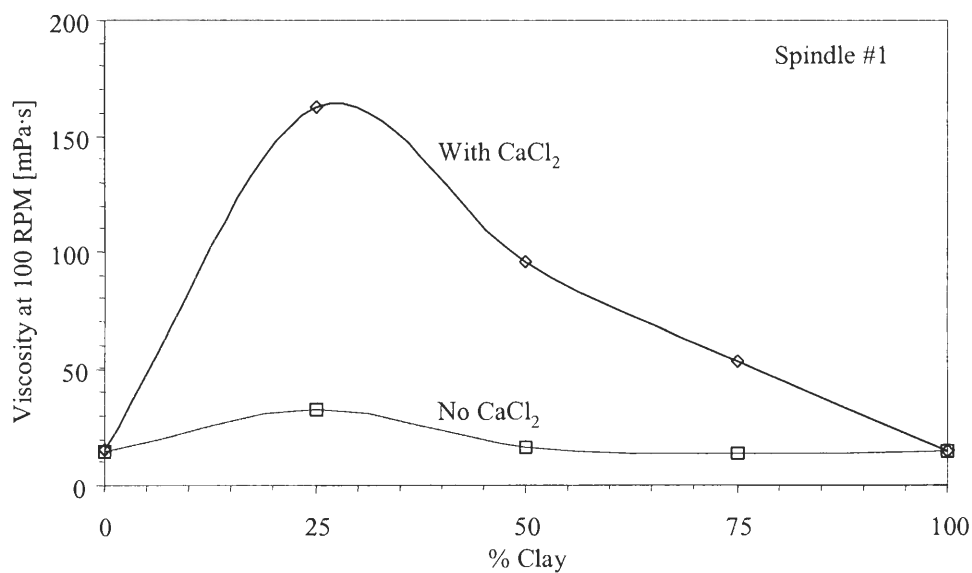


Figure 7.9 Premier-PCC viscosity at 100 RPM with and without CaCl₂.

liquid limit for each system is plotted according to clay percentage in Figure 7.10. The liquid limit remains fairly constant between clay:carbonate= 0:100 to 25:75 and decreases thereafter.

The liquid limit of the 100% Premier was not obtained (Figure 7.10). (Note: a drying sequence was not attempted). The pure polymer-treated clay is difficult to prepare for fall cone testing. The preparation process includes intermittently mixing the clay between additions of small volumes of water. With increasing water content, the clay becomes increasingly difficult to mix thoroughly. Yet, the moisture content is inadequate for even the initial cone penetration measurement. The material behavior is more like a shear-thickening fluid in that it flows under its own weight but cannot be punctured by the falling cone. Since additional water cannot be uniformly distributed and the behavior of the wetted clay is more of a shear thickening fluid, the liquid limit for the 100% Premier case is not measured.

With CaCl_2 . Figure 7.10 also shows the measured liquid limits for the Premier-PCC mixtures prepared with CaCl_2 . Values and trends are almost identical to those for the corresponding mixtures without CaCl_2 .

7.4 Discussion

Without CaCl_2 . Overall, particle associations are observed to increase with increasing carbonate content. The decreasing induction period, increasingly flocculative settling behavior, increasing sediment volume and increasing liquid limit correspond to increasing particle associations with carbonate content for the Premier-PCC mixtures.

Structure formation in free-forming sediments may be attributed to particle packing, increasing particle flocculation, or both (Figure 7.11). While the lengths of the PCC and

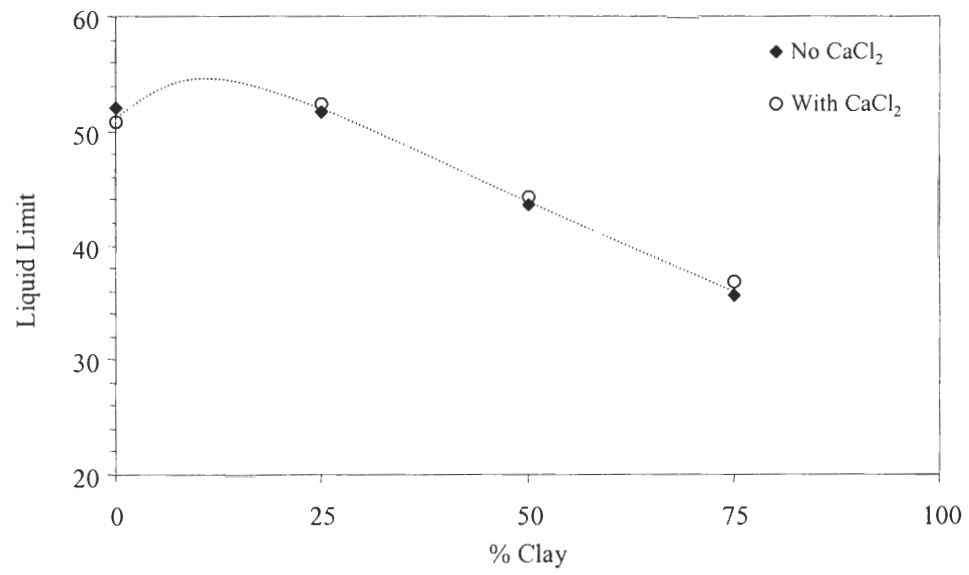
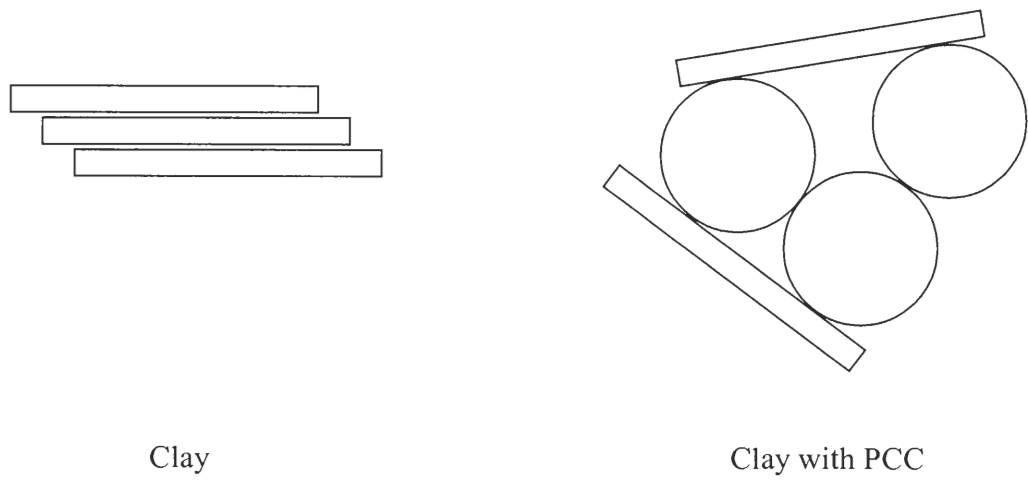
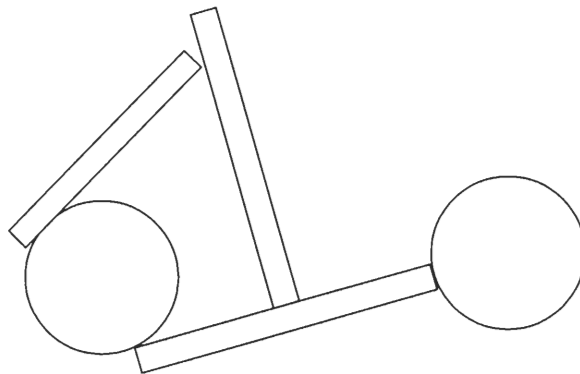


Figure 7.10 Liquid limits of Premier-PCC mixtures with and without



(a)



(b)

Figure 7.11 Effects of (a) particle packing and (b) flocculation on sediment height.

clay particles are approximately the same, the PCC diameters are approximately half this dimension. Neglecting electrical forces, at this length to diameter ratio (~ 2) the platy particles may bridge the rounder particles and increase the void ratio (Guimaraes, 2002). Particle bridging in the 25:75 clay:PCC system can be seen in Figure 7.7-c.

If electrical forces are considered, a flocculated system will settle relatively quickly into an open, voluminous structure (Patton, 1979; van Olphen, 1977). Table 7.2 lists the pore fluid pH for each suspension. The supernatant for 25:75 system has pH 8.56, which is above the typical range for untreated kaolinite edge isoelectric point, and so dispersive behavior would be expected. However, the polyacrylate molecules should be nearly completely ionized at this pH, and hence, have a high negative charge (Micheals & Morelos, 1955). The electrostatic attraction between the negatively charged carboxyl groups and the positive surface sites promotes polyacrylate adsorption onto the calcium carbonate. The adsorption of NaPAA onto calcium carbonate increases with increasing pH. At high pH ($\text{pH} > 8$), the adsorption of NaPAA onto carbonate surfaces is greater than adsorption onto kaolinite surfaces (Järnström, 1993). Therefore, particle attraction between the two mineral types should be observed.

The largest sediment height in this study corresponds to the 25:75 kaolinite:PCC mixture. This contrasts the observations made by Huber and Weigl (1972) who use natural ground calcium carbonate ($d=0.5$ to $5\mu\text{m}$) and kaolinite ($d=0.3$ to $5\mu\text{m}$) at the optimum dispersant concentration and find the maximum relative sediment volume to occur at 80:20 clay:carbonate.

The primary particle association mode may vary with mineral content. In other words, the relative availability of clay and PCC surface as well as the locations of the

polymer chains on the clay particle influences the final sediment structure. The chain length, at least in terms of the molecule extension from the particle, plays a less significant role in that it most likely binds to the clay surface in a fairly flat conformation (Berg et al., 1993). Since the polyacrylate is adsorbed at the positively charged sites, primarily the clay particle edges, (Michaels and Morelos, 1955), then the most likely association of NaPAA-treated clay particles with the carbonate particles is a pseudo edge-to-face formation Figure 7.12. In other words, the clay particle edges will attach along the lateral surface of the PCC in a perpendicular fashion.

At moderate solids content, the dispersive nature of the higher clay-content mixtures is consistent with the sedimentation behaviors. However, the viscosity of the 100:0 clay:PCC suspension becomes measurable at high RPM. Most likely this slight dilatancy is not an indication of increasing particle associations. In fact, one would expect decreasing viscosity with increasing shear rate for particles with an anisotropic shape. Particle rotation (and resulting larger hydrodynamic radius) due to Brownian motion at low shear succumbs to particle alignment at high shear, thereby reducing particle interference and decreasing the viscosity (Hunter, 1993). However, a suspension containing particles with large repulsive forces may also exhibit larger viscosities at higher shear rates. The suspension develops a slight resistance to shear as it becomes more and more difficult for the particles to move past each other at increased shear rates (van Olphen, 1977).

The 25:75 clay:PCC blend has the highest degree of flocculation. The measured viscosity at 100 RPM is almost twice that of the other four suspensions (Figure 7.6). While the ratio is in contrast with that of Hagemeyer (1960) in which the viscosity peaks

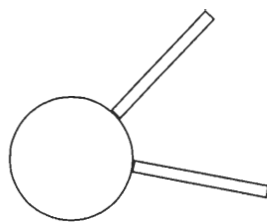


Figure 7.12 Pseudo edge-to-face flocculation of kaolinite and PCC particles.

at 80:20 clay:calcium carbonate, the existence of a peak viscosity for some apparent critical ratio is consistent. The peak is observed for mixtures of kaolinite ($L=90\% < 2\mu\text{m}$) and either needle ($L=0.5$ to $1.5\mu\text{m}$, $d=0.1$ to $0.3\mu\text{m}$) or rhomb-shaped ($d=0.1$ to $1\mu\text{m}$) carbonate particles as well as over a range of total solids volume fraction. In other words, with the materials tested by Hagemeyer (1960) the magnitude changes with carbonate shape and total solids content, but the trend does not.

The liquid limits of the clay-carbonate mixtures presented in Chapter 5 increase with increasing clay content. Without a polymer, increasing the total mineral surface area is one of the factors that influences the liquid limit with increasing clay content. However, for the mixtures presented in this study, the liquid limit *decreases* with increasing clay content and peaks at ~25:75 clay:PCC. The greater the percentage of NaPAA-treated clay, the more the system is dispersed.

As the Premier clay particles hydrate, they repulse one another. At such a high solids concentration, the particles minimize their interactions with their nearest neighbors by adopting a minimum energy configuration, that is, they tend to align with respect to each other. The electrostatic repulsion between the polymer chains allow the particles to easily slide past one another at a minimal water content.

Adding PCC to the Premier clay has several implications. First, in addition to surface sites, slight dissolution of the carbonate provides a source of Ca^{2+} ions. The concentration of released calcium ions is approximately 10^{-3} mol/L based on the increase in pH. Particle association may then occur either between clay and carbonate particles, or if polymer chains adsorb Ca^{2+} ions, associations take place between the Premier particles (through some combination of double layer reduction and ion bridging). Second, the

PCC particles are similar in size to the clay particles, but not in shape (Figures 3.3-b, 3.4-b and 7.11), and the PCC crystals have a subrounded cross-section perpendicular to the long axis. Combining these two factors means that the PCC and clay particles have a higher association rate due to the presence of the Ca^{2+} ions (and surface sites), yet, the flocs will have an open structure. A well-coated clay particle may have polyacrylate chains associated with most of its positive sites along both the edge and basal plans of the particle (Diz and Rand, 1990). Binding sites for carbonate particles on the clay particle then include both the clay particle edge and face, and flocs with a pseudo FF or EE may form. The total fabric should become increasingly flocculated with increasing mass carbonate. This tendency is observed in the increase in liquid limit with increasing PCC content.

With CaCl_2 . Since the kaolinite particles are pretreated with NaPAA, the results show the interaction between the Ca^{2+} ions in solution and the clay surface polymer chains and carbonate surfaces. The influence of Ca^{2+} ions include: (1) clay particle double layer reduction due to Ca^{2+} ion surface adsorption, (2) altered surface charge density, (3) Ca^{2+} ion bridge formation between polymer molecules (Berg et al., 1993) and (4) decreasing the polyacrylate solubility, and hence, net repulsive force through Ca^{2+} ion adsorption at the carboxylate groups (Daklvik, 1995; Järnström, 1993).

Given that the clay particles are pretreated with NaPAA, other relevant phenomena for the systems presented in this study are: (1) the amount of dispersant within the mixtures is in proportion to the clay content and (2) clay-clay particle interactions compete with and may be more favorable than clay-carbonate interactions. Hence, the ratio of total Ca^{2+} to the number of NaPAA binding sites plays critical role in the mineral

mixture behavior (Chapter 4). Table 7.5 lists the estimated ratios of $[\text{Ca}^{2+}]_{\text{add}}/C_{\text{PPA}}$ for the tests presented in this chapter. The exact molecular weight and density of the NaPAA used to treat the kaolinite is not given by the manufacturer. Estimates are based on values of Colloid 211, and so the $[\text{Ca}^{2+}]_{\text{add}}/C_{\text{PPA}}$ ratios are relative and not absolute.

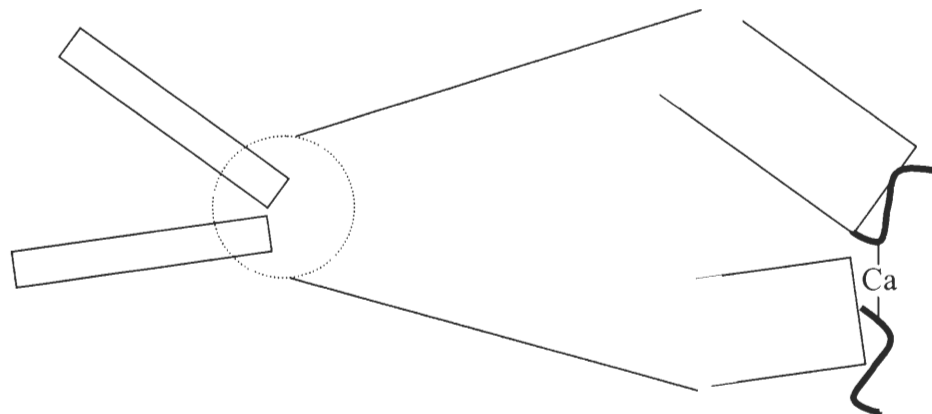
In comparing the sedimentation behavior with and without CaCl_2 , several important observations can be made. At low clay contents, there is little difference between induction times of suspensions with and without CaCl_2 , yet the observed sedimentation behavior indicates significant differences in particle associations. Also, CaCl_2 has little effect on the sediment height. At higher clay contents, Ca^{2+} has significant influence on induction period and greatly increases the sedimentation height. This would suggest an increase in degree of flocculation, particularly in edge-to-face formations. Notice the similarities between Figures 7.4 and 7.5 in response to CaCl_2 .

The particle associations for the 100:0 clay:carbonate suspension are most likely in edge-to-edge or edge-to-face. If the polymer chains are located primarily along the particle edges, Ca^{2+} ions may bind two particle edges together and/or reduce the negative face charge through adsorption, thus allowing the edge of one particle to approach the face of another as shown in Figure 7.13.

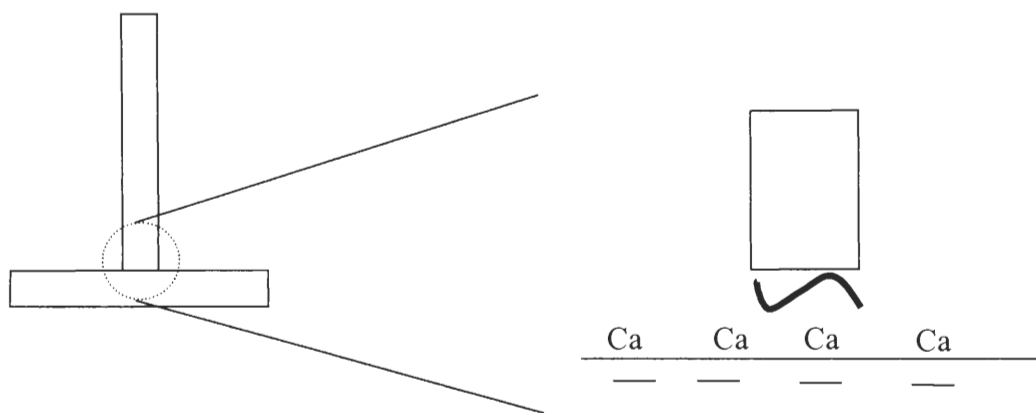
With increasing carbonate content, the sedimentation height and accordingly the degree of flocculation, also decreases. Since in the clay-carbonate suspensions only the clay particles are coated in NaPAA, in the presence of Ca^{2+} the interactions between the clay particles are much stronger than the interactions between the clay and PCC particles. Also, a reduction in clay content corresponds to a reduction in the total concentration of NaPAA. So, the flocculation effect of CaCl_2 is lessened.

Table 7.5 Estimated Ratios of added Ca^{2+} to NaPAA Monomers $[\text{Ca}^{2+}]_{\text{add}}/C_{\text{PPA}}$ for Premier Kaolinite (calculations are given in Mathgram 7.1)

| Premier:PCC Ratio | Sedimentation | Viscosity | Fall Cone |
|-------------------|---------------|-----------|------------|
| 100:0 | 0.925 | 0.272 | Not Tested |
| 75:25 | 1.233 | 0.359 | 0.04 |
| 50:50 | 1.85 | 0.533 | 0.037 |
| 25:75 | 3.701 | 1.057 | 0.124 |
| 0:100 | 0.25 | 0.035 | 0.025 |



(a)



(b)

Figure 7.13 Premier kaolinite particle associations in the presence of Ca^{2+} : (a) edge-to-edge and (b) edge to face.

It is interesting to note that without added divalent cations, the most voluminous structure is obtained at clay:PCC=25:75. But, in the presence of added CaCl_2 , the 75:25 clay:carbonate blend settles in the most open network. So, a greater mass percentage of PCC is required to achieve a lesser sediment height in the absence of CaCl_2 .

For the given moderate solids content $\phi=0.07$ and CaCl_2 concentration, the suspension degree of flocculation is enhanced by increasing carbonate content, except at 100% PCC. Dahlvik et al. (1995) report similar observations with yield stress as a structure indicator. This trend is clearly seen in Figure 7.8 and is opposite to that observed with the sedimentation parameters. The sedimentation height of the 100% Premier case with CaCl_2 is much greater than the final height without CaCl_2 (Figure 7.4), suggesting an increase in particle associations. However, the rheological response of the 100:0 Premier:PCC case shows no such structure development. The apparent inconsistency may reflect the different ratio of Ca^{2+} ions per polyacrylate binding site: this value is too low at the high Premier concentration in rheological measurements. That is, there are not enough calcium ions in the pore fluid to either reduce the effective polymer distance (decrease polymer solubility) or to bind enough particles together to form measurable flocculation. As the clay content decreases, the ratio of Ca^{2+} to number of polymer binding sites increases. So, the addition of CaCl_2 magnifies the trend seen in the no- CaCl_2 series as shown in Figure 7.9.

The minimal floc formation indicated by the low viscosity of the 100% carbonate suspension is consistent with the sedimentation findings, i.e. the concentration of CaCl_2 in the suspension has very little effect on PCC flocculation in the presence of NaPAA.

The PCC particles remain primarily dispersed with their anisotropic shape contributing to the viscosity increase at 100 RPM.

The liquid limit for the series without CaCl_2 differs very little from the liquid limit for mixtures with CaCl_2 . The high clay concentration and subsequent NaPAA concentration reduces the Ca^{2+} to polymer binding site ratio, and thus reduces the effectiveness of the divalent cation. The salt concentration in the pore fluid is 0.002 M CaCl_2 , as in the previous sedimentation and viscosity tests. However, at higher clay percentages, less water is required to mobilize the particles. So, there are less Ca^{2+} ions available to exchange with the bound sodium ions on the polymer chains. Without enough Ca^{2+} ions to induce flocculation through either double layer reduction or cation bridging, the overall trend is the same with and without the given concentration of CaCl_2 .

7.5 Conclusions

The variation in and underlying mechanisms controlling fabric formation of kaolinite-calcium carbonate mixtures in the presence of sodium polyacrylate with and without calcium chloride is explored. Interpretations incorporate observations and measurements made from sedimentation, rheological, and liquid limit observations. These tests represent a wide range of solids content and strain conditions.

A flocculated fabric may be achieved in mineral mixtures even in the presence of a polymer dispersant. Electrostatic interactions between the anionic polymer molecules bound to the kaolin surface and the positive sites on the PCC particles create an open sediment structure.

The fabric of the mineral mixtures is influenced not only by electrostatic interactions, but also by relative particle shape and size. The thin platy kaolin particles

bridge the more prismatic PCC particles and increase the free-formed sediment volume. However, this effect is maximized at a particular clay-carbonate ratio. While this apparent critical ratio may be material dependent, it can be altered with solids content and the ratio of Ca^{2+} ions to amount of polymer.

The introduction of calcium chloride induces a general increase in flocculation compared to those mixtures without added salt. The efficiency of Ca^{2+} as a flocculant in the presence of NaPAA depends on the ratio of total calcium ions to polyacrylate binding sites. This ratio is altered as the relative masses of clay and carbonate change, as well as with changes in the solids volume fraction. For the low to moderate solids content systems, the efficiency is much greater than the high solids content systems for the same CaCl_2 concentration. Also, the polymer-treated clay particles have stronger interactions with each other than with the carbonate particles even at supernatant pH values above the kaolinite edge isoelectric point.

At high solids content and high applied strain, the liquid limit showed no significant change with the addition of calcium chloride. This is a consequence of the primary mechanism governing particle flocculation in a NaPAA- CaCl_2 system: Ca^{2+} adsorption by the polyacrylate molecule and subsequent interparticle cation bridging. The number of available Ca^{2+} ions is significantly reduced at such low water contents. Without significant Ca^{2+} adsorption, the polymer efficiency as a dispersant remains the same.

While particle shape and relative particle size influence the final fabric of clay-calcium carbonate mineral mixtures, the final fabric is determined by particle surface charges. By modifying these charges with variation in polymer and ionic concentration, particle associations are also altered.

Mathgram 7.1. $[\text{Ca}^{2+}]_{\text{add}}/\text{C}_{\text{PAA}}$ Ratios

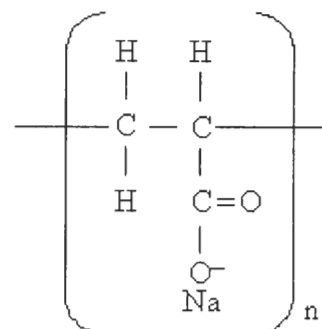
Sodium Polyacrylate, $\text{CH}_2\text{CH}(\text{COONa})$

Approximate Molecular Weight and density, manufacturer's data:

Colloid 211 -- 3400 g/mole

$$\text{MW} := 3400 \frac{\text{gm}}{\text{mole}}$$

$$\rho_{211} := 1.30 \frac{\text{gm}}{\text{mL}}$$



Individual Atom Molecular Weights

$$\text{H} := 1.007947 \frac{\text{gm}}{\text{mole}}$$

$$\text{C} := 12.01078 \frac{\text{gm}}{\text{mole}}$$

$$\text{O} := 15.99943 \frac{\text{gm}}{\text{mole}}$$

$$\text{Na} := 22.9897702 \frac{\text{gm}}{\text{mole}}$$

Equation Based on Chemical Formula

$$n \cdot (3 \cdot \text{C} + 3 \cdot \text{H} + 2 \cdot \text{O} + \text{Na}) + 2 \cdot n \cdot \text{H} = \text{MW}$$

Approximate Number of Monomers Per Molecule, n :

$$n_{\text{monomer}} := \frac{\text{MW}}{(3 \cdot \text{C} + 5 \cdot \text{H} + 2 \cdot \text{O} + \text{Na})} \quad n_{\text{monomer}} = 35.4$$

Approximate Number of NaPAA Molecules Per mL Colloid 211, $N_{\text{molecules}}$:

$$N_{\text{av}} := 6.022 \cdot 10^{23} \cdot \frac{1}{\text{mole}}$$

$$N_{\text{molecules}} := N_{\text{av}} \cdot \frac{1}{\text{MW}} \cdot \rho_{211} \quad N_{\text{molecules}} = 2.303 \times 10^{20} \frac{1}{\text{mL}}$$

$$V_{\text{PAA}} := \frac{0.35 \text{ gm}}{\rho_{211}} \quad V_{\text{PAA}} = 0.269 \text{ mL} \quad \text{per 100g Premier}$$

Sedimentation

Initial Solution: 84.49 mL 0.002M CaCl_2

$$n_{\text{monomer}} = 35.394 \quad i := 0..4$$

Total number of NaPAA monomers (potential binding sites for Ca^{2+} ions)

$$\text{MassPremier}_i := \begin{pmatrix} 5 \\ 3.75 \\ 2.5 \\ 1.25 \\ 0 \end{pmatrix} \cdot \text{gm} \quad \text{Vol}_{\text{PAA}_i} := \frac{\text{MassPremier}_i \cdot V_{\text{PAA}}}{100\text{gm}}$$

$$\text{Vol}_{\text{PAA}} = \begin{pmatrix} 0.013 \\ 0.01 \\ 6.731 \times 10^{-3} \\ 3.365 \times 10^{-3} \\ 0 \end{pmatrix} \text{mL}$$

$$T_{\text{monomers}_i} := N_{\text{molecules}} \cdot \text{Vol}_{\text{PAA}_i} \cdot n_{\text{monomer}}$$

$$T_{\text{monomers}} = \begin{pmatrix} 1.097 \times 10^{20} \\ 8.228 \times 10^{19} \\ 5.485 \times 10^{19} \\ 2.743 \times 10^{19} \\ 0 \end{pmatrix}$$

Volume of 0.002M CaCl_2 solution added to mineral solids:

Solids volume fraction:

$$\phi := \begin{pmatrix} 0.0223 \\ 0.0221 \\ 0.0219 \\ 0.0216 \\ 0.0214 \end{pmatrix} \quad \text{TotVol} := 86.14 \text{mL}$$

$$\text{CaCl2Vol}_i := \text{TotVol} - (\phi_i \cdot \text{TotVol}) \quad \text{CaCl2Vol} = \begin{pmatrix} 84.219 \\ 84.236 \\ 84.254 \\ 84.279 \\ 84.297 \end{pmatrix} \text{ mL}$$

There is one mole of Ca^{2+} ions for every mole CaCl_2

$$\text{CaCl2Concen} := 0.002 \frac{\text{mole}}{\text{L}}$$

$$\text{CaIons}_i := \text{CaCl2Vol}_i \cdot \text{CaCl2Concen} \cdot N_{\text{av}} \quad \text{CaIons} = \begin{pmatrix} 1.014 \times 10^{20} \\ 1.015 \times 10^{20} \\ 1.015 \times 10^{20} \\ 1.015 \times 10^{20} \\ 1.015 \times 10^{20} \end{pmatrix}$$

Ratio of Ca^{2+} ions to total number of COO^- sites (potential binding sit

$$j := 0..3$$

$$R_j := \frac{\text{CaIons}_j}{T_{\text{monomers}_j}} \quad R = \begin{pmatrix} 0.925 \\ 1.233 \\ 1.85 \\ 3.701 \end{pmatrix}$$

Viscosity

$$n_{\text{monomer}} = 35.394 \quad i := 0..4$$

Total number of NaPAA monomers (potential binding sites for Ca^{2+} io

$$\text{MassPremier} := \begin{pmatrix} 93.5 \\ 70.9 \\ 47.8 \\ 24.10 \\ 0 \end{pmatrix} \cdot \text{gm} \quad \text{Vol}_{\text{PAA}_i} := \frac{\text{MassPremier}_i \cdot V_{\text{PA}}}{100\text{gm}}$$

$$\text{Vol}_{\text{PAA}} = \begin{pmatrix} 0.252 \\ 0.191 \\ 0.129 \\ 0.065 \\ 0 \end{pmatrix} \text{mL}$$

$$T_{\text{monomers}_i} := N_{\text{molecules}} \cdot \text{Vol}_{\text{PAA}_i} \cdot n_{\text{monomer}}$$

$$T_{\text{monomers}} = \begin{pmatrix} 2.052 \times 10^{21} \\ 1.556 \times 10^{21} \\ 1.049 \times 10^{21} \\ 5.288 \times 10^{20} \\ 0 \end{pmatrix}$$

Volume of 0.002M CaCl_2 solution added to mineral solids:

Solids volume fraction:

$$\phi := 0.072$$

$$\text{TotVol} := 500\text{mL}$$

$$\text{CaCl2Vol} := \text{TotVol} - (\phi \cdot \text{TotVol})$$

$$\text{CaCl2Vol} = 464 \text{ mL}$$

There is one mole of Ca^{2+} ions for every mole CaCl_2

$$\text{CaCl2Concen} := 0.002 \frac{\text{mole}}{\text{L}}$$

$$\text{CaIons} := \text{CaCl2Vol} \cdot \text{CaCl2Concen} \cdot N_{\text{av}} \quad \text{CaIons} = 5.588 \times 10^{20}$$

Ratio of Ca^{2+} ions to total number of COO^- sites (potential binding

$$j := 0..3$$

$$R_j := \frac{\text{CaIons}}{T_{\text{monomers}_j}} \quad R = \begin{pmatrix} 0.272 \\ 0.359 \\ 0.533 \\ 1.057 \end{pmatrix}$$

Fall Cone

$$n_{\text{monomer}} = 35.394 \quad k := 0..2$$

Total number of NaPAA monomers (potential binding sites for Ca^{2+} ions)

$$\text{MassPremier}_k := \begin{pmatrix} 262.5 \\ 200 \\ 75 \end{pmatrix} \cdot \text{gm} \quad \text{VolFC}_{\text{PAA}_k} := \frac{\text{MassPremier}_k \cdot V_{\text{PAA}}}{100\text{gm}}$$

$$\text{VolFC}_{\text{PAA}} = \begin{pmatrix} 7.067 \times 10^{-7} \\ 5.385 \times 10^{-7} \\ 2.019 \times 10^{-7} \end{pmatrix} \text{m}^3$$

$$\text{TFC}_{\text{monomers}_k} := N_{\text{molecules}} \cdot \text{VolFC}_{\text{PAA}_k} \cdot n_{\text{monomer}}$$

$$\text{TFC}_{\text{monomers}} = \begin{pmatrix} 5.76 \times 10^{21} \\ 4.388 \times 10^{21} \\ 1.646 \times 10^{21} \end{pmatrix}$$

Volume of 0.002M CaCl_2 solution added to mineral solids:

$$\text{CaCl}_2 \text{VolFC} := \begin{pmatrix} 192 \\ 135 \\ 169 \end{pmatrix} \cdot \text{mL}$$

There is one mole of Ca^{2+} ions for every mole CaCl_2

$$\text{CaCl}_2 \text{Concen} := 0.002 \frac{\text{mole}}{\text{L}}$$

$$\text{CalonsFC}_k := \text{CaCl}_2 \text{VolFC}_k \cdot \text{CaCl}_2 \text{Concen} \cdot N_{\text{av}} \quad \text{Calons} = 5.588 \times 10^{20}$$

Ratio of Ca^{2+} ions to total number of COO^- sites (potential binding sites)

$$\text{RFC}_k := \frac{\text{CalonsFC}_k}{\text{TFC}_{\text{monomers}_k}} \quad \text{RFC} = \begin{pmatrix} 0.04 \\ 0.037 \\ 0.124 \end{pmatrix}$$

CHAPTER 8

CONCLUSIONS AND RECOMMENDATIONS

8.1 Conclusions

This study provides a far-reaching analysis of microscale particle interactions, for different minerals exposed to a wide range of chemical and physical conditions. Single mineral particle associations can be captured in a pH-ionic concentration space. Mapping these associations provides a robust understanding of competing forces and their region of dominance. The proposed kaolinite fabric map includes both a physics-based approach to defining interparticle forces as well as an in-depth interpretation of experimental behavior observed by previous researchers.

The proposed kaolinite fabric map is verified with an untreated, commercially available kaolinite using wide-ranging volumetric solids contents and strain conditions. Fabric map verification implies that maps may be developed for specific minerals and counterions by defining characteristic behavioral regions based on the particle edge isoelectric point, the particle or face isoelectric point, and the ionic concentration convergence point. These three points define two horizontal lines and a vertical line that divide the pH-c space into various regions where either face charge, edge charge or van der Waals attraction dominate.

The fabric map is extended into a third dimension with an added anionic polymer, to control fabric through surface charge alteration. Variations in single mineral fabric are accomplished by first compensating excess positive charges and then inducing associations through the use of divalent cations. The extent of polymer influence is mineral dependent.

Fabric is opened with increasing edge to face and edge to edge associations promoted by bridging between the calcium ions and the anionic polymer located on the mineral surface. However, the effect of increasing particle associations is limited by the ratio of cations to polymer bonding sites and the overall solids volume fraction. At low cation-to-bonding site ratios, few bridges may form and associations are minimized. This effect is evident at high solids volume fraction where the number of accessible calcium ions is reduced due to the relatively low pore fluid volume.

Particle associations also vary in the case of mineral mixtures. Not only is fabric affected by relative particle shape and size, but it is also dependent on relative mineral content and competing dissolution effects. Bridging of prismatic carbonate particles by platy clay particles opens the pore spaces. The presence of calcium carbonate, even in small percentages, elevates the pore fluid pH in kaolinite-carbonate mixtures. Electrostatic-based associations develop when the negatively charged clay particles at high pH interact with the positively charged carbonate particles. Hence, clay particle associations can occur at pH away from the edge isoelectric point of the individual minerals. These effects are maximized at a particular mixing ratio (e.g., clay-carbonate) that is also mineral dependent.

The relevance of these effects is altered through changes in surface charge. Positive surface charge compensation is accomplished through anionic polymer addition. By minimizing the electrostatic attraction between particles, the final fabric is primarily due to particle packing where relative particle shape and size become more important. But, increasing particle associations through cation bridging is also solids content dependent and the maximized fabric mineral ratio is altered.

In summary, fabric may be controlled by taking advantage of the relative influences of mineral surface-fluid interactions, particle geometry and differences in particle mineralogy. The effect of surface charges can be altered with changes in pH, ionic concentration and polymer charge compensation.

8.2 Recommendations

Develop applications for both geotechnical use (clay liners) as well as other mineral-based industries (e.g. paper coatings). Surface-treated clays enhance the performance of a protective barrier (durability issues remain). Polymers are carefully chosen to minimize edge-to-face or edge-to-edge associations that may increase permeability, yet have resistance to changes in pore fluid chemistry. Paper coating techniques are improved through the coating application process. Engineered coating fabrics are produced by treating paper surfaces in stages rather than with a single coating application.

Consider the control distance between particles by varying polymer and/or molecule length. Fabric is altered by controlling the overall void ratio for a given dominance of particle interaction. For example, the density of a sediment made of primarily face-to-face aggregates is decreased by polymer expansion. The face-to-face association remains intact, but the distance between individual particles is a function of the polymer molecule length.

Include an intercalation study in the context of mineral mixtures (sandwiched nanofabrics). The interlayer spaces in clay particle layers are expandable, allowing for entrance of charge controlling polymers or nanoparticles. Exposed charged sites provide distinct locations for mineral or other material precipitation.

Explore a wider range of particle shapes (halloysite). The halloysite tube-like shape coupled with internal surface charge makes this clay particle a unique additive to mineral mixtures.

Explore other forms of fabric control, e.g. imposed AC electric fields. Manipulation of the relative motion between the particle and surrounding double layer as well as net particle motion within the applied field is achievable through both frequency and signal variation.

REFERENCES

- Ahmad, N.S., Karunaratne, G.P., Chew, S.H., and Lee, S.L. (2000), "Bentonite-Kaolinite Mix for Barrier Systems", *Geotechnical Special Publication, no. 105, Environmental Geotechnics, Proceedings of Sessions of Geo-Denver 2000: August 5-8, 2000, Denver, Colorado*, T.F. Zimmie, ed. ASCE Reston, VA, 93 – 104.
- Alinec, B. and Lepoutre, P. (1983a), "Flow Behavior of Pigment Blends", *Coating Conference, Proceedings of the Technical Association of the Pulp and Paper Industry*, 201 – 206.
- Alinec, B. and Lepoutre, P. (1983b), "Viscosity, Packing Density, and Optical Properties of Pigment Blends", *Colloids and Surfaces*, 6, 155 – 165.
- Allen, T. (1990), *Particle Size Measurement*, 4th ed., Chapman and Hall, New York, 806 p.
- Amirtharajah, A. and Mills, K.M., (1982), "Rapid-Mix Design for Mechanisms of Alum Coagulation", *Journal of the American Water Works Association*, 74(4), April, 210 – 216.
- Anandarajah, A. (1997), "Structure of sediments of kaolinite", *Engineering Geology*, 47, 313 – 323.
- Andersson, L.G. (1993), "Typical Coating Components", Chapter 2, Section 1 in *The Coating Process*, Prepared by the Coating Process Committee of the Coating and Graphic Arts Division Committee Assignment No. 1571-.870110.02, Walter, J.C., chairman, TAPPI Press, Atlanta, 260 p.
- Arkin, Y. and Michaeli, L. (1989), "Strength and Consistency of Artificial Clay-Carbonate Mixtures: Simulation of Natural Sediments", *Engineering Geology*, 26, 201 – 213.
- Barak, P. and Nater, E.A.. (2003). "The Virtual Museum of Minerals and Molecules", 1998-2003. [Online]. [c. 100 p.] Available at http://www.soils.wisc.edu/virtual_museum/ and http://www.soils.umn.edu/virtual_museum/ (modified 09 JUL 2003; accessed 22 OCT 2003). Univ. of Wisconsin-Madison, Madison, WI.
- Baumgartner, W. (2002), "Chemical markets of the Future", *Pulp & Paper*, 76(4), 25.
- Bell, F.G. and Coulthard, J.M. (1990), "Stabilization of Clay Soils with Lime", *Municipal Engineer*, 7(3), 125 – 140.

- Berg, J.M., Claesson, P.M., and Neuman, R.D. (1993), "Interactions Between Mica Surfaces in Sodium Polyacrylate Solutions Containing Calcium Ions", *Journal of Colloid and Interface Science*, 161, 182 – 189.
- Bergström, L., Sjöberg, M., and Järnström, L. (1996), "Concentrated Kaolinite Suspensions – Polymer Adsorption and Rheological Properties", *Science of Whitewares*, V.E. Henkes, G.Y. Onoda, and W.M. Carty, eds., Proceedings of the Science of Whitewares Conference, Alfred University July 16 – 20, 1995, 65 – 77.
- Bjorklund, R.B., Arwin, H., and Järnström, L. (1994), "Adsorption of Anionic and Cationic Polymers on Porous and Non-Porous Calcium Carbonate Surfaces", *Applied Surface Science*, 75, 197 – 203.
- Bohn, H.L., McNeal, B.L., and O'Connor, G.A. (1985), *Soil Chemistry*, 2nd Edition, John Wiley & Sons, New York, 341 p.
- Bradford, J.M. and Blanchar, R.W. (1999), "Mineralogy and Water Quality Parameters in Rill Erosion of Clay-Sand Mixtures", *Soil Science Society of America Journal*, 63, 1300 – 1307.
- Brady, P.V. and Walther, J.V. (1989), "Controls on Silicate Dissolution Rates in Neutral and Basic pH Solutions at 25°C", *Geochimica et Cosmochimica Acta*, 53, 2823 – 2830.
- Branston, R. (1999), "Flourescent Whiting Agents (FWA's) and Dyes in Paper Coating", 1999 Coating Materials: Pigments, Binders, and Additives Short Course: Auburn University Hotel & Conference Center, Auburn, AL, April 12 – 14, 1999, Course Notes, TAPPI Press, Atlanta, pp. 567 – 636.
- British Standard 1377-90 Section 4, "Determination of Liquid Limit".
- CCPA (2003), "Kaolin Geology in Middle Georgia", China Clay Product Association, accessed September 24, 2003, <<http://www.kaolin.com/geology/index.htm>>.
- Chen, J. and Anandarajah, A. (1998), "Influence of pore fluid composition on volume of sediments in kaolinite suspensions", *Clays and Clay Minerals*, 46(2) 145 – 152.
- Chonde, Y., Salminen, P., and Roper, J. (1995), "A Review of Wet Coating Structure: Pigment/Latex/Cobinder Interaction and Its Impact on Rheology and Runnability", *1995 Coating Fundamentals Symposium*, TAPPI Proceedings, 57 – 62.
- Chu, S.-C. and Kao, H.-S. (1993), "A Study of Engineering Properties of a Clay Modified by Fly Ash and Slag", *Fly Ash for Soil Improvement*, Geotechnical Special Publication No.36, E.D. Sharp, editor, American Society of Civil Engineers, New York, 89 – 99.
- Connors, T.E. and Banerjee, S., eds. (1995), *Surface Analysis of Paper*, CRC Press, Boca Raton, 346 p.

- Dahlvik, P., Ström, G. and Salminen, P. (1995), "Effect of pH and Calcium Ion Concentration on the Flow Behaviour and Structure Formation of Clay/Calcium Carbonate Suspensions", *1995 Coating Fundamental Symposium*, TAPPI Proceedings, 63 – 69.
- de Kretser, R.G., Scales, P.J., and Boger, D.V. (1998), "Surface Chemistry-Rheology Inter-relationships in Clay Suspensions", *Colloids and Surfaces A: Physicochemical and Engineering Aspects*, 137, 307 – 318.
- Delville, A. (2002), "The Influence of Electrostatic Forces on the Stability and the Mechanical Properties of Clay Suspensions", Chemo-Mechanical Coupling in Clays: From Nano-Scale to Engineering Applications, Edts., C. Di Maio, T. Hueckel, and B. Loret, Proceedings of the Workshop on Chemo-Mechanical Coupling in Clays: From Nano-Scale to Engineering Applications, Maratea, Italy, June 28 -30, A.A. Balkema, Lisse, 75 – 92.
- Di Maio, C. (1996), "Exposure of Bentonite to Salt Solution", *Geotechnique*, 46(4), 695 – 707.
- Diz, H.M.M. and Rand, B. (1990), "The Mechanism of Deflocculation of Kaolinite by Polyanions", *British Ceramic Transactions and Journal*, 89, 77 – 82.
- Drever, J.I. (1997), The Geochemistry of Natural Waters, 3rd Edition, Prentice Hall, Upper Saddle River, NJ, 436 p.
- Fam, M. and Dusseault, M (1998), "Evaluation of surface-related phenomena using sedimentation tests", *Geotechnical Testing Journal*, 21(3), 180 – 184.
- Fogle, A.W., Barfield, B.J., and Evangelou, V.P. (1991), "Solution sodium/calcium ratio effects on bentonite floc density", *Journal of Environmental Science & Health, Part A: Environmental Science & Engineering*, 26(6), 1003 – 1012.
- Gregory, J. (1997), "The density of particle aggregates", *Water Science & Technology*, 36(4), 1 – 13.
- Grim, R.E. (1968), Clay Mineralogy, Second Edition, McGraw-Hill, New York, 596 p.
- Guimaraes, M. (2002), Crushed Stone Fines and Ion Removal from Clay Slurries: Fundamental Studies, Ph.D. Dissertation, Georgia Institute of Technology, Atlanta, GA.
- Hagemeyer, R.W. (1960), "The Effect of Pigment Combination and Solids Concentration on Particle Packing and Coated Paper Characteristics: I. Relationship of Particle Shape to Particle Packing", *TAPPI*, 43(3), 277 – 288.
- Hagemeyer, R.W., ed. (1984), Pigments for Paper, TAPPI Press, Atlanta, 292 p.
- Hagemeyer, R.W., ed. (1997), Pigments for Paper, TAPPI Press, Atlanta, 254 p.

- Hayes, K. F. and Leckie, J. O. (1987), "Modeling Ionic Strength Effects on Cation Adsorption at Hydrous Oxide/Solution Interfaces", *Journal of Colloid and Interface Science*, 115(2), 564 – 572.
- Hiemenz, P.C. (1986), Principles of Colloid and Surface Chemistry, 2nd ed., Marcel Dekker, Inc., New York, 815 p.
- Hogg, R., Klimpel, R.C., and Ray, D.T. (1987), "Agglomerate structure in flocculated suspensions and its effect on sedimentation and dewatering", *Minerals and Metallurgical Processing*, 4(2), 108 – 114.
- Huber, O. and Weigl, J. (1972), "Die Füllstoff- und Pigmentqualit und ihr Einflu auf das Papier", *Papier*, 26(10A), 545 – 554.
- Hunter, R.J. (1993), Introduction to Modern Colloid Science, Oxford University Press, New York, 344 p.
- Hunter, R.J. (2001), Foundations of Colloid Science, 2nd ed., Oxford University Press, New York, 806 p.
- Imai, G. (1980), "Settling behavior of clay suspension", *Soils and Foundations*, 20(2), 61 – 77.
- Irani, R.R., and Callis, C.F. (1963), Particle Size: Measurement, Interpretation, and Application, John Wiley & Sons, New York, 165 p.
- Jrnstrm, L. (1993), "The Polyacrylate Demand in Suspensions Containing Ground Calcium Carbonate", *Nordic Pulp and Paper Research Journal*, 8(1), 27 – 33.
- Jrnstrm, L. and Stenius, P. (1990), "Adsorption of Polyacrylate and Carboxy Methyl Cellulose on Kaolinite: Salt Effects and Competitive Adsorption", *Colloids and Surfaces*, 50, 47 – 73.
- Kanbara, T., Yamamoto, T., Ikawa, H., Tagawa, T., and Imai, H. (1989), "Preparation and Characterization of Porous and Electrically Conducting Carbon-Clay Composites", *Journal of Materials Science*, 24, 1552 – 1558.
- Keren, R. (1989), "Rhology of Mixed Kaolinite-Montmorillonite Suspensions", *Soil Science Society of America Journal*, 53, 725 – 730.
- Klein, K. (1999), Electromagnetic Properties of High Specific Surface Minerals, Ph.D. Dissertation, Georgia Institute of Technology, Atlanta, GA.
- Klimpel, R.C., Dirican, C., and Hogg, R. (1986), "Measurement of agglomerate density in flocculated fine particle suspensions", *Particulate Science & Technology*, 4, 45 – 59.

- Lagvankar, A.L. and Gemmell, R.S. (1968), "A size-density relationship for flocs", *Journal of the American Water Works Association*, 60, 1040 – 1046.
- Lambe, T.W. and Whitman, R.V. (1969), *Soil Mechanics*, John Wiley & Sons, New York, 553 p.
- Langmuir, D. (1997), *Aqueous Environmental Geochemistry*, Prentice Hall, Upper Saddle River, NJ, 600 p.
- Leelanitkul, S. (1989), "Improving Properties of Active Clay by Sand Admixtures", *Foundation Engineering and Current Principles and Practices*, Vol. 1, F.H. Kulhawy, ed., ASCE, New York, 381 – 391.
- Levlin, J.E. and Söderhjelm, L., eds. (1999), *Pulp and Paper Testing*, Fapet Oy, Helsinki, Finland, 287 p.
- Lovgren, L., Sjöberg, S., and Schindler, P.W. (1990), "Acid/Base Reactions and Al(III) Complexation at the Surface of Goethite", *Geochimica et Cosmochimica Acta*, 54, 1301 – 1306.
- Lyklema, J. (1995), *Fundamentals of Interface and Colloid Science Volume II: Solid-Liquid Interfaces*, Academic Press, New York.
- Ma, C. and Eggleton, R.A. (1999), "Cation Exchange Capacity of Kaolinite", *Clays and Clay Minerals*, 47(2), 174-180.
- Malla, P.B., Starr, R.E., and Werkin, T.J. (1999), "The Effects of Kaolin Particle Size, Structured Clay Loading, and Binder Level on Glossing and Offset Print Properties – A CLC Coating Study", *1999 TAPPI Coating Conference*, May 2 – 5, 1999, Toronto, p. 387 – 411.
- Mallett, A.S. and Craig, R.L. (1977), "The Effect of the Molecular Weight of Sodium Polyacrylate on Pigment Dispersions", *TAPPI*, 60(11), 101 – 104.
- Marion, D., Nur, A., Yin, H., and Han, D. (1992), "Compressional Velocity and Porosity in Sand-Clay Mixtures", *Geophysics*, 57(4), 554 – 563.
- Melton, I.E. and Rand, B. (1977), "Particle interactions in aqueous kaolinite suspensions III Sedimentation volumes", *Journal of Colloid and Interface Science*, 60(2), 331 – 336.
- Michaels, A.S. and Bolger, J.C. (1964), "Particle Interactions in Aqueous Kaolinite Dispersions", *Industrial and Engineering Chemistry Fundamentals*, 3(1), 14 – 20.
- Michaels, A.S. and Morelos, O. (1955), "Polyelectrolyte Adsorption by Kaolinite", *Industrial and Engineering Chemistry*, 47(9), 1801 – 1809.

- Mitchell, J.K. (1993), Fundamentals of Soil Behavior, John Wiley & Sons, New York, p. 437.
- Mitchell, J.K. and Dermatas, D. (1992), "Clay Soil Heave Caused by Lime-Sulfate Reactions", *Innovations and Uses for Lime, ASTM STP 1135*, D.D. Walker, Jr., T.B. Hardy, D.C. Hoffman, and D.D. Stanley, editors, American Society for Testing and Materials, Philadelphia, 41 – 64.
- Moore, J. (2002), "Kaolin Pigment Advances", *Pulp & Paper*, 76(1), 29.
- Muhunthan, B. (1991), "Liquid Limit and Surface Area of Clays", *Geotechnique*, 41(1), 135 – 138.
- Mukerjee, M. (2000), "Superabsorbers", *Scientific American*, December 19, accessed July 17, 2003, http://www.sciam.com/print_version.cfm?articleID=00028414-AF72-1C72-9EB7809EC588F2D7.
- Murray, H.H. (2000), "Traditional and New Applications for Kaolin, Smectite, and Palygorskite: A General Overview", *Applied Clay Science*, 17, 207 – 221.
- Nagy, K.L. (1995), "Dissolution and Precipitation Kinetics of Sheet Silicates", Chemical Weathering Rates of Silicate Minerals, Reviews in Mineralogy, Volume 31, Edts. A.F. White and S.L. Brantley, 173 – 233.
- Neaman, A. and Singer, A. (2000), "Rheology of Mixed Palygorskite-Montmorillonite Suspensions", *Clays and Clay Minerals*, 48(6), 713 – 715.
- Nicol, S.K. and Hunter, R.J. (1970), "Some Rheological and Electrokinetic Properties of Kaolinite Suspensions", *Australian Journal of Chemistry*, 23, 2177 – 2186.
- Nishimura, S., Biggs, S., Scales, P. J., Healy, T. W., Tsune-matsu, K., and Tateyama, T. (1994), "Molecular-Scale Structure of the Cation Modified Muscovite Mica Basal Plane", *Langmuir*, 10, 4554 – 4559.
- O'Brien, D.K., Manghnani, M.H., Tribble, J.S., and Wenk, H.-R. (1993), "Preferred Orientation and Velocity Anisotropy in Marine Clay-Bearing Calcareous Sediments", Carbonate Microfabrics, Chapter 11, R. Rezak and D.L. Lavoie, editors, Springer-Verlag, New York, 313 p.
- O'Brien, N.R. (1971), "Fabric of Kaolinite and Illite Floccules", *Clays and Clay Minerals*, 19, 353 – 359.
- Orr, C. Jr., and Dallavalle, J.M. (1959), Fine Particle Measurement: Size, Surface, and Pore Volume, The Macmillan Company, New York, 353 p.

- Pamukcu, S., Tuncan, M., and Fang, H.-Y. (1990), "Influence of Some Environmental Activities on Physical and Mechanical Behavior of Clays", *Physico-Chemical Aspects of Soil and Related Materials, ASTM STP 1095*, K.B. Hoddinott and R.O. Lamb, editors, American Society for Testing and Materials, 91 – 107.
- Patton, T.C. (1979), Paint Flow and Pigment Dispersion, 2nd ed., John Wiley & Sons, New York, 631 p.
- Pierre, A.C. and Ma, K. (1999), "DLVO theory and clay aggregate architectures formed with $AlCl_3$ ", *Journal of the European Ceramic Society*, 19(8), 1615 – 1622.
- Pierre, A.C., Ma, K., and Barker, C. (1995), "Structure of kaolinite flocs formed in an aqueous medium", *Journal of Materials Science*, 30, 2176 – 2181.
- Pierre, A.C., Zou, J., and Barker, C. (1993), "Structure reorganization in montmorillonite gels during drying", *Journal of Materials Science*, 28, 5193 – 5198.
- Rahaman, M.N. (1995), Ceramic Processing and Sintering, Marcel Dekker, Inc., New York, 770 p.
- Rand, B. and Melton, I.E. (1977), "Particle interactions in aqueous kaolinite suspensions I. Effect of pH and electrolyte upon the mode of particle interaction in homoionic sodium kaolinite suspensions", *Journal of Colloid and Interface Science*, 60(2), 308 – 320.
- Rand, B., Pekenc, E., Goodwin, J. W., and Smith, R. W. (1980), "Investigation into the Existence of Edge-Face Coagulated Structures in Na-Montmorillonite Suspensions", *Journal of the Chemical Society, Faraday Transaction I*, (76), 225 – 235.
- Ravisangar, V. (2001), The Role of Sediment Chemistry in Stability and Resuspension Characteristics of Cohesive Sediments, Ph.D. Dissertation, Georgia Institute of Technology, Atlanta, GA.
- Riggin, W.M. (1999), "The Nature of Coating Clays", 1999 Coating Materials: Pigments, Binders, and Additives Short Course: Auburn University Hotel & Conference Center, Auburn, AL, April 12 – 14, 1999, Course Notes, TAPPI Press, Atlanta, pp. 11 – 39.
- Robinson, J.V., Millman, N., and Whitley, J.B. (1997), "The Dispersion of Pigments for Paper Coating", Pigments for Paper, R.W. Hagemeyer, ed., 21 – 53.
- Sacks, M. (2001), Fine Particle Technology, class notes, Georgia Institute of Technology, Atlanta, Georgia.
- Sanders, N.D. (1991), "The Effect of Surface Modification of Pigments on Colloidal Stability and Structural Performance", *CPPA/TAPPI Symposium on Papercoating Fundamentals*, Montreal, Canada, May 17 – 18, 1991, 51 – 60.

- Santamarina, J.C. (2002), Soil Behavior at the Microscale: Particle Forces, in “Soil Behavior and Soft Ground Construction”, *Soil Behavior and Soft Ground Construction – The Ladd Symposium*, October, MIT, Boston, ASCE Special Publications #119, pp. 25-56.
- Santamarina, J.C., Klein, D.A., Palomino, A., and Guimaraes, M.S. (2002), “Micro-Scale Aspects of Chemical-Mechanical Coupling: Interparticle Forces and Fabric”, Chemo-Mechanical Coupling in Clays: From Nano-Scale to Engineering Applications, Edts., C. Di Maio, T. Hueckel, and B. Loret, Proceedings of the Workshop on Chemo-Mechanical Coupling in Clays: From Nano-Scale to Engineering Applications, Maratea, Italy, June 28 -30, A.A. Balkema, Lisse, 47 – 64.
- Santamarina, J.C., Klein, K.A., and Fam, M.A. (2001), Soils and Waves, John Wiley & Sons, Chichester, UK, 488 p.
- Schofield, R.K. and Samson, H.R. (1953), “The Deflocculation of Kaolinite Suspensions and the Accompanying Change-Over from Positive to Negative Chloride Adsorption”, *Clay Minerals Bulletin*, 2(9), 45 – 51.
- Schofield, R.K. and Samson, H.R. (1954), “Flocculation of Kaolinite Due to the Attraction of Oppositely Charged Crystal Faces”, *Faraday Society Discussions*, no. 18, 135 – 145.
- Schweins, R. and Huber, K. (2001), “Collapse of Sodium Polyacrylate Chains in Calcium Salt Solutions”, *The European Physical Journal E*, 5, 117 – 126.
- Scott, W.E. (1996), Principles of Wet End Chemistry, TAPPI Press, Atlanta, 185 p.
- Secor, R.B. and Radke, C.J. (1985), “Spillover of the Diffuse Double Layer on Montmorillonite Particles”, *Journal of Colloid and Interface Science*, 103(1), 237 – 234.
- Siffert, B. and Fimbel, P. (1984), “Parameters Affecting the Sign and the Magnitude of the Electrokinetic Potential of Calcite”, *Colloids and Surfaces*, 11, 377 – 389.
- Sjöberg, M, Bergström, L., Larsson, A., and Sjöström, E. (1999), “The Effect of Polymer and Surfactant Adsorption on the Colloidal Stability and Rheology of Kaolin Dispersions”, *Colloids and Surfaces A: Physicochemical and Engineering Aspects*, 159, 197 – 208.
- Sposito, G. (1989), The Chemistry of Soils, Oxford University Press, New York, 277 p.
- Sposito, G. (1998), "On Points of Zero Charge", *Environmental Science & Technology*, 32(19), 2815 – 2819.

- Sridharan, A. and Prakash, K. (1999), "Influence of clay mineralogy and pore-medium chemistry on clay sediment formation", *Canadian Geotechnical Journal*, 36, 961 – 966.
- Stenius, P., Järnström, L., and Rigdahl, M. (1990), "Aggregation in Concentrated Kaolin Suspensions Stabilized by Polyacrylate", *Colloids and Surfaces*, 51, 219 – 238.
- Ström, G., Härdin, A.-M., and Salminen, P. (1995), "A Novel Formulation Approach for Improving Fibre Coverage During Blade Coating", *Nordic Pulp and Paper Research Journal*, 10(4), 227 – 233.
- Stumm, W. (1992), Chemistry of the Solid-Water Interface, John Wiley & Sons, New York, 428 p.
- Tari, G., Fonseca, A.T., and Ferreira, J.M.F. (1998), "Influence of Kaolinite Delamination on Rheological Properties and Sedimentation Behaviour of Ceramic Suspensions", *British Ceramic Transactions*, 97(6), 259 – 262.
- Testing Machines, Inc. (2002), "Guide to Pulp and Paper Testing", <http://www.testingmachines.com/pdfs/guidindx.pdf>, accessed September 30, 2002.
- Theng, B.K.G. (1979), Formation and Properties of Clay-Polymer Complexes, Elsevier Scientific Publishing Company, Amsterdam, 362 pp.
- Tiller, F.M. and Khatib, Z. (1984), "The Theory of Sediment Volumes of Compressible, Particulate Structures", *Journal of Colloid and Interface Science*, 100(1), 55 – 67.
- UGA (2003), University of Georgia, "The Geology of Georgia", University of Georgia Department of Geology, <http://www.gly.uga.edu/GAGeology.html>, accessed September 24, 2003,
- USGS (2001), United States Geological Survey, Minerals Yearbook, State of Georgia, <http://minerals.usgs.gov/minerals/pubs/state/2001/gastmyb01.pdf>, accessed September 24, 2003.
- USGS (2003), United States Geological Survey, Mineral Commodity Summaries 2003, <http://minerals.usgs.gov/minerals/pubs/mcs/2003/mcs2003.pdf>, accessed September 24, 2003.
- van Olphen, H. (1951), "Rheological Phenomena of Clay Sols in Connection with the Charge Distribution on the Micelles", *Discussions of the Faraday Society*, no. 11, 82 – 84.
- van Olphen, H. (1977), An Introduction to Clay Colloid Chemistry, 2nd ed., Krieger Publishing Company, Malabar, Florida, 318 p.

- Vanerek, A., Alince, B. and van de Ven, T.G.M. (2000), "Colloidal Behaviour of Ground and Precipitated Calcium Carbonate Fillers: Effects of Cationic Polyelectrolytes and Water Quality", *Journal of Pulp and Paper Science*, 26(4), April, 135 – 139.
- Vipulanandan, C. and Leung, M. (1991), "Effect of Methanol and Seepage Control in Permeable Kaolinite Soil", *Journal of Hazardous Materials*, 27, 149 – 167.
- Wieland, E. and Stumm, W., (1992), "Dissolution Kinetics of Kaolinite in Acidic Solutions at 25°C", *Geochimica et Cosmochimica Acta*, 56, 3339 – 3355.
- Wroth, C.P. and Wood, D.M. (1978), "The correlation of index properties with some basic engineering properties of soils", *Canadian Geotechnical Journal*, 15(2), 137 – 145.
- Wygant, R.W., Iyer, R.R., Jones, J.P.E., and Cummings, D.O. (1998), "Glossing Properties of Engineered Kaolins", *1998 TAPPI Proceedings Coating/Papermakers Conference*, Book 2, May 4 – 6, 1998, New Orleans, pp. 837 – 852.
- Yariv, S. and Cross, H., eds., (2002), Organo-Clay Complexes and Interactions, Marcel Dekker, New York, 688 pp.
- Yuan, J. and Murray, H.H. (1997), "The Importance of Crystal Morphology on the Viscosity of Concentrated Suspensions of Kaolins", *Applied Clay Science*, 12, 209 – 219.

VITA

Angelica M. Palomino was born on May 13, 1974, in San Benito, Texas. She received both her Bachelor of Arts degree in Natural Sciences from Our Lady of the Lake University, San Antonio, Texas, and her Bachelor of Civil Engineering degree from the Georgia Institute of Technology, Atlanta, Georgia, in 1998. Ms. Palomino continued her studies at Georgia Tech as a National Science Foundation Graduate Fellow and Georgia Tech Presidential Fellow, receiving her Master of Science in Civil Engineering in 1999. Ms. Palomino received her Ph.D. degree from the Georgia Institute of Technology in 2004. Her research interests include mineral surface chemistry and modification and microscale engineered particulate fabrics.